Universidade do Minho
Escola de Engenharia

Juliana Alice Ferreira Oliveira

Radiation detectors based on printing technologies

outubro de 2018

Juliana Alice Ferreira Oliveira **Radiation detectors based on printing technologies**

UMinho | 2018

Universidade do Minho
Escola de Engenharia

Juliana Alice Ferreira Oliveira

Radiation detectors based on printing technologies

Tese de Doutoramento em Engenharia de Materiais

Trabalho efetuado sob a orientação do
Professor Senentxu Lanceros-Mendez
e do
Professor Gerardo Rocha

outubro de 2018

STATEMENT OF INTEGRITY

I hereby declare having conducted my thesis with integrity. I confirm that I have not used plagiarism or any form of falsification of results in the process of the thesis elaboration.

I further declare that I have fully acknowledge the Code of Ethical Conduct of the University of Minho.

University of Minho, 29 de Outubro de 2018

Full name: Juliana Alice Ferreira Oliveira

Signature: Juliana Oliveira

Acknowledgments

I would like to express my gratitude to every person who somehow contributed for the development of this thesis.

The Foundation for Science and Technology (FCT), grant SFRH/BD/98219/2013, for the financial support to this project.

All the work at the thesis would not have been accomplished without the accompaniment and effort of my supervisors. Thus, I'm thankful to Professor Gerardo Rocha and Professor Senentxu Lanceros-Mendez for the given opportunity, all support, sympathy, understanding and for all the scientific knowledge given to me.

I also want to thank the good times spent in the Technical Chemnitz University and off course, in special, all the support given by Enrico Sowade.

To the Electroactive Smart Materials group (ESMG), I would like to thank all the great and amazing team spirit and the friendship given. A special thank to Dr. Pedro Martins, Dr. Pedro Costa, Dr. Renato Gonçalves and Dr. Vitor Correia, for all the help, effort and support at the laboratory. A special thank for my friend Sylvie Ribeiro for the friendship, unconditional support and for all the effort always shown to make me feel good and happy.

I would like to thank all my friends for the unconditional support, good moments and vibes and for always being by my side at good and even in the difficult times.

To my parents and my sister Diana, for all the affection, understanding, and strength given not only during the development of the thesis, but in all the journeys of my life and for always believe in my capability. Thank you for everything you do for me! What I am today I owe it to you.

At last, I would like to thank my husband Nuno for the unconditional love, support, encouragement given and for always being by side. Love you.

Thank you.

To my mum

and my daughter Benedita

Abstract

X-ray imaging is being increasingly implemented in a variety of areas, ranging from security to industry and medical devices. Since the discovery of the X-ray radiation by Wilhelm Roentgen in 1895, the development in the field of radiography has been notorious. Conventional radiography presents relevant limitations such as the requirement of high radiation doses, low quality images, long time of radiographic processing and the use of chemicals with strong environmental impact. Thus, different technologies are being developed to overcome these limitations. The demand for improved spatial resolution to obtain more clear and accurate images, while reducing the radiation doses led to the progressive replacement of the traditional techniques based on X-ray film chemical processing by digital processing techniques. Further, X-ray digital images allow real-time imaging. The detection process in digital radiography can be based in two different approaches: indirect detection, where radiation is absorbed by a scintillator material that converts it into visible light, which is later converted to an electrical signal by a photodetector, and the direct method, where the photons are directly converted into an electrical signal. However, radiation detection methods for digital radiography face serious limitations and high costs when large areas or flexible applications are required. In this context, the main objective of this work is the development of printable indirect X-ray detectors based on novel polymer-based scintillators, prepared in the form of inks. This approach will set the basis for a new generation of X-ray detectors for low-cost, large area and flexible applications. For this purpose, polymer scintillator film composites were prepared based on $Gd_2O_3:Eu^{3+}$ (GDO) scintillator nanoparticles, which are responsible for converting X-rays into visible light. Different types of polymer matrix were used within the composites to optimize scintillator response and to allow specific X-ray imaging applications. First, a polymer-based scintillator composite was developed using poly(vinylidene fluoride), P(VDF), as polymer matrix. The main objective of this work was to determine the influence of the inclusion of fluorescence molecules (FL) (2,5 diphenyloxazole (PPO), 1 wt.%, and 0.01 wt.% of 1,4 di[2-(5phenyloxazolyl)]benzene (POPOP)), together with the scintillator GDO nanoparticles, to enhance X-ray to visible radiation overall conversion, allowing the reduction of incident X-ray radiation.

Further, polystyrene (PS) was used as polymer matrix due to its intrinsic scintillator characteristics. The introduction of FL and GDO nanoparticles leads to a decrease of the optical transmittance of the composites films compared with P(VDF)-based scintillator composites, but also to the enhancement of visible light yield in around 2000%. Overall, it was not found a significant increase of X-ray conversion performance with the

substitution of P(VDF) by PS, despite the scintillating characteristics of the latter. Regarding to the development of new materials for stretchable applications, polymer-based scintillator composites were developed based on thermoplastic elastomer Styrene-Ethylene/Butadiene-Styrene (SEBS). After the optimization of the best concentration of GDO (0.50 wt.%) a scintillator ink was produced. Tests of stretchability were performed and it was observed that increasing applied strain up to 100% leads just to a decrease of 13% in the visible radiation intensity, remaining scintillator composite fully functional. This behavior was explained by the effective decrease of the film thickness upon stretching, reducing thus the amount of scintillator material in the X-ray beam. Following, an environmentally-friendly approach was implemented for the development of printable X-ray radiation detectors. Thus, water-based scintillator inks, suitable for spray, screen and doctor blade printing, were produced by combining water soluble poly(vinyl) alcohol as polymer matrix, scintillator nanoparticles and fluorescence molecules. The optimal concentration of scintillator nanoparticles in the water-based ink for spray-printing was 0.75 wt.% and the ink formulation, with a viscosity around 0.1 Pa.s, exhibits a Newtonian behavior. The ink was printed on a photodetector matrix and the results show that the ink is suitable for the fabrication of spray-printed indirect X-ray detectors by a green-solvent approach, once the conversion of the X-ray radiation into visible light of the different photodetectors are linear, stable and reproducible. Finally, an all-printed functional prototype was fabricated to demonstrate the concept proposed in the present thesis. Thus, inkjet-printed photodetector arrays, based on an organic thin-film transistor (OTFT) architecture, was fabricated and applied for indirect detection of X-ray radiation using a screen printing scintillator ink based on polymer SEBS dissolved on toluene with 0.50 wt.% of GDO scintillator nanoparticles and 1 wt.% of PPO and 0.01wt.% of POPOP, as X-ray absorber. The electrical response of the photodetector shows a dark current about 300 nA, while under illumination the photocurrent was about 660 nA. The increase of around 120 % shows the suitable performance of the printed device as a photodetector. Further, the scintillation response of the scintillator when located on top of the photodetector proves the suitability of the printed device for X-ray detection applications once its current intensity increases 93 % under X-ray radiation. In conclusion, it was demonstrated the possibility of fabricating a complete printed X-ray indirect radiation detector based on the new developed scintillator polymer composites.

Resumo

A imagiologia baseada em radiação raios-X (RX) encontra-se cada vez mais presente em diversas áreas tais como inspeção industrial, segurança e imagiologia médica. Desde a descoberta da radiação RX, por Wilhelm Roentgen em 1895, têm sido notórios os vários desenvolvimentos adquiridos na área da radiografia. A radiografia convencional apresenta várias limitações, tais como a exigência de altas doses de radiação, baixa qualidade de imagem, longo tempo de processamento e o uso de produtos químicos com alto impacto no meio ambiente. Assim, diversas tecnologias têm vindo a ser desenvolvidas de forma a superar essas limitações. A transição da radiografia convencional para a radiografia digital leva a importantes vantagens para a imagiologia de radiação RX. Em particular, a necessidade em melhorar a resolução espacial de forma a obter imagens mais nítidas e precisas, bem como a redução da dose de radiação aplicada, levou à substituição progressiva das técnicas tradicionais de processamento de imagem de RX por técnicas de processamento digital. A obtenção de radiografia digital divide-se em dois diferentes métodos: direto e indireto. No método direto, a radiação de RX é absorvida pelo detetor que a converte diretamente num sinal elétrico. No método indireto, os RX são previamente convertidos em radiação visível, por um material cintilador, sendo posteriormente transformada num sinal elétrico. No entanto, ambos enfrentam sérias limitações e custos elevadas quando necessárias aplicações em grandes áreas e/ou aplicações flexíveis. Assim, o principal objetivo deste trabalho consiste no desenvolvimento de um detetor de RX por método indireto, baseado numa nova geração de cintiladores poliméricos preparados sob a forma de compósitos e tintas.

Para este efeito, os compósitos cintiladores poliméricos foram preparados com base em nanopartículas cintiladoras, $Gd_2O_3:Eu^{3+}$ (GDO), que são responsáveis pela conversão da radiação RX em luz visível. Além disso, foram utilizados diferentes tipos de polímeros de forma a obter algumas aplicações específicas de imagiologia baseada em RX. Primeiramente, um compósito cintilador polimérico foi desenvolvido usando fluoreto de polivinilideno (P(VDF)) como matriz polimérica. Este trabalho centrou-se em determinar a influência da inclusão de moléculas fluorescentes (FL), 1 wt.% de 2,5 diphenyloxazole (PPO) e 0,01 wt.% de 1,4 di[2-(5phenyloxazolyl)] benzeno (POPOP)), juntamente com as nanopartículas de GDO, no melhoramento da conversão de RX de forma a permitir a redução da dose de radiação incidente de RX. Desta forma, determinou-se a concentração ótima de GDO (0.50 wt.%) e das FL e verificou-se que a sua inclusão levou a uma maior eficiência de conversão da radiação. Seguidamente, foi utilizado o poliestireno (PS) como matriz polimérica devido às suas características cintiladoras. A introdução de FL e de

GDO levou a uma diminuição da transmitância ótica dos compósitos cintiladores de PS em comparação com os compósitos cintiladores à base de P(VDF), e a um aumento do rendimento de luz visível em cerca de 2000 %. O aumento do desempenho de conversão de RX relativamente aos compósitos de P(VDF) foi pouco significativo, apesar das características cintiladoras do PS. Para proceder ao desenvolvimento de novos materiais para aplicações flexíveis e estiráveis, foram desenvolvidos compósitos cintiladores poliméricos baseados no termoplástico elastómero estireno-etileno/butadieno-estireno (SEBS). Após a otimização da composição das nanopartículas cintiladoras (0.50 wt.%), foi produzida uma tinta cintiladora e realizados testes de estiramento nos filmes impressos observando-se que um aumento do estiramento aplicado até 100% leva a uma diminuição de 13 % na intensidade da radiação visível, permanecendo o filme cintilador totalmente funcional. Seguidamente, foram produzidas tintas cintiladoras à base de água, adequadas para as técnicas de impressão por *spray*, serigrafia e *doctor blade*, pela combinação do polímero álcool polivinílico, nanopartículas de GDO e FL. A concentração ótima de nanopartículas cintiladoras na tinta para impressão por *spray* foi de 0,75 wt.% e, a tinta apresentava uma viscosidade de ~0.1 Pa.s exibindo um comportamento Newtoniano. Após caracterização, a tinta foi impressa sobre uma matriz de fotodetetores e depois de vários testes realizados, os resultados mostraram que a tinta é adequada para a fabricação de detetores indiretos de RX impressos por *spray*, uma vez que a conversão da radiação de RX em luz visível pelos diferentes fotodetetores é reprodutível e linear. Finalmente foi fabricado um protótipo totalmente impresso como prova de conceito. Foram fabricadas matrizes de fotodetetores por impressão a jato de tinta, baseadas na arquitetura de transístores orgânicos de filme fino (OTFT), e aplicadas para deteção indireta de radiação de RX usando uma tinta cintiladora otimizada para serigrafia, baseada numa solução de SEBS, nanopartículas de GDO (0.50 wt.%) e FL. A resposta elétrica do fotodetetor com e sem iluminação incidente era de 660 nA e 300 nA respetivamente. O aumento em 120% demonstra o desempenho adequado do protótipo como fotodetetor. Além disso, quando o cintilador é impresso sobre a matriz, a eficiência de conversão de radiação obtida (aumento de 93%) demonstra que o dispositivo impresso é adequado para aplicações de deteção indireta de RX. Em conclusão, demonstrou-se a possibilidade e a viabilidade de fabricar um detetor de radiação RX de método indireto totalmente impresso, baseado em compósitos cintiladores poliméricos

Table of Contents

List of figures

List of tables

List of symbols

ρ	Density
Z_{eff}	Atomic number
L_R	Generated light,
λ	Emission wavelength
τ	Scintillation decay time
I	Intensity of the radiation
I_0	Initial intensity of the radiation
μ	Coefficient of linear absorption of the material
α	Fine-structure constant
σ_{pair}	Pair Production
r_e	Classic electron radius
β	β-phase
γ	γ-phase
wt.%	Weight percentage
ε’	Real part of dielectric constant
tan δ	Dielectric loss
ε_0	Vacuum permittivity
ε’’	Imaginary part of dielectric constant
σ_{AC}	AC conductivity
η_0	Zero shear viscosity
η_S	Shear viscosity
ϕ	Volume fraction of spherical particles

List of abbreviations

A

AC	Alternating Current
a. u.	Arbitrary units

B

BAS	Block Acquisition System

C

CCD	Charge Coupled Device
CMOS	Complementary Metal Oxide Semiconductor
c-PVP	Cross-linked poly-4-vinylphenol
CT	Computed tomography

D

DMF	N, N-dimethylformamide
DSC	Differential scanning calorimetry
DMP	Dimatix Materials Printer
DVD	Digital Versatile Discs

E

EDX	Energy Dispersive X-ray

F

FIB	Focused gallium ion beam
FL	Fluorescence molecules
FTIR	Fourier transformed infrared spectroscopy

G

GDO	$Gd_2O_3:Eu^{3+}$

H

HOMO	Highest Occupied Molecular Orbital

I

IC	Integrated circuit
I_{DS}	Current Drain-Source

L

LUMO	Lowest Unoccupied Molecular Orbital

M

MCU	Micro Control Unit

O

OTFT	Organic Thin-Film Transistor
OPDs	Organic Photodetectors
OSC	Organic Semiconductor

P

PEN	Polyethylene naphthalate
PET	Polyethylene terephthalate
PD	Printed photodetectors
PGMEA	Propylene glycol monomethyl ether acetate
PL	Photoluminescence
PMFM	Poly(melamine-coformaldehyde) methylated
P(VDF)	Poly(vinylidene fluoride)
PS	Polystyrene

PVA	Poly(vinyl) alcohol
PPO	2,5 diphenyloxazole
POPOP	1,4 di[2-(5phenyloxazolyl)]benzene

R

RF	Radio frequency

S

SC	Scintillator material
SEBS	Styrene-Ethylene/Butadiene-Styrene
SBS	Styrene-Butadiene-Styrene
SEM	Scanning Electron Microscope
S-D	Source-Drain

T

TFT	Thin Film Transistor
TPE	Thermoplastic elastomers

U

UV-VIS	Ultraviolet–Visible spectroscopy

V

V_{DS}	Voltage Drain-Source
V_{GS}	Voltage Gate-Source
V.R.I.	Visible Radiation Intensity

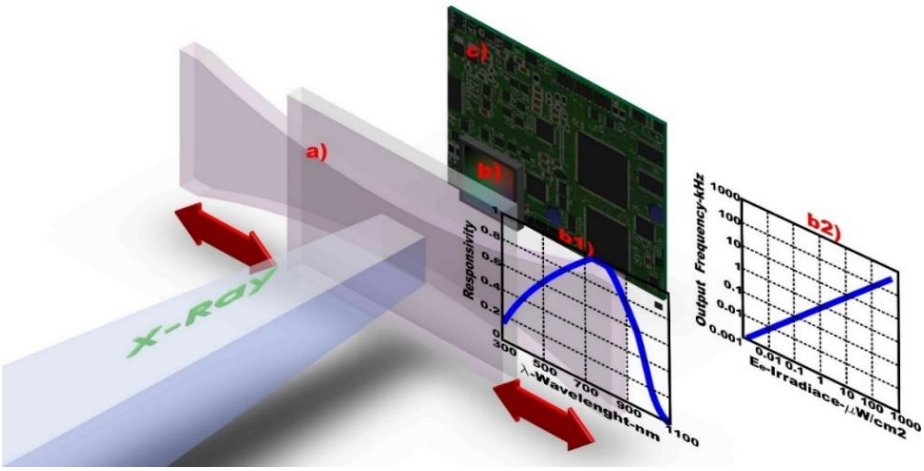

Chapter 1. Introduction

Advances on digital radiography and X-ray radiation detectors are taking place and new digital technologies are available for a wide spectrum of applications ranging from medical imaging detectors, inspection and safety industries, healthcare industry, military applications, among others. The present work represents a contribution to the development of novel materials for X-ray radiation detectors, to be implemented by printing technologies. Thus, this chapter introduces the main concepts related to X-ray radiation detectors and technologies with special focus on scintillator materials and photodetectors, as they are the main focus of the present work. This chapter also presents the main objectives of the study, the research methodology and the structure of the thesis.

1.1. X-ray imaging and detectors

Smart and multifunctional materials are getting increasing interest by the scientific and technological communities as an attractive group of materials for a new generation of devices [1]. Through almost all industries, ranging from medicine, sports, security and consumer electronics, this kind of materials are adding value to traditional devices and allowing the development of new ones, providing also improved integration possibilities and novel fabrication approaches [1, 2]. In this way, smart and multifunctional materials are a very active research topic which will allow novel emerging applications [2, 3].

In particular, the development of a new generation of materials is needed in order to improve the performance of existing X-ray image detectors and to extend their range of applicability to fields in which larger areas and/or flexibility are required.

The discovery of X-ray radiation by Roentgen in 1895 led to a revolution in many fields, including medicine, due to the possibility of image diagnosis [4]. X-ray detectors are undergoing fast development in the area of digital radiography with improved spatial resolution with reduction of the radiation dose, but despite the strong technological advances, continuously taking place in this field, the detectors currently in use are unable to provide the demanded performances concerning the improvement of the resolution and absorption efficiency which would result in more clear and accurate images [5].

Given the disadvantages of conventional radiography, such as the required high radiation doses, the variability in the quality of the obtained image, long radiographic processing time, the use of chemicals with high environmental impact, the need for a proper location for radiographic processing and the impossibility of modifying the image after it was acquired, several technologies have been developed to minimize them, leading to the development and application of digital image radiography [6]. The digital image can be obtained indirectly by scanning conventional radiographs or by directly using image detectors [7]. There are numerous advantages of the latter system, including the elimination of chemical processing, the possibility of copying images without the need for new radiographic images, and the reduction of the exposure dose to X-rays [6].

Further, recent advances in manufacturing technologies allow the possibility of a new generation of large-area, flat-panel detectors with integrated thin-film transistors (TFT) readout mechanisms. The main advantages of this approach are [8]:

✓ Reduction of the radiation dose: the radiation dose used on conventional radiography is determined by the receptor's sensitivity and the film's depth brightness. In digital

radiography the only concern involving the radiation dose is due to the signal-noise relationship that must maintain satisfactory values while reducing the radiation dose. Any image contrast loss can be restored using image processing techniques.

- ✓ Improvement in the image acquisition and processing: Digital radiography allows image acquisition without waiting for the film processing, and uses digital processing techniques through the application of sophisticated algorithms, including contrast change, equalization and image subtraction [9],
- ✓ Image acquisition, visualization, storage and recovery are simplified: The image acquired is displayed in a screen instead of a film and can be stored in databases which make it easier to recover and transmit it.

These characteristics and possibilities have led to an increased use of radiology in applications ranging from medical imaging to structural health monitoring and security, among many others.

Despite the advantages of digital radiography, current techniques face severe limitations and high costs when large areas or flexible applications are involved.

Image quality is intimately linked to the precise and accurate acquisition of information from the X-ray beam transmitted through the object/patient, i.e. to the performance of the X-ray detector. Depending on the application, a detector must fulfil various requirements to present a good performance and in specific applications some requirements rule out certain detector types. The main important X-ray detector parameters are spatial resolution, uniformity of response, contrast sensitivity, sensitivity and dynamic range, acquisition speed and detection efficiency. Some of these requirements and characteristics are difficult to combine in one type of photodetector. For example, it is usually difficult to combine high sensitivity and high detection bandwidth [10, 11].

One of the most important requirement is the sensitivity. This parameter is related to the detector response due to a change on X-ray photon intensity. A detector should be sensitive in some specific spectral region and suitable for specific power ranges: the maximum detected power can be limited by damage issues or by a nonlinear response, whereas the minimum power is normally determined by noise. The magnitude of the dynamic range (typically specified as the ratio of maximum and minimum detectable power) is often most important. Relative to the detection efficiency, a high quantum efficiency is required to get a good efficiency conversion of X-ray photons into electrons and recorded signal. This parameter indicates the quantity of phonons that is required to

generate a sufficiently signal response. Contrast is the capacity of distinguish an object compared with the background. It is necessary that the detector can reveal an object size and type (bone or metals, among others), with the maximum details as possible. Another requirement of a detector are a high reliability and low noise for reduced errors. The noise represents the lowest level of detectability due to small intrinsic fluctuations on the electrical signal.

X-ray radiation detectors can be produced by two distinct main approaches identified as direct and indirect method [8]. The direct method is characterized by just one conversion step of the X-ray radiation into electrical signal (see Figure 1.1), when materials are directly exposed to the X-rays [12]. Some examples are pixel arrays of CdZnTe [13] and CdTe [14]. Direct method detectors present important drawbacks, in particular due to the high acquisition time. Indirect-conversion detectors, on the other hand, are characterized by a two-step process for X-ray detection. A scintillator material is the primary material which is in direct contact with the X-ray radiation. The scintillator converts the incident X-ray energy into visible light which will be then converted into an electrical signal, and the light image is recorded by means of different possible readout systems, that include CMOS (Complementary Metal Oxide Semiconductor), CCD (Charge Coupled Device) electronics, and TFT (Thin Film Transistor) (Figure 1.1). Detectors that used indirect conversion are characterized by their high stability and linearity. However, their spatial resolution is limited by the light scattering in the scintillator and the pixel size of the photodetector.

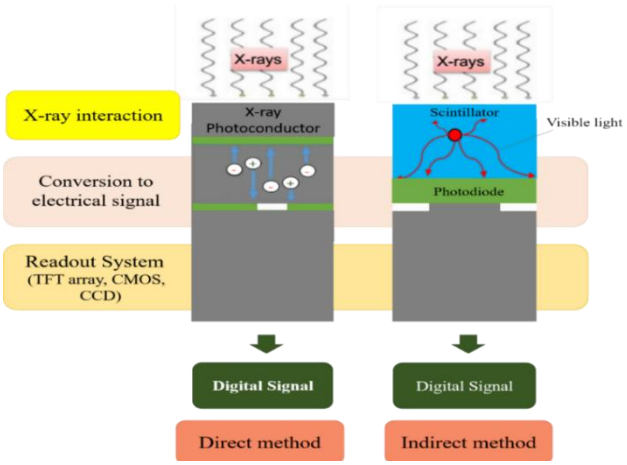

Figure 1.1 - Direct and Indirect conversion of X-ray detectors (adapted from [15]).

The indirect method is thus an interesting method for the development of X-ray detectors due to the conversion efficiency of the scintillators. They do not need bias voltages which will allow the reduction of X-ray radiation doses using a high atomic number and high-density scintillator materials [15]. Further, having also a lower effective cost than current technologies, allows overcoming the size limitation of the existing X-ray imagers.

1.2. Scintillators materials

The scintillator is one of the main components of an indirect X-ray detector and its main function is the conversion of X-rays into visible light: X-ray photons are absorbed in the scintillator and visible light is emitted proportional to the X-ray photon's energy [8, 15].

Among all types of scintillator materials, organic and inorganic scintillators are both used for the development of applications [16]. Inorganic scintillators are the ones with the best radiation yield output and linearity, but they show limitations with respect to the response times. Organic scintillators, on the other hand, show faster responses but lower conversion efficiency. In terms of X-ray detection, the most suitable scintillators are inorganic materials. This type of scintillator is typically composed by crystalline solids, most of them being halogen and alkali metal crystals. Some representative examples are thallium doped cesium iodide (CsI:Tl), thallium doped sodium iodide (NaI:Tl) and cesium iodide doped with sodium (CsI:Na), showing a high efficiency and a scintillation emission wavelength in the visible region, between 400 nm and 600 nm [15].

Scintillator-based architectures have been developed aiming to improve detector responses. Nevertheless, those techniques are appropriate for the fabrication of detector prototypes for small images, but they are not suitable for mass production or for the development of large area applications [17, 18].

In the field of large area panels, amorphous silicon technology coated with scintillators [19] has been developed. The disadvantages of this technology are the dispersion of light in the scintillator and the difficulty of manufacturing electronic readout systems near the photodetectors. In order to overcome the major disadvantages of this type of devices, new scintillator-based radiation detectors have been studied and developed [5].

Some essential properties and characteristics must be taken into account for the practical use of a scintillator [19, 20]:

- ✓ High efficiency, in order to effectively convert the absorbed energy, enabling radiation dose reduction;
- ✓ Linearity between absorbed energy and the number of generated photons;
- ✓ Transparency to the generated visible photons, so that the radiation is transmitted to a readout system;
- ✓ Short decay time of the material, which implies a short emission period allowing a correct and accurate particle counting.

The scintillator spectral zone is another very important property, since the scintillator emission spectrum must coincide with the detection zone of the readout system.

Table 1.1. shows some types of scintillators and their main properties, including density (ρ), atomic number (Z_{eff}), generated light (L_R), emission wavelength (λ) and scintillation decay time (τ).

Table 1.1 - Some representative X-ray scintillators and their main properties [22, 23].

Scintillator Material	ρ (g/cm^3)	Z_{eff}	L_R (phot/MeV)	λ (nm)	τ (ns)	Main Advantage	Main Disadvantage
Halides							
TlCl:I	7.0	74.8	~1000	465		High ρ and Z_{eff}	Low L_R
NaI (77 K)	3.67	50.8	76000	303		High L_R + short τ	Hygroscopic
NaI:Tl	3.67	50.8	43000	415		High L_R + short τ	Hygroscopic + non-linear
CsI:Na	4.51	54	43000	420		High L_R	long τ
CsI:Tl	4.51	54	65900	560		High L_R	long τ
CaI_2	3.96	51.1	86000	410		High L_R	Very hygroscopic
HgI_2	6.38	68.8	6000	580	)^3	High ρ and Z_{eff}	Low L_R
Oxides							
$LuAlO_3:Ce^{3+}$	8.34	64.9	11400	365	17	High initial intensity	Small crystals
$Gd_2SiO3:Ce^{3+}$	6.71	59.4	10000	430	56600	High dose resistance	Fragile
$Lu_2SiO3:Ce^{3+}$	7.4	66.4	27000	420	40	High L_R + short τ	Small crystals
$Lu_3Al_5O_12:Sc$	6.7	62.9	22500	270	610	High L_R	long τ
$CdWO_4$	7.9	64.2	19700	495	(2-15) x 10^3	High ρ and Z_{eff}	long τ
$PbWO_4$	8.28	75.6	~100	~475	~10	High ρ and Z_{eff}	Low L_R
$Bi_3Ge_4O_{12}$	7.13	75.2	8200	505	300	High ρ and Z_{eff}	Low L_R
Chalcogenide							
$Gd_2O_2S:Pr,Ce,F$	7.34	61.1	~40000	511	~3x10^3	High ρ and Z_{eff}	long τ
ZnS:Ag	4.1	27.4	73000	450	10^5	High L_R	Only dust-state
CdS:Te	4.8	48	17000	640	~270-3000	High L_R	Low ρ and Z_{eff}
Glasses							
CsF	4.64	53.2	1900	390	2-4	Short τ	Hygroscopic
BaF_2	4.88	52.7	1430	175	0.8	Short τ	Low λ
CeF_3	6.16	53.1	4500	330	30	High dose resistance	Low L_R

There are many desired properties for scintillators, such as high density, fast operation speed, low cost, radiation hardness, and simple production capability among others. From Table 1.1 it is possible to conclude that the existing scintillator materials despite of being similar to each other in certain characteristics, differ in many parameters and the choice of the best one to use in certain application is the most important aspect to take into account. Additionally, it is possible to observe that some scintillator groups show the highest generated light but also show the lowest decay time, which can be a disadvantage for some applications. Besides that, the oxides scintillator group shows high atomic number and also high density which is an advantage once they can be used in applications where high stopping power or a high conversion efficiency for electrons or photons is required.

The most used scintillator materials, as already referred are organic and inorganics crystals [24]. Organic scintillators show fast-response but also show lower efficiency, while inorganic scintillators show limitation on response time but better radiation output and linearity [16]. To maximize the spatial resolution performance and the applicability of an indirect detector, the scintillator should possess high density (> 5 g/cm^3), high atomic number (> 50) and high yield (> 15 ph/keV) [21]. The selected scintillator material for this work was gadolinium oxide doped with europium (Gd_2O_3:Eu^{3+} - GDO) due to its high yield efficiency of 20.000 ph/MeV, high atomic number, relatively high density (~ 7.4 g/cm^3) and low scintillation decay time (< 2 ns). In addition to these features, the main advantages of this material are that it can be obtained in the form of nanoparticles, which allows its inclusion in different polymer matrices, and its emission wavelength is 611 nm, which is in agreement with the detection wavelength of the photodetectors.

1.3. Radiation detection

There are several radiation detection methods, and each one has its own advantages and disadvantages [22]. Among them, the detection modes with the most interesting response for the present application are pn junctions, based on working principle of thermal effects, photoconductors and scintillators. Each method has its own advantages and disadvantages.

The method based on pn junctions is usually implemented in amorphous silicon substrates and electron-hole pairs are created in the pn junction region due to the absorption of X-ray photons. The main advantage of this method is the low quantity of

energy necessary to produce one electron-hole pair (little more than 1 eV of energy), although the X-ray absorption power of silicon is much reduced.

The working principle of the thermal effect method is based on the Seebeck effect, which consists in detecting the increase in temperature caused by the absorption of X-rays by a material with high atomic number and density. The temperature variation is detecting by two thermoelectric materials with different Seebeck coefficients[23]. In this case, a bias voltage is not necessary since the output signal appears as an electric voltage. However, the frequency response is just of the order of Hz.

The method based on photoconductors uses materials (like amorphous selenium) whose conductivity changes proportional to the amount of absorbed radiation. These detectors show higher radiation absorption than silicon (a 525 µm thick detector would absorb approximately 12.7% of 100 keV X-rays) but need 50 eV to produce an electron-hole pair and a high bias voltage to operate properly (about 10 V/µm) [24].

1.3.1. X-ray detectors based on scintillator materials

As previously indicated, several X-ray detectors use scintillator materials which convert the energy of the absorbed X-ray radiation into visible light. Then, the visible light is detected by a photodetector and converted into electrical signal. For this application, the scintillator material should be constituted by elements of high atomic number and present high density in order to improve radiation absorption [25]. The scintillation mechanism involves two different steps and is determined by the energy band structure of the material [26, 27].

Figure 1.2 shows the schematic representation of the structure of an X-ray image detector based on scintillators.

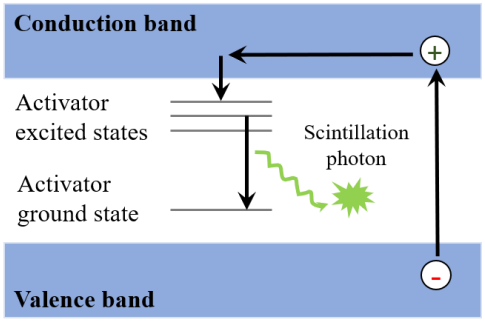

Figure 1.2 - Schematic representation of the main physical process within a scintillator material

When the scintillator absorbs X-ray radiation, the electrons undergo an excitation from the valence band to the conduction band. This process leads to the creation of holes in the valence band. Electrons tend to return to their stable energy state, so they de-excite back to the valence band, producing a high-energy photon. In order to obtain a lower energy photon, it is necessary to modify the forbidden band (band gap).

Thus, small amounts of impurities, known as activators, are added to the inorganic scintillator. This will create energy states within the forbidden band through which the electron can de-excite back to the valence band. This process allows increasing the probability of visible photon emission during de-excitation. Thus, the scintillation process occurs through the de-excitation of the electrons from activator states to the ground state by the emission of photons, the transition occurring in the visible range [17, 27].

Scintillators present high X-ray absorption ability and high frequency responses (usually in the GHz range) without the need of bias voltage [22]. However, restrictions imposed by the height of the scintillator result in limitations in spatial resolution: increasing the height of the scintillator increases the number of X-ray photons absorbed, but the amount of light that reach neighboring pixels is also higher, decreasing spatial resolution [28].

This issue has been solved by using an individual scintillator for each photodetector pixel, separated by layers of a reflection material, as is shown in Figure 1.3 [29].

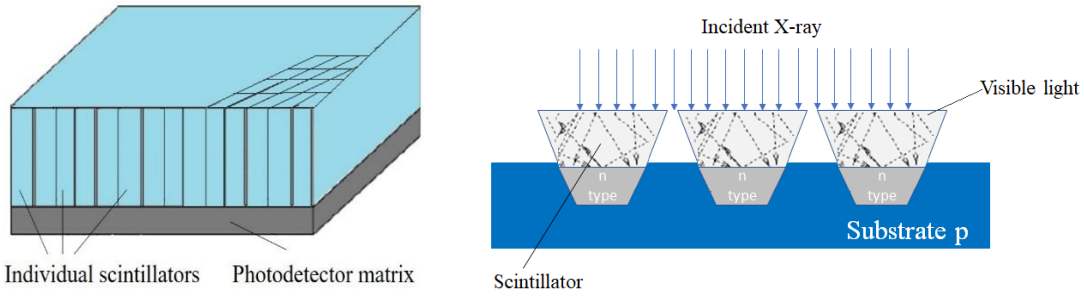

Figure 1.3 - a) Schematic representation of a structure based on an individual scintillator for each photodetector (adapted from [33]); b) Schematic diagram of an X-ray imaging detector based in scintillators (adapted from [30]).

Figure 1.3b shows a schematic of a detector using aluminum as reflective material and a scintillator for each detection pixel. The aluminum layer allows the penetration of

X-rays due to its low atomic number and density while its high reflectivity for visible light guides it to the corresponding photodetector.

During this process, some critical steps that can influence the efficiency and the noise of the signal must be taken in account, such as [22, 30, 31]:

- Transmission of the X-rays through the aluminum reflective layer;
- Absorption of X-rays by the scintillator and their conversion into visible light;
- Transmission of visible light to the photodetector;
- Detection of visible light and its conversion into electrical signals.

The absorption of the X-ray radiation by a material occurs according to the Lambert-Beer law [31]:

$$I = I_0 e^{-\mu x} \qquad (1.1)$$

where I is the intensity of the radiation, I_0 is the initial intensity of the radiation and μ is the coefficient of linear absorption of the material.

Considering this equation, it is observed that higher thickness of the reflective layer leads to lower the radiation transmission. Figure 1.4a shows the relation between the aluminum layer thickness and the transmissivity of the X-ray radiation.

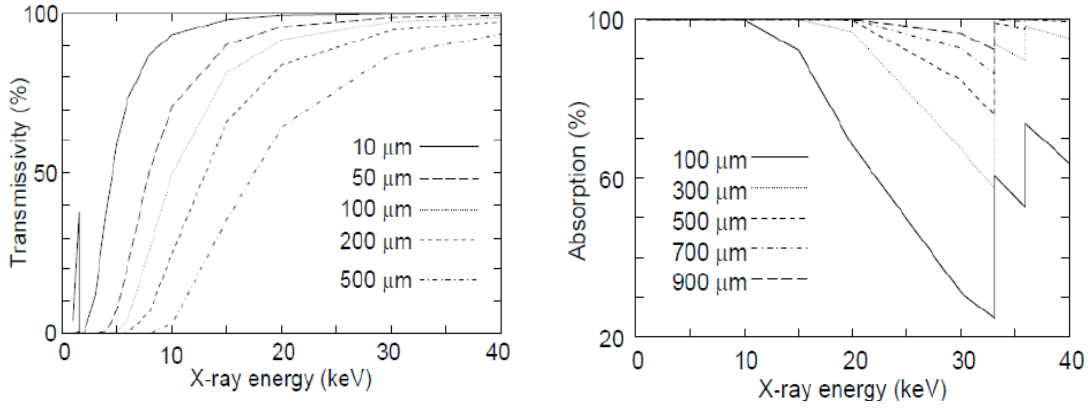

Figure 1.4 - a) Transmissivity to X-rays for different aluminium thickness; b) absorption of X-ray radiation by CsI:Tl scintillator with different thickness [31]

When an X-ray beam penetrates some material, it is absorbed according to equation 1.1. As it can be observed, there is a reduction of the transmissivity with increasing the

thickness of the layer. It is observed that the transmissivity decreases with increasing layer thickness between 10 and 500 µm.

Other important aspect to take into account is the scintillator layer thickness and the absorption ratio. The absorption of X-rays by the scintillator depends also on equation 1.1. However, the mass absorption coefficient must be calculated separately for each element that form the scintillator, using equation 1.2, where α is the fine-structure constant and Z is the atomic number [22].

$$\sigma_{pair} \approx \frac{7}{9} 4\alpha r_e^2 Z^2 \ln\left(\frac{183}{Z^2}\right) \qquad (1.2)$$

Figure 1.4b shows the relation between the CsI:Tl scintillator thickness between 100 and 900 µm and the absorption ratio. As expected, the X-rays absorption increases with increasing thickness.

After the scintillation process, the light will spread as it crosses the scintillator and this diffusion of light will limit the image resolution, the dispersion being proportional to the distance the light has to travel to the detector and, therefore, a thinner scintillator will result in a higher resolution than a thicker one (see Figure 1.5). On the other hand, a thinner scintillator will absorb less X-ray radiation which leads to a higher relative noise level. Thus, the selection of the scintillator thickness is a compromise between high resolution and low noise.

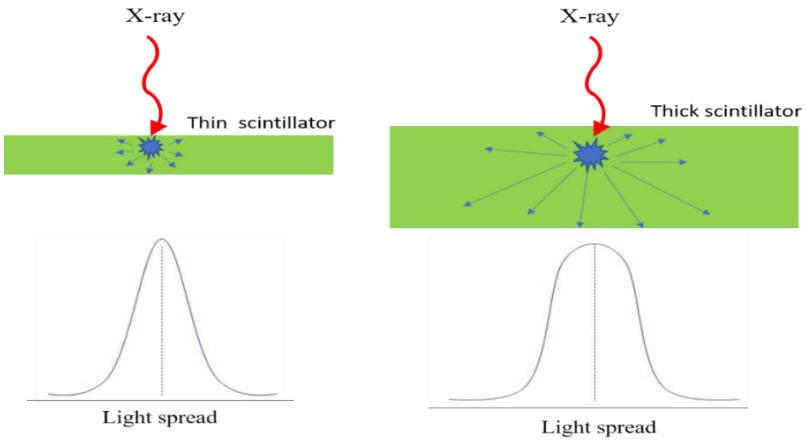

Figure 1.5 - Relation between the scintillator thickness and the light spread.

1.3.2. Polymer composites based on scintillator nanoparticles

Polymer matrix composites are gaining increasing interest as their properties can be adjusted by controlling the composition, content and morphology of the fillers, processing techniques or by modification of the polymer matrix [32]. The type of filler and content within the composite have a significant influence on the physical properties of the material, including active response, thermal, mechanical, electrical and optical properties. Polymeric materials are found in our daily lives in various forms and in the most varied areas [33], showing very advantageous characteristics compared to inorganic materials such as high corrosion resistance, low molecular density and excellent mechanical properties [33]. From an industrial point of view, these materials are widely used today due to their low cost and ease of processing and handling [34]. The choice of the polymer to be used is quite important, since it is the one that provides the mechanical characteristics desired for the chosen application.

Polymer-based scintillators are extensively used in a wide range of areas, from nuclear physics to security or medical applications, due to their effective cost, ease of fabrication and fast response times [35].

The development of polymer-based composites has allowed the emergence of a growing number of new applications, including functional textile fibres, biomedical materials, sensors for radiation detection as well as materials for energy generation and storage, among others.

The incorporation of scintillator nanoparticles into polymer matrix materials allows to tailor optical properties including absorption, fluorescence and luminescence. The development of polymer composites, with the inclusion of scintillator nanoparticles allows new application opportunities [36]. These materials also offer exclusive characteristics such as high flexibility, adequate response time, chemical and mechanical stability, low cost, easy manufacturing in large areas and different geometries, and the possibility of adapting properties through composition modification [35, 37].

Polymer composites with the inclusion of scintillating nanoparticles have been developed for X-ray radiation detectors [38] but show low light emission resulting from quenching of the fluorescence and their low transparency [39]. In order to achieve good energy conversion efficiency, new studies have dictated the need to use materials with higher atomic numbers [38, 40]. A proposed solution for the substitution of conventional

matrices is the use of polymers conjugated with inorganic scintillators with high atomic number. The nanoparticles not only increase the effective density of the composite but also increase the effective atomic number, thus increasing scintillation efficiency. However, the use of this type of composites for detection of X-ray radiation remains little explored [41-44], being this area at continuously investigated for improving their potential applications. The intensive research for innovative solutions to overcome limitations and improve the materials application is linked with obtaining shorter scintillation decay period, wider thermal stability, higher flexibility and lower production cost [45-47]. Polymer composites with scintillator particles come up as a solution and option to be used in radiation detection [40, 47].

1.4. Photodetection technologies

Since X-ray imaging is used in medical diagnostics and security, the interest in a flat panel active matrix for digital X-ray imaging is a reality. These imagers are becoming available in large sizes (larger than 25 x 25 cm) with pixel sizes as small as 100 x 100 micrometres. The smaller panels are fabricated in crystalline silicon and the larger ones in amorphous silicon, but due to the relatively poor absorption of X-rays by silicon, it is required an additional X-ray detection layer on top of the active matrix panel. In the field of large area panels, most devices are fabricated in amorphous silicon coated with scintillators [48].

Regarding the visible light imaging devices that work together with scintillators, the market is dominated by the charge coupled device (CCD) technology [7, 49] and the active pixel complementary metal oxide semiconductor (CMOS) technology [50, 51] that is also explored.

CCD sensors consist in an array or matrix of pixels (or light sensitive cells) capable of generating electrical charge proportional to the light intensity. A CCD pixel is formed from a biased p-n junction, and the incident light generates an electron-hole pairs in the depletion region [47]. CMOS detectors are formed by a matrix capable of generating electrical charges proportional to the incident light. However, the acquisition process of light is different from the first one, since each CMOS pixel employs a photodiode, a capacitor and a transistor. The main difference between CCD and CMOS system architectures is the integration of the readout system. Figure 1.6 shows that CMOS

technology, contrarily to CCD, allows the integration of the pixel array and the corresponding complementary electronics readout system.

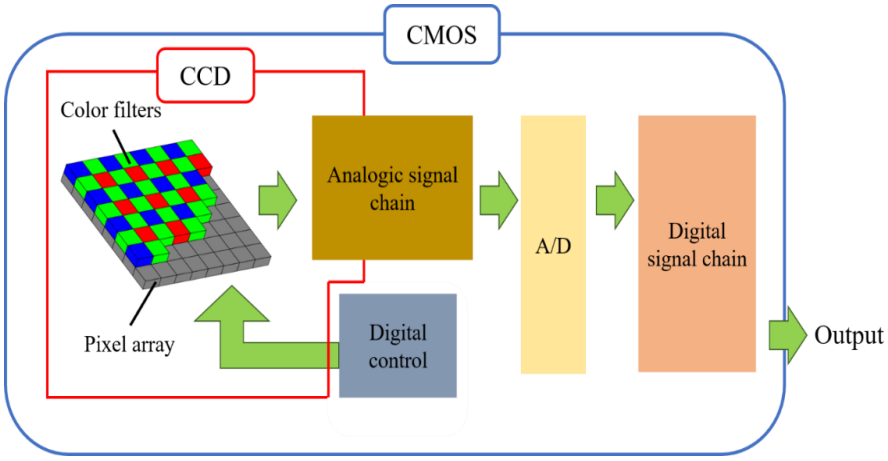

Figure 1.6 - CCD and CMOS system architectures (adapted from [52]).

The integration of all electronic readout components allows CMOS to show advantages relative to CCD such as being more compact, lower power consumption and one single supply high integration capability, lower production effective cost and the possibility to be developed on flexible modules [53, 54]. The first method used on this work was based on CMOS technology due to the referred advantages.

Recent advances in the area of microfabrication allows the onset of a new approach of development of large area X-ray detectors, using the technology of thin-film transistor (TFT). Thus, photodetectors and electronics are implemented by organic photodiodes and TFTs, respectively, built in a flexible organic substrate [55-57]. Organic thin film transistors (OFTFs) have a great potential due to its low-cost and the possibility of being flexible relative to amorphous silicon thin film transistors for electronic applications. During the last decade, the industry related to printed electronics is experiencing significant growth. Printed electronics refers to a set of printing methods, such as screen printing, flexography, spray printing, inkjet printing, etc., used to create electronic devices on various substrates. Printed photodetectors can achieve and overcome some limitations that the actual photodetectors based on silicon have. A well-known limitation of these devices based on silicon technology is the lower absorption coefficient, the high temperature, complex and expensive fabrication process. Besides that, silicon technology is not appropriate for the development of flexible and large areas devices.

In order to develop and design a sustainable, flexible and a large detection system, the final prototype of the present work is based on polymer-based printed photodetectors using the TFT technology.

1.5. Printed technologies

It is essential to explore and promote the development and application of more sustainable engineering principles, regarding to the production, applications and development of innovative materials to achieve novel and better devices and to add value to photodetectors. For that, the main steps are to reach better performance on photodetector material characteristics and properties, such as, wavelength range response, flexibility, large area application and higher integrability, among others, to address new developments and applications. Besides that, the achievement of large area application and flexibility is limited by the actual silicon technologies. However, printed radiation detectors can achieve and overcome these limitations and also allow device fabrication on a large variety of substrates, rigid and flat as well as flexible and curved, opening the way for the development of non-fragile, conformable electronics [58].

Printing technologies are in a significant growth and present many advantages when compared to traditional lithographic methods, including low effective cost, low material wastage, processing flexibility and the possibility to print into large areas [59]. The increasing interest of printing technologies is mainly relative to the achievement of a wide range of new functionalities which will allow new applications, and/or the improvement of applications already present in our daily life.

The choice of the printing technology is determined by the characteristics of the printed layers, by the properties of printed materials as well as the effective cost of the final device.

The aim of this work is to design an X-ray detector that can overcome conventional limitations that radiography face, such as large and/or flexible detection areas.

The formulation of materials on solution, such as inks, allows the fabrication of these devices by printing technologies. The transformation of nanocomposites into polymer-based inks enables printable electronic components to be obtained. Printing on all types of substrates makes these materials promising and attractive to the industry due to their production in large areas, high production speed, high resolution and the possibility of miniaturizing devices [60].

The two most popular approaches for the development of coating/printing systems are non-contact and contact printing. Figure 1.7 schematically represent the printing technologies classification diagram.

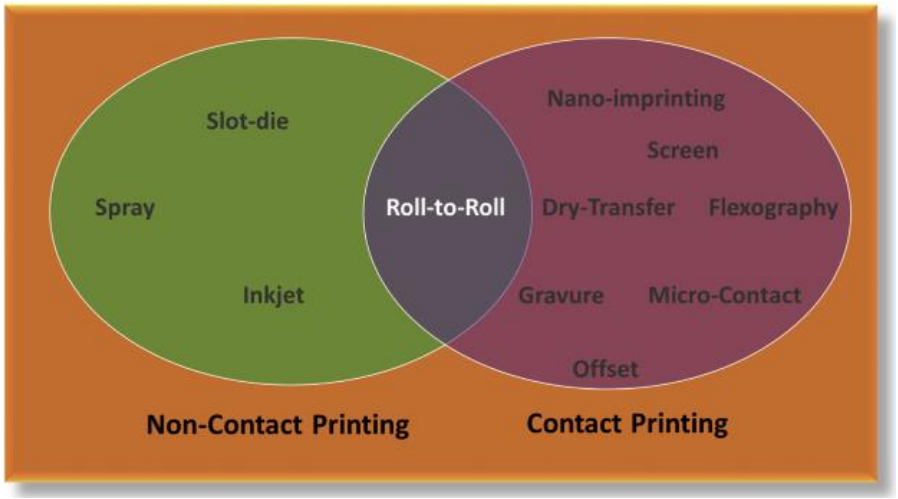

Figure 1.7 - Schematic representation of printing technologies classification [61].

The process involved in contact printing is characterized by the patterned structures with printed surfaces that are in contact with the substrate. In contrast, when a non-contact process is used, the ink is printed through nozzles or holes and the assemblies are developed by moving the substrate holder (or stage) in a pre-designed pattern [62]. Printing technologies by the contact process include screen, gravure printing, dry-transfer, flexography, micro-contact and offset printing. All of them present some drawbacks [62], namely pattern resolution and higher cost production. Due to the limitations of contact printing technique, non-contact printing (inkjet and spray printing) has emerged as a suitable approach to produce printed devices.

The most used printing technologies are inkjet, screen and spray printing. They require different and optimized characteristics such as viscosity, surface tension, conductivity, maximum particle diameter, type of substrate and optimum temperature (see Table 1.2)

Table 1.2 - Printing techniques characteristics and ink/substrate requirements for each printing techniquePrinting techniques characteristics and ink/substrate requirements for each printing technique [61].

Printing Technology	Characteristics	Ink's limitations	Substrate limitations
Inkjet	✓ Allows a large variety of patters; ✓ Simple process, widely used in the industry; ✓ Ideal for small and medium production volumes; ✓ Low time to market; ✓ Typical resolution of 0.01 [mm]	✓ Viscosity: 8-20 cPs ✓ Surface Tension ✓ 25-36mN/m ✓ Max. particle diameter 0.2µm ✓ Flash point: >45ºC	✓From very small to large size areas; ✓Flat substrate with small roughness.
Screen	✓ Needs a different frame for each different pattern; ✓ Simple process, widely used in the industry; ✓ Ideal for small, medium and high production volumes; ✓ Low time to market; ✓ Typical resolution of 0.2 [mm] ✓ Low-cost equipment.	✓ Viscosity: 1k-40k cPs ✓ Surface Tension: 25-36mN/m ✓ Max particle diameter depends on the mesh	✓ From small to medium size areas; ✓ Flat and curved substrates with small roughness.
Spray	✓ Low resolution patterns ✓ Simple process, ✓ Low time to market; ✓ Low-cost equipment. ✓ Very low resolution typically up to 1 [mm]	✓ Viscosity: 1-1000cPs ✓ Max particle diameter 10µm; ✓ Flash point: >45 ºC.	✓ From small to very large size areas; ✓ Any substrate; ✓ Any roughness.

From Table 1.2 it is possible to conclude that the existing printing technologies despite to intercept each other in certain characteristics, differ in many key issues, such as simplicity and resolution in the equipment setup, scalability and the choice of materials features that are more suitable for printing, among others [63].

Proper printable materials are essential to produce smart products with the required characteristics. A high variety of factors can influence the material selection for printable applications. Thus, inks are at the basis of printed technologies and need to be tailored printable materials are a key element for a specific printing technology in terms of surface

tension and viscosity. Further, the substrate is another key element that affects the application of printing systems and the production of printable materials [64].

1.6. Objectives

The main objective of this work is the development a novel polymer-based scintillator composites for a new generation of indirect X-ray imaging detector. Further, another objective is the applicability of the developed materials by printing technologies, in order to facilitate implementation into devices. Together with the new materials, the main innovation of this thesis will be the demonstration of fully printed X-ray detectors, based on the implementation of the developed materials on printed photodetectors.

1.7. Methodology and thesis structure

This thesis is divided in seven chapters, five of them based on published research papers. In this way, a comprehensive and logic report is provided on the progress achieved during the present research as well as on the research methodology, as the chapters represent the sequential progress obtained during this work, involving the development of the general strategy for the implementation of scintillator polymer based composites (chapter 2), novel scintillator polymer composites (chapter 3), stretchable scintillator composites (chapter 4), water processable scintillator inks (chapter 5) and the development of all-printed X-ray detectors (chapter 6). Thus, the present thesis is divided in the following chapters:

Chapter 1 presents a general introduction to the work, the motivation and the objectives, as well as the methodology and structure of the thesis. In particular, a brief state of the art on the subject of the work is presented, focusing on the different types of X-ray detectors, scintillator materials and photodetection techniques. It is to notice that the specific state of the art is placed in each of the different chapters.

Chapter 2 is based on the published research work "Increasing X-ray to visible transduction performance of $Gd_2O_3:Eu^{3+}$/P(VDF) composites by 2,5 dipheniloxazol (PPO) and (1,4-bis (2-(5-phenioxazolil))-benzol (POPOP) addition". A polymer-based scintillator composite is produced and optimized by combining poly (vinylidene fluoride (P(VDF)) and GDO scintillator nanoparticles. The visible light yield under X-ray

irradiation is further improved by the introduction of two different fluorescence molecules, PPO and POPOP.

Chapter 3 is based on the published scientific paper "Gd_2O_3:Eu^{3+}/PPO/POPOP/PS composites for digital imaging radiation detector". A polymer-based scintillator composite based on polystyrene, a polymer with scintillator properties, is presented, optimized and fully characterized.

Chapter 4 is based on the published work "Stretchable scintillator composites for indirect X-ray detectors". A scintillator composite based on the thermoplastic elastomer Styrene-Ethylene/Butadiene-Styrene (SEBS) is developed for applications in polymer-based flexible and stretchable indirect X-ray detectors. The scintillator films exhibit suitable X-ray into visible radiation conversion performance for deformation up to 100%. It shows also low mechanical hysteresis.

Chapter 5 is based on the work "Environmentally-friendly scintillator ink for printed radiation detectors". A scintillator ink based on thermoplastic elastomeric polyvinyl alcohol (PVA) together with scintillator nanoparticles and fluorescence molecules is developed and fully characterized. The new water processable ink is implemented by spray-printing in the development of X-ray detectors, which performance is presented.

Chapter 6 is based on the work "Indirect X-ray detectors based on inkjet-printed photodetectors with a screen-printed scintillator layer". This chapter is dedicated to the all-printed X-ray photodetector prototype. An inkjet-printed photodetector array was fabricated, based on an organic thin-film transistor (OTFT) architecture, and applied for the indirect detection of X-ray radiation using a scintillator ink as X-ray absorber, also applied by printing technologies. The fabrication and characterization of both photodetector and X-ray detector are presented and discussed.

Finally, **Chapter 7** presents the main conclusions of the thesis, as well some suggestions for future work.

1.8. References

1. Schroeter, K., *Printed sensors: Enabling new applications.* Sensor Review, 2008. 28(1): p. 6-11.

2. Bogue, R., *Smart materials: A review of capabilities and applications.* Assembly Automation, 2014. 34(1): p. 16-22.

3. Murphy, E.B. and F. Wudl, *The world of smart healable materials.* Progress in Polymer Science, 2010. 35(1–2): p. 223-251.

4. Selman, J., *The Fundamentals of X-ray and Radium Physics*. 1954: Thomas.

5. Rocha, J.G., G. Minas, and S. Lanceros-Mendez, *Pixel readout circuit for X-ray imagers.* IEEE Sensors Journal, 2010. 10(11): p. 1740-1745.

6. Körner, M., et al., *Advances in digital radiography: Physical principles and system overview*. Radiographics, 2007. 27(3): p. 675-686.

7. Han, Y., et al., *Development of an advanced X-ray detector for inspecting inner microscopic structural details in industrial applications.* Nuclear Instruments and Methods in Physics Research, Section A: Accelerators, Spectrometers, Detectors and Associated Equipment, 2009. 600(2): p. 440-444.

8. Rocha, J.G., et al., *X-ray image detector based on light guides and scintillators.* IEEE Sensors Journal, 2009. 9(9): p. 1154-1159.

9. Smathers, R.L. and W.R. Brody, *Review article. Digital radiography: Current and future trends.* British Journal of Radiology, 1985. 58(688): p. 285-307.

10. Nalwa, H.S., *Photodetectors and fiber optics*. 2012: Elsevier.

11. Donati, S., *Photodetectors*. Vol. 1. 1999: Prentice Hall PTR.

12. Rocha, J.G., L.M. Goncalves, and S. Lanceros-Mendez. *Flexible x-ray detector based on the seebeck effect*. in *TRANSDUCERS 2009 - 15th International Conference on Solid-State Sensors, Actuators and Microsystems*. 2009.

13. Barber, H.B., et al., *Progress in developing focal-plane-multiplexer readout for large CdZnTe arrays for nuclear medicine applications.* Nuclear Instruments and Methods in Physics Research, Section A: Accelerators, Spectrometers, Detectors and Associated Equipment, 1996. 380(1-2): p. 262-265.

14. Chambron, J., et al., *Pixellated γ-camera based on CdTe detectors clinical interests and performances.* Nuclear Instruments and Methods in Physics Research, Section A: Accelerators, Spectrometers, Detectors and Associated Equipment, 2000. 448(3): p. 537-549.

15. Rocha, J.G. and S. Lanceros-Mendez, *Review on X-ray detectors based on scintillators and CMOS technology*. Recent Patents on Electrical Engineering, 2011. 4(1): p. 16-41.

16. Van Eijk, C.W.E., *Inorganic scintillators in medical imaging detectors.* Nuclear Instruments and Methods in Physics Research, Section A: Accelerators, Spectrometers, Detectors and Associated Equipment, 2003. 509(1-3): p. 17-25.

17. Knoll, G.F., *Radiation Detection and Measurement*. 3rd edition ed. 1999: John Wiley & Sons.

18. Blasse, G., *Scintillator materials.* Chemistry of Materials, 1994. 6(9): p. 1465-1475.

19. Rodnyi, P.A., *Physical Processes in Inorganic Scintillators*, in *Physical Processes in Inorganic Scintillators*, C. Press, Editor. 1997: Russia.

20. Ronda, C.R., *Luminescence: From Theory to Applications*. 2007: Wiley.

21. Martin, T., et al., *LSO-based single crystal film scintillator for synchrotron-based hard X-ray micro-imaging.* IEEE Transactions on Nuclear Science, 2009. 56(3): p. 1412-1418.

22. Rocha, J.G. and S. Lanceros-Méndez, *Review on X-ray detectors based on scintillators and CMOS technology.* 2011.

23. Rocha, J.G., L.M. Goncalves, and S. Lanceros-Mendez. *Flexible x-ray detector based on the seebeck effect*. in *2007 IEEE International Symposium on Industrial Electronics*. 2007. IEEE.

24. Sakellaris, T., et al., *Monte Carlo simulation of primary electron production inside an a-selenium detector for x-ray mammography: physics.* Phys Med Biol, 2005. 50(16): p. 3717-38.

25. Martins, P.M., et al., *Gd2O3: Eu nanoparticle-based poly (vinylidene fluoride) composites for indirect X-ray detection.* Journal of Electronic Materials, 2015. 44(1): p. 129-135.

26. Rodnyi, P.A., *Physical Processes in Inorganic Scintillators*. 1997: Taylor & Francis.

27. Nikl, M., *Scintillation detectors for x-rays.* Measurement Science and Technology, 2006. 17(4): p. R37-R54.

28. Rocha, J.G. and S. Lanceros-Mendez, *X-ray imaging matrix with light guides and intelligent pixel sensors, radiation or high energy particle detector devices that contain it, its fabrication process and its use*. 2008, Google Patents.

29. Kleimann, P., et al. *An X-ray imaging pixel detector based on a scintillating guides screen*. in *Nuclear Science Symposium, 1999. Conference Record. 1999 IEEE*. 1999. IEEE.

30. Rocha, J.G., et al., *X-Ray image detector based on light guides and scintillators.* 2009.

31. Rocha, J.G. and S. Lanceros-Mendez, *3-D modeling of scintillator-based X-ray detectors.* IEEE Sensors Journal, 2006. 6(5): p. 1236-1242.

32. Camargo, P.H.C., K.G. Satyanarayana, and F. Wypych, *Nanocomposites: Synthesis, structure, properties and new application opportunities.* Materials Research, 2009. 12(1): p. 1-39.

33. Botelho, G., Apontamentos da Unidade Curricular: Química, Tecnologia e novos materiais, Universidade do Minho, 2011/2012.

34. Obitayo, W. and T. Liu, *A review: Carbon nanotube-based piezoresistive strain sensors.* Journal of Sensors, 2012. 2012.

35. Quaranta, A., et al., *Optical and scintillation properties of polydimethyl-diphenylsiloxane based organic scintillators.* IEEE Transactions on Nuclear Science, 2010. 57(2 PART 2): p. 891-900.

36. Martins, P.M., et al., *Gd2O3:Eu Nanoparticle-Based Poly(vinylidene fluoride) Composites for Indirect X-ray Detection.* Journal of Electronic Materials, 2014. 44(1): p. 129-135.

37. Righetti, M.C., et al., *Thermal and mechanical properties of PES/PTFE composites and nanocomposites.* Journal of Applied Polymer Science, 2013. 130(5): p. 3624-3633.

38. Cai, W., et al., *Synthesis of bulk-size transparent gadolinium oxide-polymer nanocomposites for gamma ray spectroscopy.* Journal of Materials Chemistry C, 2013. 1(10): p. 1970-1976.

39. Zhong, H., et al., *Photoluminescence quenching of conjugated polymer nanocomposites for gamma ray detection.* Nanotechnology, 2008. 19(50).

40. Zhao, Y.S., H. Zhong, and Q. Pei, *Fluorescence resonance energy transfer in conjugated polymer composites for radiation detection.* Physical Chemistry Chemical Physics, 2008. 10(14): p. 1848-1851.

41. Gibson, R.F., *A review of recent research on mechanics of multifunctional composite materials and structures.* Composite Structures, 2010. 92(12): p. 2793-2810.

42. Murali, M.G., et al., *Thiophene-based donor-acceptor conjugated polymer as potential optoelectronic and photonic material.* Journal of Chemical Sciences, 2013. 125(2): p. 247-257.

43. Sen, S., et al., *Organic-Inorganic Composite Films Based on Gd3Ga3Al2O12:Ce Scintillator Nanoparticles for X-ray Imaging Applications.* ACS Applied Materials and Interfaces, 2017. 9(42): p. 37310-37320.

44. Novais, S.M.V., et al., *Hydrothermal synthesis of CdWO4 for scintillator-polymer composite films development.* Journal of Luminescence, 2018. 199: p. 225-231.

45. Rocha, J.G., L.M. Goncalves, and S. Lanceros-Mendez, *Bi2Te3-Sb2Te3 on polymeric substrate for X-ray detectors based on the seebeck effect.* Microsystem Technologies, 2012. 18(1): p. 1-8.

46. Milbrath, B.D., et al., *Radiation detector materials: An overview.* Journal of Materials Research, 2008. 23(10): p. 2561-2581.

47. Cai, W., et al., *Synthesis of bulk-size transparent gadolinium oxide–polymer nanocomposites for gamma ray spectroscopy.* Journal of Materials Chemistry C, 2013. 1(10): p. 1970-1976.

48. Lai, J., A. Nathan, and J. Rowlands, *High dynamic range active pixel sensor arrays for digital x-ray imaging using a-Si:H.* Journal of Vacuum Science and Technology A: Vacuum, Surfaces and Films, 2006. 24(3): p. 850-853.

49. Peng, J.L., et al. *Space solar EUV and X ray imaging camera*. in *Proceedings of SPIE - The International Society for Optical Engineering*. 2008.

50. Arvanitis, C.D., et al., *Signal and noise transfer properties of CMOS based active pixel flat panel imager coupled to structured CsI:Tl.* Medical Physics, 2009. 36(1): p. 116-126.

51. Taghibakhsh, F., et al., *X-ray detection using a two-transistor active pixel sensor array coupled to an a-Se X-ray photoconductor.* IEEE Sensors Journal, 2009. 9(1): p. 51-56.

52. Litwiller, D., *CMOS vs. CCD: Maturing Technologies, Maturing Markets-The factors determining which type of imager delivers better cost performance are becoming more refined.* Photonics Spectra, 2005. 39(8): p. 54-61.

53. Bigas, M., et al., *Review of CMOS image sensors.* Microelectronics Journal, 2006. 37(5): p. 433-451.

54. Vinayagam, P. and P. Anandan, *A review on pixel performance in CMOS image sensors.* Journal of Advanced Research in Dynamical and Control Systems, 2017. 2017 (Special Issue 5): p. 20-25.

55. Gwoziecki, R., et al. *Organic electronics application overview from automotive HMI to X-ray detectors*. in *2016 6th Electronic System-Integration Technology Conference, ESTC 2016*.

56. Gelinck, G.H., et al., *X-ray imager using solution processed organic transistor arrays and bulk heterojunction photodiodes on thin, flexible plastic substrate.* Organic Electronics: physics, materials, applications, 2013. 14(10): p. 2602-2609.

57. Basiricò, L., et al., *Direct X-ray photoconversion in flexible organic thin film devices operated below 1v.* Nature Communications, 2016. 7.

58. Pace, G., et al., *Printed photodetectors.* Semiconductor Science and Technology, 2015. 30(10): p. 104006.

59. Azzellino, G., et al., *Fully inkjet-printed organic photodetectors with high quantum yield.* Advanced Materials, 2013. 25(47): p. 6829-6833.

60. Andò, B. and S. Baglio, *Inkjet-printed sensors: A useful approach for low cost, rapid prototyping [instrumentation notes]*. IEEE Instrumentation and Measurement Magazine, 2011. 14(5): p. 36-40.

61. Oliveira, J., et al., *Polymer-based smart materials by printing technologies: Improving application and integration.* Additive Manufacturing, 2018. 21: p. 269-283.

62. Khan, S., L. Lorenzelli, and R.S. Dahiya, *Technologies for printing sensors and electronics over large flexible substrates: A review.* IEEE Sensors Journal, 2015. 15(6): p. 3164-3185.

63. Ru, C., et al., *A review of non-contact micro- and nano-printing technologies.* Journal of Micromechanics and Microengineering, 2014. 24(5).

64. Hoffman, J., et al., *The standardization of printable materials and direct writing systems.* Journal of Electronic Packaging, Transactions of the ASME, 2013. 135(1).

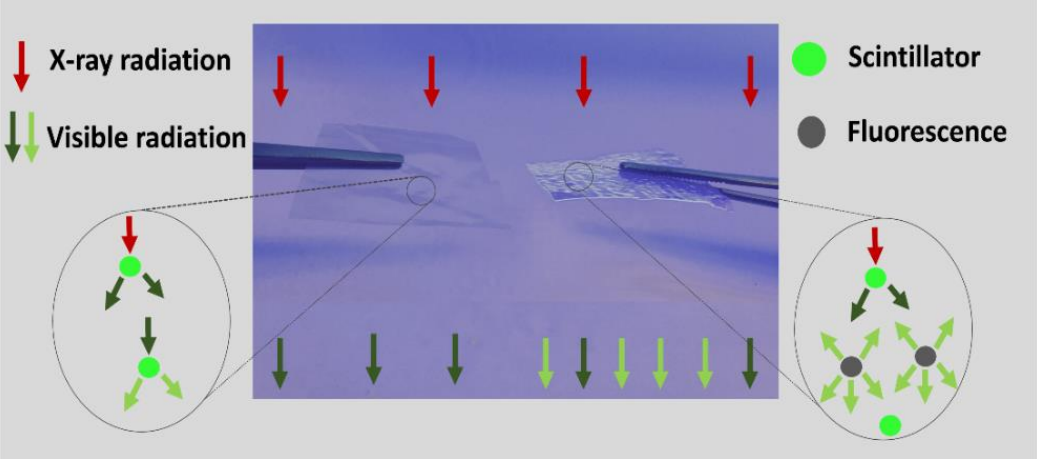

Chapter 2. Increasing X-ray to visible transduction performance of $Gd_2O_3:Eu^{3+}$/ P(VDF) composites by PPO/POPOP addition

Polymer based scintillator composites have been produced by combining poly(vinylidene fluoride (P(VDF)) and gadolinium oxide doped with europium ($Gd_2O_3:Eu^{3+}$ - GDO) scintillator nanoparticles. Additionally, 2,5 diphenyloxazol and (1,4-bis (2-(5-phenioxazolil))-benzol were introduced in the polymer matrix in order to improve visible light yield under X-ray irradiation.

This chapter is based on the following publication: J. Oliveira, P.M. Martins; P. Martins, V. Correia, J.G. Rocha, S. Lanceros-Méndez, *Increasing X-ray to visible transduction performance of $Gd_2O_3:Eu^{3+}$/ P(VDF) composites by PPO/POPOP addition*; Composites Part B: Engineering 91, 610-614, 2016.

2.1. Introduction

The onset of polymer nanocomposites was an important step for the development of novel application oriented materials [1]. Such composites have been extensively studied for an increasing number of applications including catalysts, functional textiles, biomedical materials, sensors, actuators and materials for energy conversion and storage, among others [2, 3]. It has been shown that, in such composites, both physical and chemical properties can be enhanced and/or tailored by the presence of suitable amounts of micro or nanofillers [4]. Thus, mechanical, electrical, optical and thermal properties have been improved with respect to the single polymer or co-polymer matrix [1].

Nanocomposites can be also used to develop polymer-based materials able to convert X-ray radiation into visible light, with appropriate mechanical properties, thermal, chemical and radiation stability, as well as with high energy resolution [5]. The conversion of X-ray radiation into visible light is based in the scintillation process: the interaction of the X-rays with electrons within the scintillators nanoparticles leads to their promotion to the conduction band across the forbidden gap. Then, the electrons migrate to the activation center excited-state orbitals and the holes in the valence band to the activation center ground-state orbitals [6]. Finally, the transition of electrons from an activated center excited-state orbital to an activation center ground-state orbital produces a scintillation photon. Polymer-based scintillators offer unique important properties such as mechanical flexibility and relatively high scintillation efficiency [1]. Additionally, such polymeric scintillators allow suitable response time, air-stability, low cost, easy fabrication in large areas in a wide range of geometries and tailored property possibilities through composition modification [7, 8]. Polymer composites have been used for the development of X-ray detectors for several applications [9]. Among the best ones, $Gd_2O_3:Eu^{3+}$/poly(vinylidene fluoride) composites were found to be able to convert X-ray radiation into visible light [4]. In this system, poly(vinylidene fluoride) (P(VDF)) was used as a binder since it is a flexible and stable matrix and due to its low surface tension and high thermal and light degradation resistance [4, 10]. Gadolinium oxide doped with europium ($Gd_2O_3:Eu^{3+}$ - GDO) nanoparticles were selected as scintillators due to their wide band gap (~5.2 eV), atomic number, high density (~7.4 $g.cm^{-3}$), suitable light yield (~2×104 photons. MeV^{-1}) and radioluminescence.

Nevertheless, in order to meet industry requirements, the light yield in such innovative polymeric composites needs to be improved, without sacrificing the

homogeneity and transparency of the scintillators [11-14]. Such improvement will allow X-ray dose reduction, decreasing signal to noise ratio, increasing sensitivity and optimizing the detection efficiency [11, 12].

In this way, aiming to fulfil the present needs in the field of X-ray detection, this work focus on the improvement of the light yield in the overall X-ray to electrical conversion process by the inclusion of fluorescence PPO and POPOP on the scintillator composites. Such light yield improvement allied with the good mechanical properties, thermal, chemical and radiation stability, large areas potentiality, homogeneity and transparency found on the GDO/P(VDF) composites will allow the use of GDO/PPO/POPOP/P(VDF) scintillator composites on novel X-ray detectors [5, 11, 15, 16].

2.2. Experimental Section

2.2.1. Materials

P(VDF) was purchased from Solvay (Belgium), N, N-dimethylformamide (DMF) from Merck (analytical grade), GDO nanoparticles were obtained from Nanograde and the fluorescence molecules, PPO and POPOP were obtained from Sigma-Aldrich. All chemicals were used as provided by the suppliers.

2.2.2. Samples Preparation

Composite films of GDO/P(VDF), with and without PPO/POPOP, with a thickness of ~50 μm were prepared by solvent casting and melt processing. First, based on [1], the desired content of GDO (0.25 and 0.5 wt.%) nanoparticles was added to dymethylformamide (DMF) and placed in an ultrasound bath. Then, P(VDF) was added to the mixture and placed in a Teflon™ mechanical stirrer until complete dissolution of the polymer. After the fluorescence material, 1wt.% of PPO and 0.01wt.% of POPOP, was added the solution, it was spread in a clean glass substrate and placed in an oven at 210 °C for 10 min before cooling down to room temperature. Such fluorescence content has been previously optimized in order to maximize light yield [17-19]. Additionally, the selected weight ratio allows to achieve high phenyl concentration in the matrix, hereby

increasing the number of excimer states which transfer the network excitation energy and avoids the rise to optical inhomogeneity and opacity [14].

2.2.3. Samples characterization

The phase of P(VDF) was determined by Fourier transformed infrared (FTIR) spectra collected in a Perkin-Elmer Spectrum 100 over a range of 650–4000 cm^{-1}.

The optical transmittance was obtained by a double beam spectrophotometer UV-2501PC Ultraviolet-Visible (UV-VIS) set up in the 200 to 800 nm range with a 1nm step. ε' and ε'', real and imaginary parts of the dielectric function, were obtained [20, 21] through the measurement of the capacity and tan δ (dielectric loss) with an automatic Quadtech 1929 Precision LCR meter. The samples were previously coated with circular Au electrodes with 5 mm diameter onto both sides of the sample in order to obtain a parallel capacitor geometry.

Characteristic I–V curves were measured at room temperature with a Keithley 6487 picoammeter/voltage source in a voltage range from −75 to 75 V. The DC conductivity of the samples was obtained from the slope of the I-V curves and the geometrical characteristics of the samples. The efficiency of the X-ray radiation into visible light conversion was measured with the help of a Bruker D8 Discover diffractometer using Cu Kα incident radiation at 40 kV applied voltage and current varying from 10-40 mA. The output visible light from the samples at the corresponding wavelength was detected by a TSL2560 photodiode from Texas Ad. Optoelectronic Solutions Inc.

2.3. Results and Discussion

Figure 2.1a shows the FTIR spectra of neat P(VDF) and GDO/P(VDF) composites, with and without PPO/POPOP, in order to evaluate the influence of the filler on the polymer phase. Further, optical transmittance as a function of wavelength for the polymer and composite films is shown in figure 2.1b. The following nomenclature will be adopted in the text: P(VDF)/0.25S-FL means a P(VDF) sample with 0.25 wt.% of scintillator nanoparticles (S) in the present of fluorescent molecules (FL).

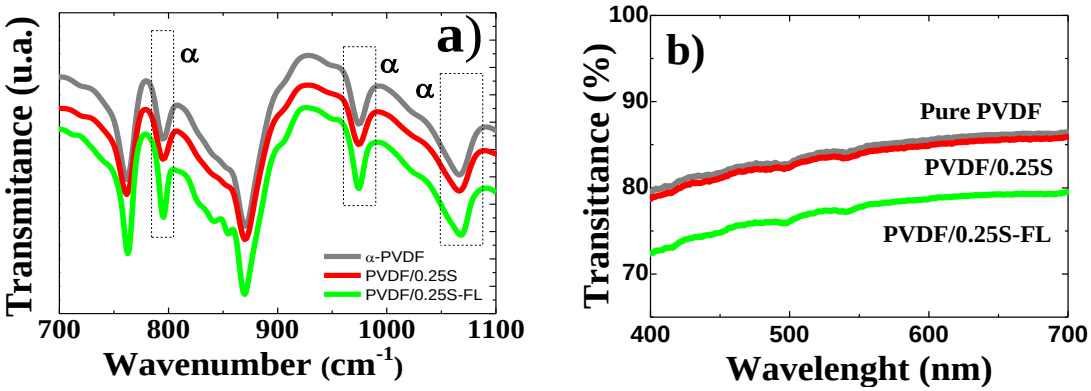

Figure 2.1- a) Infrared transmittance vs. wavenumber for the GDO/P(VDF), GDO/PPO/POPOP/P(VDF) composites and for P(VDF); b) Optical transmittance of the films in the visible range as a function of wavelength.

The introduction of GDO nanoparticles and fluorescence molecules into the P(VDF) matrix has no influence in the polymer phase content. The polymer crystallized in the α-phase, as demonstrated by the presence of the 766, 795 and 976 cm^{-1} characteristic bands and absence of the bands related to the polar β- and γ-phases [1, 22]. This fact is related with the sample preparation conditions [1], melting and recrystallizations, but also indicates that there is no nucleation of the polar phases due to strong electrostatic surface interaction between fillers and the monomer dipolar moments, as it has been previously observed for other nanocomposites systems [23-25].

Figure 2.1b shows just a small decrease of ~8% in the optical transmittance of the samples with the introduction of fluorescence molecules, when compared to α-P(VDF) and to the composite without fluorescence molecules. This fact is related to the higher nanoparticle and fluorescence molecules content of the samples, leading to a more heterogeneous and defective microstructures, which causes dispersion of the light and leads to lower visible light transmittance [22].

Since the energy resolution of the systems can be improved by increasing the dielectric permittivity of the scintillator material [26, 27], dielectric properties of the composite have been determined (Figure 2.2).

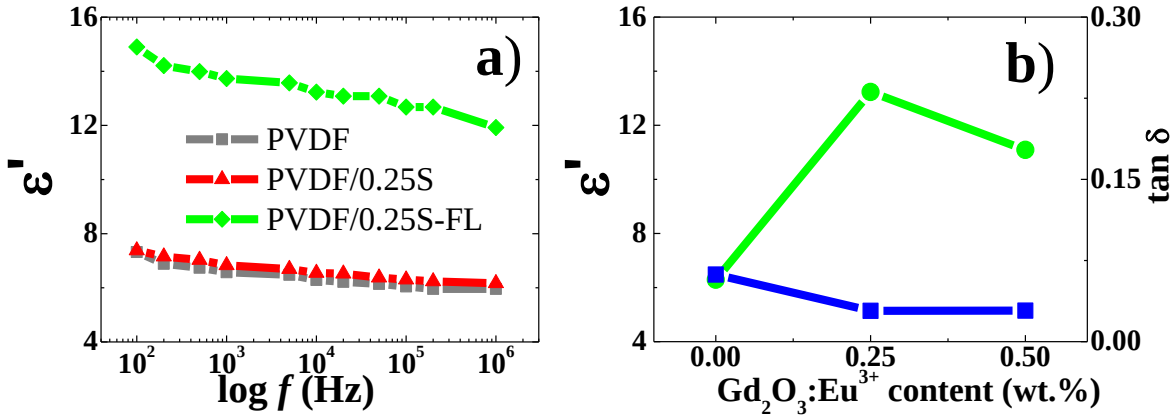

Figure 2.2 - a) Frequency-dependent dielectric constant for P(VDF)/GDO based composites. b) Variation of the dielectric constant (circles) and dielectric loss (squares) of the P(VDF)/S-FL nanocomposites as a function of GDO content at room temperature and 10 kHz.

Figure 2.2a shows that the dielectric response of P(VDF) slightly increases with the incorporation of GDO nanoparticles, from ε'=6 to ε'=7, and shows a significant increase, from ε'=6 to ε'=14, with the incorporation of fluorescent molecules (Figure 2.2b). The first effect is related with the interfacial effects and ionic conductivity of the P(VDF) matrix with the introduction of GDO nanoparticles [1], whereas the high dipolar moments of the fluorescence molecules explain the second one [28]. This increase does not occur in the behaviour of tan δ, which remains practically constant with increasing nanoparticle concentration and introduction of fluorescence molecules at a given frequency (Figure 2.2b).

In order to evaluate the performance of the developed composites for X-ray detector applications, X-Ray radiation was projected into the composite films and the conversion into visible light measured by a photodetector (Figure 2.3).

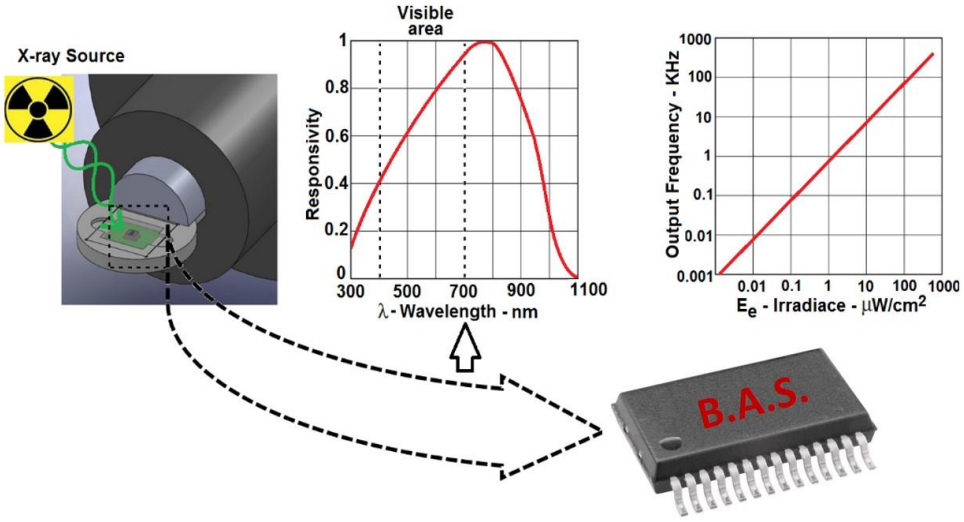

Figure 2.3 - Schematic representation of the system developed to study the X-ray conversion into an electrical signal.

The samples were placed on the sample holder, that included the block acquisition system (B.A.S.) constituted by the electronic read-out circuit, a battery, a TSL235 light sensor and a Micro Control Unit (MCU) CC1111 [29] both from Texas Instruments (Figure 2.3).

Figure 2.4a shows the variation of the visible radiation intensity (V.R.I.) as a function of X-ray intensity. The variation of the visible radiation intensity as a function of GDO content is shown in figure 2.4b.

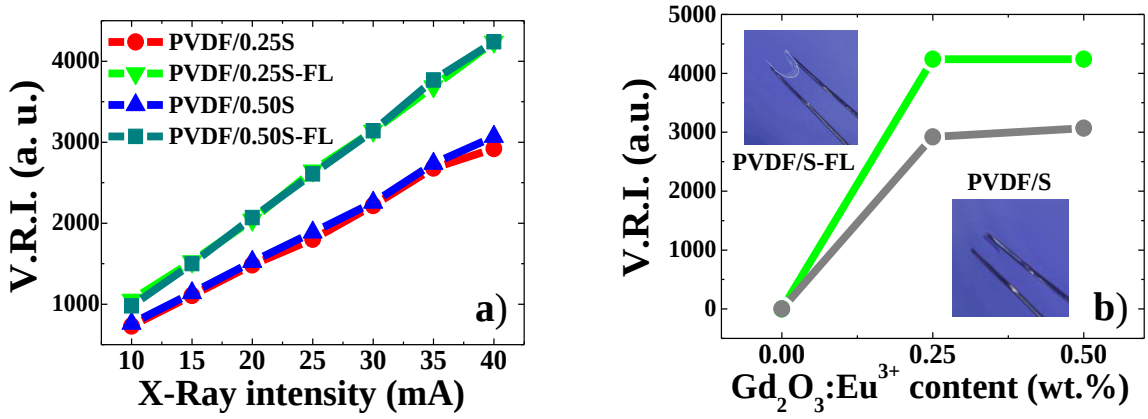

Figure 2.4 - a) Variation of the visible radiation intensity as a function of X-ray intensity (mA). b) Variation of the visible radiation intensity as a function of GDO content (wt. %).

Results show that visible light yield increases with GDO filler content as well as with the introduction of fluorescence materials up to 0.50 wt.%.

Due to the interaction with the X-rays, electrons within the GDO nanoparticles are promoted across the forbidden gap to the conduction band. Then, electrons migrate to the activation center excited-state orbitals and the holes in the valence band to the activation center ground-state orbitals giving rise to the scintillation light [1, 30, 31]. The overall visible light yield is strongly increased with the addition of fluorescence molecules. In particular, it is observed that the overall increase in the efficiency of the X-ray to visible light yield is around 40% when fluorescence molecules were added to composite. The primary fluorescent molecule (PPO) absorbs the scintillation light matched to excited states in the base material and the second fluorescent molecule (POPOP) absorbs and re-emits further at longer wavelength, increasing the attenuation length [6], as it can be seen in figure 2.5.

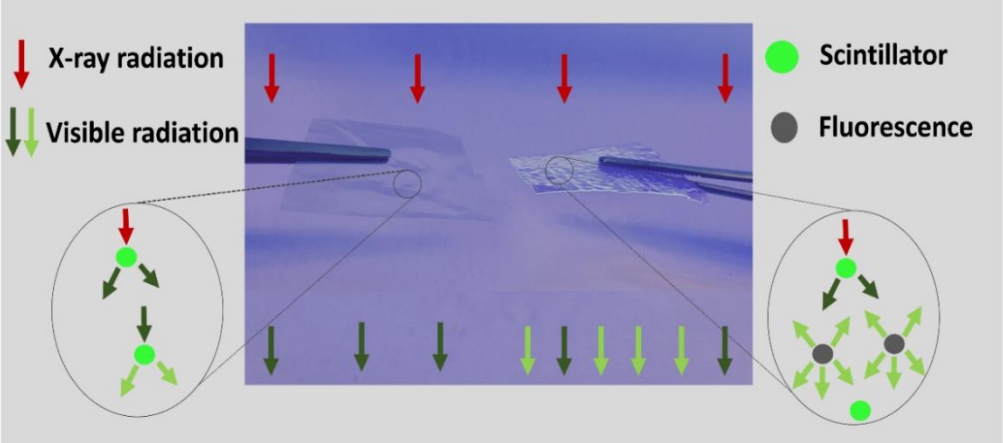

Figure 2.5 - Representation of the scintillation process. Left: P(VDF)/S composites and; right: P(VDF)/S-FL composites.

This increase is more relevant when compared to the increase of 5% in the conversion efficiency when the concentration of scintillator nanoparticles increases from 0.25 to 0.50 wt.%. It is to notice that increasing scintillator particle content above 0.50% will also lead to higher scintillator performance, however mechanical properties will be adversely affected [1], as well as optical transmittance.

In this way, the introduction of low contents of scintillator nanoparticles and fluorescence molecules seems to be the most suitable approach for improving performance of polymer-based composites for X-ray detector applications.

2.4. Conclusions

Thin polymer-based scintillators have been developed by combining GDO nanoparticles with PPO, POPOP and P(VDF) by a simple solvent casting method. The introduction of fluorescence nanoparticles has no influence in the polymer phase, slightly decreases the optical transmittance of the composites films (8%), increases the dielectric constant from ~7 to ~14 and optimizes the quantity of visible light produced in 40%. Similarly, when the content of scintillator nanoparticles was increased from 0.25 to 0.50 wt.%, it was just observed an increase of 5% in the visible light conversion efficiency.

It is thus proven that the introduction of fluorescence molecules in the scintillator composites is a suitable strategy for improving the overall X-ray to visible light conversion efficiency of the materials without sacrificing the homogeneity and transparency, allowing the development large area and/or flexible polymer-based X-ray detectors.

2.5. References

1. Martins, P., A.C. Lopes, and S. Lanceros-Mendez, Electroactive phases of poly(vinylidene fluoride): Determination, processing and applications. Progress in Polymer Science, 2014. 39(4): p. 683-706.

2. Gibson, R.F., A review of recent research on mechanics of multifunctional composite materials and structures. Composite Structures, 2010. 92(12): p. 2793-2810.

3. Murali, M.G., et al., Thiophene-based donor-acceptor conjugated polymer as potential optoelectronic and photonic material. Journal of Chemical Sciences, 2013. 125(2): p. 247-257.

4. Luan, J., et al., Synthesis techniques, properties and applications of polymer nanocomposites. Current Organic Synthesis, 2012. 9(1): p. 114-136.

5. Martins, P.M., et al., Gd2O3:Eu Nanoparticle-Based Poly(vinylidene fluoride) Composites for Indirect X-ray Detection. Journal of Electronic Materials, 2014. 44(1): p. 129-135.

6. Derenzo, S.E., et al., The quest for the ideal inorganic scintillator. Nuclear Instruments and Methods in Physics Research, Section A: Accelerators, Spectrometers, Detectors and Associated Equipment, 2003. 505(1-2): p. 111-117.

7. Righetti, M.C., et al., Thermal and mechanical properties of PES/PTFE composites and nanocomposites. Journal of Applied Polymer Science, 2013. 130(5): p. 3624-3633.

8. Quaranta, A., et al., Optical and scintillation properties of polydimethyl-diphenylsiloxane based organic scintillators. IEEE Transactions on Nuclear Science, 2010. 57(2): p. 891-900.

9. Shmurak, S.Z., et al., Spectroscopy of composite scintillators. Physics of the Solid State, 2012. 54(11): p. 2266-2276.

10. Gorelik, B.A. and M.B. Voskobojnik, Flexible highly filled coatings based on P(VDF). Journal of Fluorine Chemistry, 2000. 104(1): p. 73-77.

11. Pacella, D., Energy-resolved X-ray detectors: The future of diagnostic imaging. Reports in Medical Imaging, 2015. 8: p. 1-13.

12. Sisniega, A., et al., Dual-exposure technique for extending the dynamic range of x-ray flat panel detectors. Physics in Medicine and Biology, 2014. 59(2): p. 421-439.

13. Nillius, P., et al., Light output measurements and computational models of microcolumnar CsI scintillators for X-ray imaging. Medical Physics, 2015. 42(2): p. 600-605.

14. Quaranta, A., et al., Doped polysiloxane scintillators for thermal neutrons detection. Journal of Non-Crystalline Solids, 2011. 357(8-9): p. 1921-1925.

15. Fujita, T., et al., Two-dimensional diced scintillator array for innovative, fine-resolution gamma camera. Nuclear Instruments and Methods in Physics Research, Section A: Accelerators, Spectrometers, Detectors and Associated Equipment, 2014. 765: p. 262-268.

16. Coron, N., et al. Response of parylene-coated NaI(Tl) scintillators at low temperature. in EPJ Web of Conferences. 2014.

17. Bagan, H., et al., Crosslinked plastic scintillators: a new detection system for radioactivity measurement in organic and aggressive media. Anal Chim Acta, 2014. 852: p. 13-9.

18. Milinchuk, V.K., et al., Radiation-induced chemical processes in polystyrene scintillators. Nuclear Instruments and Methods in Physics Research, Section B: Beam Interactions with Materials and Atoms, 1999. 151(1-4): p. 457-461.

19. Santiago, L.M., et al., Synthesis of plastic scintillation microspheres: Alpha/beta discrimination. Applied Radiation and Isotopes, 2014. 93: p. 18-28.

20. Simoes, R., et al., Low percolation transitions in carbon nanotube networks dispersed in a polymer matrix: Dielectric properties, simulations and experiments. Nanotechnology, 2009. 20(3): p. 035703.

21. Martins, P., et al., Dielectric and magnetic properties of ferrite/poly(vinylidene fluoride) nanocomposites. Materials Chemistry and Physics, 2012. 131(3): p. 698-705.

22. Lopes, A.C., et al., Nucleation of the electroactive γ phase and enhancement of the optical transparency in low filler content poly(vinylidene)/clay nanocomposites. Journal of Physical Chemistry C, 2011. 115(37): p. 18076-18082.

23. Gonçalves, R., et al., Nucleation of the electroactive β-phase, dielectric and magnetic response of poly(vinylidene fluoride) composites with Fe2O 3 nanoparticles. Journal of Non-Crystalline Solids, 2013. 361(1): p. 93-99.

24. Martins, P., et al., Preparation of magnetoelectric composites by nucleation of the electroactive β-phase of poly(vinylidene fluoride) by NiZnFe 2O4 nanoparticles. Sensor Letters, 2013. 11(1): p. 110-114.

25. Martins, P., C.M. Costa, and S. Lanceros-Mendez, Nucleation of electroactive β-phase poly(vinilidene fluoride) with CoFe2O4 and NiFe2O4 nanofillers: A new method for the preparation of multiferroic nanocomposites. Applied Physics A: Materials Science and Processing, 2011. 103(1): p. 233-237.

26. Khodyuk, I.V. and P. Dorenbos, Trends and Patterns of Scintillator Nonproportionality. Ieee Transactions on Nuclear Science, 2012. 59(6): p. 3320-3331.

27. Moses, W.W., et al., Scintillator non-proportionality: Present understanding and future challenges. Ieee Transactions on Nuclear Science, 2008. 55(3): p. 1049-1053.

28. Lukavenko, O.N., et al., Solubility and fluorescence lifetime of 2,5-diphenyloxazole and 1,4-bis(5-phenyl-oxazolyl-2)benzene in water-ethanol and water-acetone solvent systems. Journal of Molecular Liquids, 2009. 145(3): p. 167-172.

29. Liu, X.-D., et al., Hydrothermal synthesis of superparamagnetic Fe3O4 nanoparticles with ionic liquids as stabilizer. Materials Research Bulletin, 2015. 62(0): p. 217-221.

30. Derenzo, S.E., et al., Scintillation studies of CdS(In): Effects of various semiconductor doping strategies. Nuclear Instruments and Methods in Physics Research, Section A: Accelerators, Spectrometers, Detectors and Associated Equipment, 2005. 537(1-2 SPEC. ISS.): p. 261-265.

31. Derenzo, S.E., M.J. Weber, and M.K. Klintenberg, Temperature dependence of the fast, near-band-edge scintillation from CuI, HgI2, PbI2, ZnO:Ga and CdS:In. Nuclear

Instruments and Methods in Physics Research, Section A: Accelerators, Spectrometers, Detectors and Associated Equipment, 2002. 486(1-2): p. 214-219.

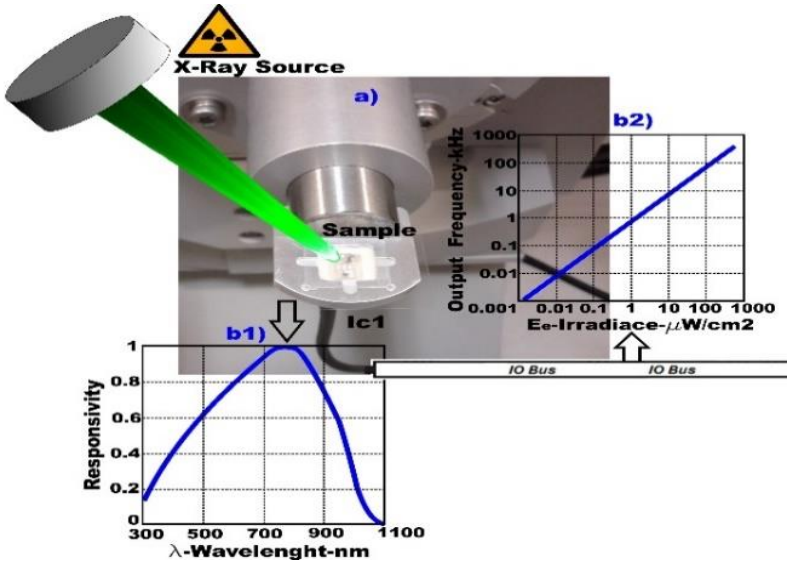

Chapter 3. $Gd_2O_3:Eu^{3+}$/PPO/POPOP/PS composites for digital imaging radiation detectors

Polymer-based scintillator composites have been produced by combining polystyrene (PS), the previously referred $Gd_2O_3:Eu^{3+}$ scintillator nanoparticles and 2,5-diphenyloxazole (PPO) and 1,4 di[2-(5phenyloxazolyl)] benzene (POPOP) fluorescence molecules. PS has been used since it is a flexible and stable binder matrix, resistant to thermal and light deterioration and with suitable optical properties.

This chapter is based on the following publication: J. Oliveira, P.M. Martins, P. Martins, V. Correia, J. G. Rocha, S. Lanceros-Méndez, S. *$Gd_2O_3:Eu^{3+}$/PPO/POPOP/PS composites for digital imaging radiation detectors*; Applied Physics A: Materials Science and Processing, 121, 2, 581-587, 2015.

3.1 Introduction

Since the discovery of scintillation in materials such as NaI(Tl), many other inorganic materials including NaI, CsI:Tl, $CdWO_4$ and $Bi_4Ge_3O_{12}$ have been investigated and used for a variety of applications such as medical image detectors and geophysical exploration, among others [1]. However, those scintillators are often limited by critical properties including efficiency, light yield, response time, surface roughness and, also important for applications, in particular when large areas are involved, cost [1]. The active research of new effective scintillators and solutions for the development of innovative X-ray detectors addressing those limitations and improving the application range of the materials is related to achieving the shortest possible scintillation decay time, extended thermal stability, flexibility and low cost for each specific application area [2-4].

Polymer-based scintillators offer thus unique prospects for their implementation in this field, such as mechanical flexibility and relatively high scintillation efficiency [5], suitable response time, air-stability, low cost, easy fabrication in large areas in a wide range of geometries and tailored property possibilities through composition modification [6, 7].

The development of polymer-based composites has allowed an increasing number of applications in several different areas, nevertheless their use for digital X-ray detection remains barely explored [8-11].

In order to develop polymer-based scintillator composites, able to convert X-ray radiation into visible light, with good mechanical properties, thermal stability and high energy resolution [5], this work reports on gadolinium oxide doped with europium ($Gd_2O_3:Eu^{3+}$ - GDO)/polystyrene (PS) composites with the same fluorescence molecules referred on Chapter 2 in section 2.1.

PS was used as it is one of the synthetic polymers with higher resistance to temperature and radiation degradation [12], it shows high transparency over a broad spectral range ($\lambda > 290$ nm) and is an efficient and stable binder [12]. GDO (particle size ~50 nm) was selected as scintillator material due to its properties already described in Chapter 2. PPO and POPOP fluorescence molecules were further added to the composite in order to increase the visible light yield efficiency as already referred in last chapter [15-17]. After the scintillation process, PPO molecules absorb the scintillation light matched to excited states in the base material and POPOP absorbs and re-emits at longer wavelength.

3.2. Experimental Section

3.2.1. Materials

PS was purchased from Solvay (Belgium), N, N-dimethylformamide (DMF) from Merck (analytical grade), GDO nanoparticles were obtained from Nanograde® and the fluorescence molecules, PPO and POPOP were obtained from Sigma-Aldrich®. All chemicals were used as provided by the suppliers.

3.2.2. Sample preparation

Nanocomposite films with ≈50 μm thick and nanoparticle content ranging from 0.25 to 7.5 in weight percentage (wt.%) were prepared by a simple solvent casting and melt processing procedure as already described in chapter 2, section 2.2.2.

The following nomenclature will be adopted in the manuscript: PS/0.25S-FL means a PS sample with 0.25 wt.% of scintillator fillers and with incorporated fluorescent (FL) molecules.

3.2.3. Sample characterization

The features at a molecular level of the polymer composites, were investigated by Fourier transformed infrared spectroscopy (FTIR) already described on Chapter 2 in section 2.2.3.

The thermal properties of the nanocomposites were determined by differential scanning calorimetry (DSC) with a Mettler Toledo 821e apparatus. Samples were cut from the central region of the film, placed in 50 μL capsules and heated from 20 to 250 ºC at a rate of 10 $^{o}C.min^{-1}$.

The optical transmittance of the samples was evaluated by Ultraviolet–visible spectroscopy (UV-VIS) described on Chapter 2 in section 2.2.3.

One of the most important requirements imposed on scintillators is their energy resolution, which can be improved by increasing the dielectric permittivity of the scintillator material. Thus, ε' and ε'', real and imaginary parts of the dielectric function, were obtained [19, 20] using the same method described on Chapter 2 in section 2.3.2. The samples were previously coated with circular Au electrodes with 5 mm diameter onto

both sides of the sample in order to obtain parallel capacitor geometry. The AC conductivity of the samples was obtained after equation 3.1:

$$\sigma_{AC} = w \times \varepsilon_0 \times \varepsilon'' \qquad (3.1)$$

where w is the frequency, ε_0 the vacuum permittivity and ε'' the imaginary part of the dielectric function.

The efficiency of the X-ray radiation conversion into visible light was measured by using the procedure reported in [5]. Then, the converted visible light from the samples at the corresponding wavelength (Figure 3.1b1) was detected by a TSL235 light-to-frequency converter supplied by Texas Advanced Optoelectronic Solutions Inc.

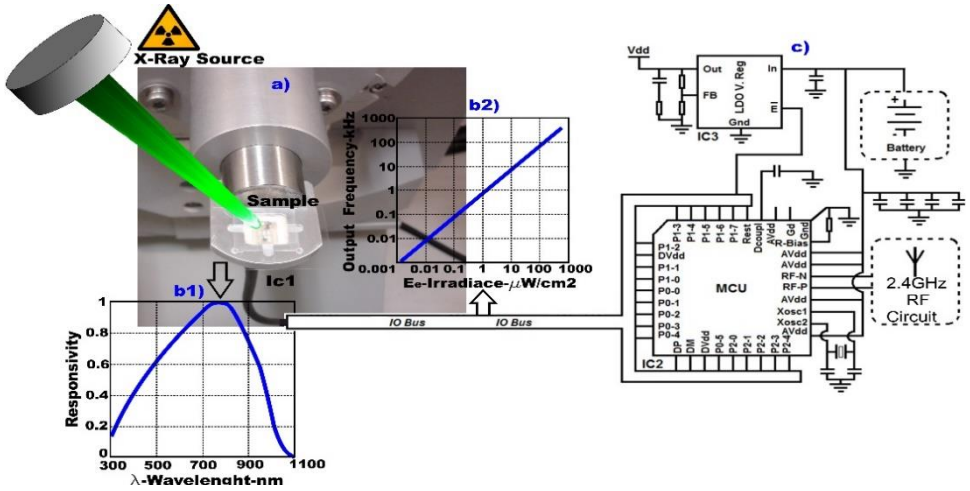

Figure 3.1 - Block diagram of the various components of the light output read-out system: a) X-ray source and sample holder, b) light frequency sensor response and c) control system diagram.

Samples were placed on a home-made sample holder (Figure 3.1a) where the electronic read-out circuit and the light sensor (IC1) was also locate, which was already described in Chapter 2 in section 2.3.The used light sensor was a TSL235 from Texas Instruments [21] and corresponds to a light-to-frequency converter combining a silicon photodiode and a current-to-frequency converter on a single monolithic CMOS integrated circuit (IC). The output frequency of this sensor varied with the irradiated power, as indicated in Figure 3.1b2.

The sensor response was then read by a Micro Controller Unit (MCU), as it represented in Figure 3.1c. The Micro Controller also saves the data in memory during the irradiation process and transmits them to a remote platform when the process is

finished. The IC3 is responsible for ensuring the 3.3V regulated voltage to the circuit. The selected IC was the LM2596 from Texas Instruments [21] which is a switching step-down voltage regulator with an efficiency higher than 80%.

3.3. Results and discussion

After flexible film composite preparation (Figure 3.2a), FTIR was performed on the GDO/PPO/POPOP/PS composites and in the neat PS (Figure 3.2b).

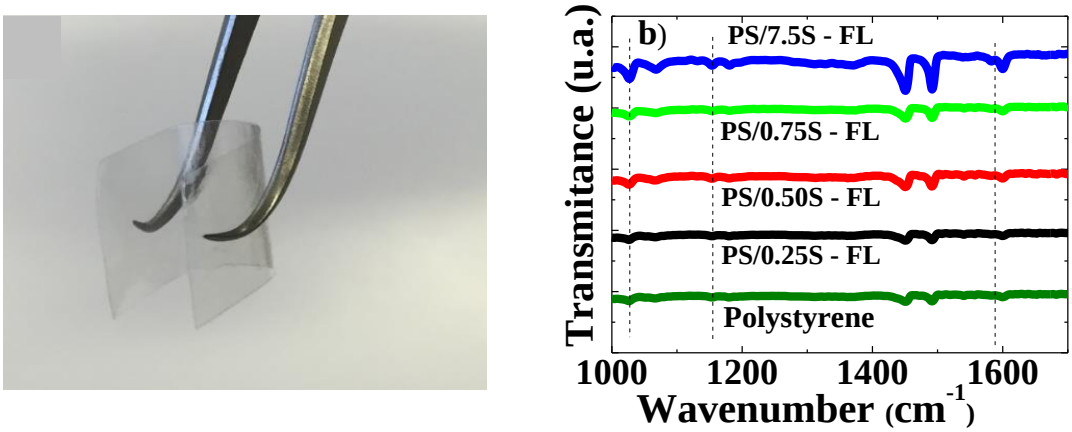

Figure 3.2 - a) Image of the GDO/PPO/POPOP/PS nanocomposites, showing their flexibility. b) Infrared transmittance vs. wavenumber for the GDO/PS/PPO/POPOP nanocomposites and the pristine polymer.

Figure 3.2a reveals that the resulting composite has a good flexibility, being able to undergo large and repeated bending deformation with no permanent deformation or cracking.

Figure 3.2b shows that the addition of GDO nanoparticles and fluorescence molecules has no influence in the infrared spectra of the polymer matrix, as indicated by the unaltered presence of the PS characteristic bands at 1583, 1154 and 1028 cm^{-1} [22]. No chemical bonds between the nanoparticles and the polymer and/or the PPO and POPOP fillers were detected. As expected, the intensity of the characteristic GDO bands at around 1500 cm^{-1} increases with increasing scintillator material content.

Since thermal stability is one of the critical parameters in the development of scintillator materials DCS was used to evaluate the thermal characteristics of the samples, such as relaxations and structural transitions [23] (Figure 3.3a).

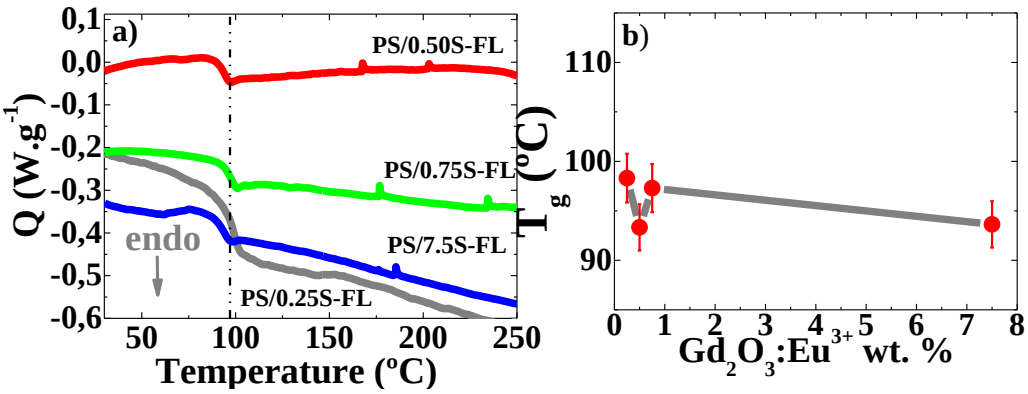

Figure 3.3 a) DSC thermograms of GDO/PPO/POPOP/PS nanocomposites as a function of temperature; b) Glass transition temperature of GDO/PPO/POPOP/PS nanocomposites as a function of GDO content.

Figure 3.3a shows that the typical PS glass transition around 100 °C [24] has not suffered significant variations with the inclusion of the fillers, indicating that the thermal stability of the PS matrix was not substantially influenced by low loadings of GDO and fluorescent molecules, as confirmed by the glass transition temperature values as a function of filler content (Figure 3.3b). Previous studies have also shown that the addition of nanofillers into the PS matrix have almost no influence in the melting temperature and crystallinity values of the polymer, not influencing in this way the performance of the PS [25, 26].

Knowing that one of the most important requirements of scintillator materials is their energy resolution. This important property of scintillators is of value for gamma-ray (e.g. nuclear medicine) or X-ray spectroscopy applications, but it is not particularly relevant for conventional X-ray imaging application. Energy resolution can be improved by increasing their dielectric permittivity [27, 28]. Thus, the real and imaginary parts of dielectric constant, the dielectric loss and the AC conductivity are shown in Figure 3.4.

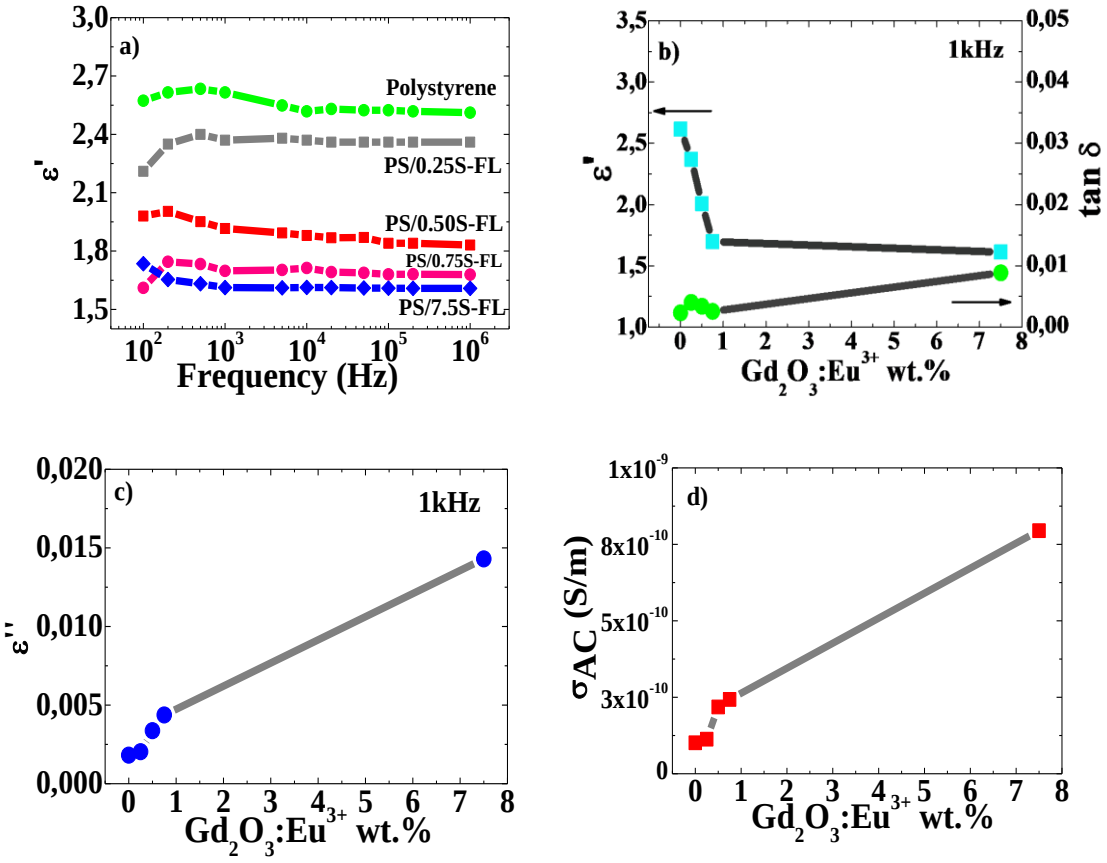

Figure 3.4 - a) Frequency-dependent dielectric constant for PS/ GDO-FL and pristine PS. b) Variation of the dielectric constant (squares) and dielectric loss (circles) of the nanocomposites, c) variation of the imaginary part of dielectric constant of the nanocomposites and d) AC conductivity as a function of GDO content at room temperature for the 1 kHz frequency.

As represented in Figure 3.4a, the dielectric response slightly decreases with increasing frequencies due to the hindered dipolar dynamic at larger frequencies [5, 20]. Figure 3.4a also shows that the dielectric response of PS [24] decreases [29] with the incorporation of GDO nanoparticles and fluorescence molecules. There are no differences on the dielectric measurements between samples with and without fluorescence molecules (results not shown). This decrease is stronger for the filler concentrations up to ≈1%, stabilizing for larger concentrations (Figure 3.4b) and can be attributed to defective polymer crystallization due to higher filler loadings, shielding due to the presence of conductive species, electrostatic interaction of the polymer chains with the

nanoparticles and decreased dipolar mobility [5]. Figure 3.4c reveals that ε'' increases from 1.74×10^{-3} to 1.43×10^{-2} with increasing contents of GDO nanoparticles. Dielectric studies also allowed the determination of the AC conductivity. Figure 3.4d reveals that the AC conductivity as a function of GDO increases from 1.13×10^{-10} to 2.81×10^{-7} S/m with increasing GDO concentration. This increase already revealed on the tan δ results is related to the increase of interfacial effects and ionic conductivity of the PS matrix with the introduction of GDO nanoparticles.

Since an ideal scintillator composite material requires high values of optical transmittance, in particular at the wavelength of scintillation in order to allow the produced visible light to reach the photodetector, Figure 3.5 shows the optical transmittance of the composites as a function of the wavelength (a) and GDO filler content (b).

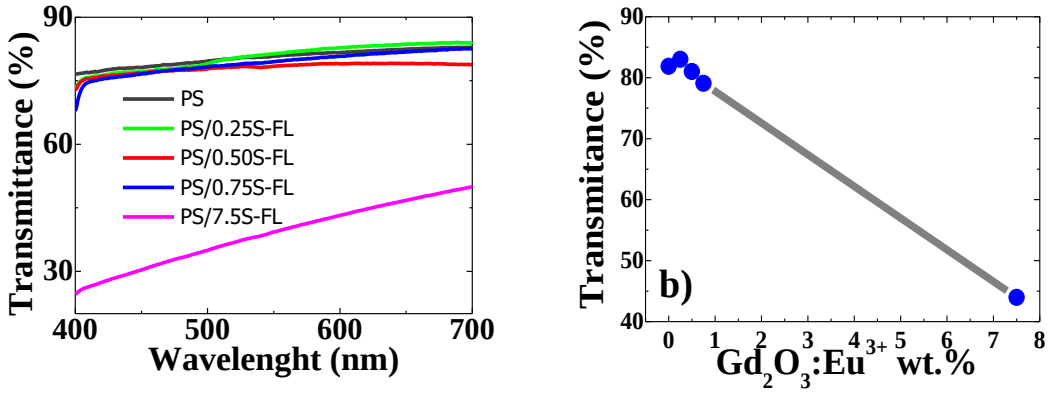

Figure 3.5 - a) Optical transmittance of the nanocomposites as a function of wavelength and b) GDO content.

Figure 3.5a shows that the optical transmittance at ≈ 611 nm decreases with increasing GDO filler content, being this decrease higher to high loadings of GDO. A decrease of ≈50% in the transmittance value was observed to the highest concentrated sample when compared to samples with low nanoparticle content (0-0.75 wt.%). There are no differences on the transmittance values between samples with and without fluorescence molecules (results not shown). The main emission peak of the GDO is observed at ≈ 611 nm, which corresponds to a red emission transition of Eu^{3+} under X-ray excitation [29]. Figure 3.5b shows the transmittance at ≈ 611 nm, which decreases with increasing scintillator filler content. This fact is explained by the fact that increasing concentration of nanoparticles leads to light dispersion and decreased optical

transparency of the films. Those results allow to infer a good scintillation performance of the developed composites. Such performance of the developed composites for X-ray detector applications was evaluated by measuring the X-ray radiation conversion into visible light in GDO nanocomposites (Figure 3.6).

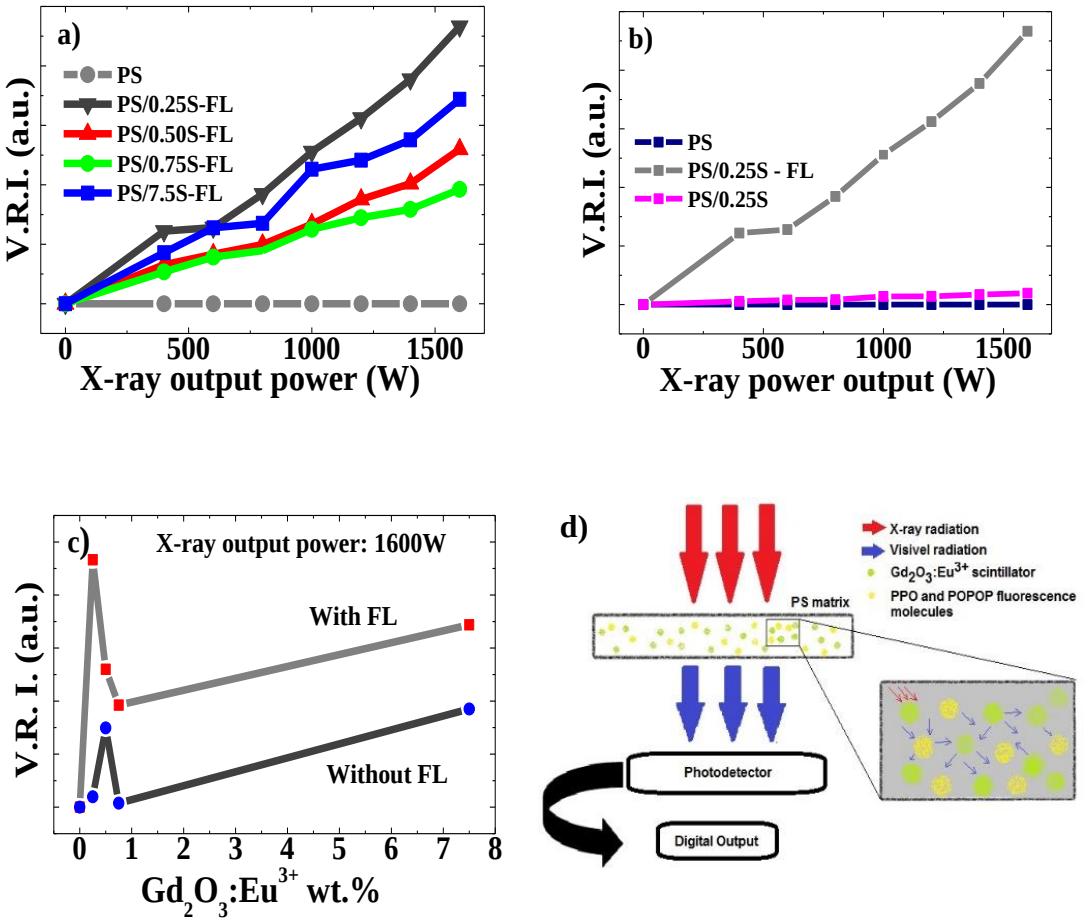

Figure 3.6 - a) Intensity of the output visible radiation as a function of the X-Ray output power. b) Intensity of the output visible radiation (V.R.I.) for the 0.25 wt.% composite, with and without fluorescence molecules as a function of X-ray output power. c) Intensity of the converted visible radiation for different GDO/PPO/POPOP/ PS, with (squares) and without (circles) fluorescence molecules, as a function GDO wt.% at 1600 W input power. d) Schematic representation of the scintillation process in the developed composites.

Figure 3.6a shows that the intensity of the converted visible radiation increases with increasing X-ray output power since with more X-rays interacting with more GDO nanoparticles, a higher number of photons will be produced [5].

The influence of the fluorescence molecules on the scintillation process was carried out in the sample with the best scintillation performance (0.25 wt.% of GDO) – Figure 3.6b. As expected, with the inclusion of scintillator nanoparticles and fluorescence molecules an improvement in the scintillation process was detected by an increase of the intensity of the output visible light as measured by the photodiode of ≈2000% when compared with the inclusion of just the scintillator nanoparticles, for a given nanoparticle concentration. Further, the inclusion of fluorescence molecules also overcomes the effect of increasing scintillator filler content, due the negative effect of light dispersion and dismissed optical transparency of the films with filler content larger than 0,25 wt.%.

Figure 3.6c reveals that for a given X-ray power, the converted visible light first increases due to the presence of the scintillating nanoparticles, then decreases due to decreased transparency of the films and finally increases again for filler concentrations higher than 0.75 wt.%, as the effect of increasing visible light yield due to increased filler content overcomes the decrease in optical transparency related to it. This effect is independent of the present of the fluorescence molecules which provide and overall and concentration independent increase of the visible light yield.

The overall characterization of the X-ray to visible conversion in the developed composites is represented in Figure 3.6d. Due to the interaction between the X-rays and the GDO nanoparticles, electrons jump across the forbidden gap to the conduction band. As previously explained, there is a migration of the electrons to the activation center excited-state orbitals and the holes in the valence band to the activation center ground-state orbitals [5, 30]. The transition of electrons from an activated center excited-state orbital to an activation center ground-state orbital produces a scintillation photon. Next, the primary fluorescent molecule (PPO) absorbs the scintillation light matched to excited states in the base material and the second fluorescent molecule (POPOP) absorbs and re-emits at longer wavelength [30]. Such dispersive process that converts X-ray radiation into visible light can be thus strongly optimized with the introduction of fluorescence molecules into the GDO/PS composites. This approach will allow for higher spatial resolution of the matrix and an increase of the amount of visible light reaching the photodiodes.

3.4. Conclusions

Thin polymer-based scintillators have been developed by developing PS composites with a combination of GDO nanoparticles and fluorescence molecules, PPO and POPOP. The introduction of fluorescence molecules and scintillator nanoparticles has no influence in the polymer structure but strongly decreases transmittance of the composites films (≈50%).

It was shown that the visible light yield increases (2000%) with increasing GDO nanoparticles filler contents up to concentrations of 7.5 wt.% and with the addition of fluorescence molecules (1 wt.% PPO and 0.01wt.% of POPOP) in the scintillator composites, to a 1600 W X-ray output power.

The increased light yield performance, independently of the scintillator filler content, has proved to be a suitable strategy for improving the overall X-ray to visible light conversion efficiency of the materials in order to develop innovative large area and/or flexible polymer-based X-ray detectors.

3.5. References

1. Weber, M.J., Inorganic scintillators: Today and tomorrow. Journal of Luminescence, 2002. 100(1-4): p. 35-45.

2. Milbrath, B.D., et al., Radiation detector materials: An overview. Journal of Materials Research, 2008. 23(10): p. 2561-2581.

3. Cai, W., et al., Synthesis of bulk-size transparent gadolinium oxide-polymer nanocomposites for gamma ray spectroscopy. Journal of Materials Chemistry C, 2013. 1(10): p. 1970-1976.

4. Rocha, J.G., L.M. Goncalves, and S. Lanceros-Mendez, Bi 2Te 3-Sb 2Te 3 on polymeric substrate for X-ray detectors based on the seebeck effect. Microsystem Technologies, 2012. 18(1): p. 1-8.

5. Martins, P.M., et al., $Gd_2O_3:Eu^{3+}$ Nanoparticle-Based Poly(vinylidene fluoride) Composites for Indirect X-ray Detection. Journal of Electronic Materials, 2014. 44(1): p. 129-135.

6. Righetti, M.C., et al., Thermal and mechanical properties of PES/PTFE composites and nanocomposites. Journal of Applied Polymer Science, 2013. 130(5): p. 3624-3633.

7. Quaranta, A., et al., Optical and scintillation properties of polydimethyl-diphenylsiloxane based organic scintillators. IEEE Transactions on Nuclear Science, 2010. 57(2 PART 2): p. 891-900.

8. Gibson, R.F., A review of recent research on mechanics of multifunctional composite materials and structures. Composite Structures, 2010. 92(12): p. 2793-2810.

9. Murali, M.G., et al., Thiophene-based donor-acceptor conjugated polymer as potential optoelectronic and photonic material. Journal of Chemical Sciences, 2013. 125(2): p. 247-257.

10. Luan, J., et al., Synthesis Techniques, Properties and Applications of Polymer Nanocomposites. Current Organic Synthesis, 2012. 9(1): p. 114-136.

11. Martins, P., A.C. Lopes, and S. Lanceros-Mendez, Electroactive phases of poly(vinylidene fluoride): Determination, processing and applications. Progress in Polymer Science, 2014. 39(4): p. 683-706.

12. Milinchuk, V.K., et al., Radiation-induced chemical processes in polystyrene scintillators. Nuclear Instruments and Methods in Physics Research, Section B: Beam Interactions with Materials and Atoms, 1999. 151(1-4): p. 457-461.

13. Paik, T., et al., Designing tripodal and triangular gadolinium oxide nanoplates and self-assembled nanofibrils as potential multimodal bioimaging probes. ACS Nano, 2013. 7(3): p. 2850-2859.

14. Gu, M., et al., Preparation and luminescence properties of transparent Gd2O3:Eu thick film. Guang Pu Xue Yu Guang Pu Fen Xi/Spectroscopy and Spectral Analysis, 2010. 30(3): p. 603-606.

15. Shmurak, S.Z., et al., Spectroscopy of composite scintillators. Physics of the Solid State, 2012. 54(11): p. 2266-2276.

16. Senchishin, V.G., et al., A new radiation stable plastic scintillator. Nuclear Inst. and Methods in Physics Research, A, 1995. 364(2): p. 253-257.

17. Nurmukhametov, R.N., et al., Fluorescence and absorption of a polystyrene-based scintillator exposed to UV laser radiation. Journal of Applied Spectroscopy, 2007. 74(6): p. 824-830.

18. Ovechkina, L., et al., Gadolinium loaded plastic scintillators for high efficiency neutron detection. Physics Procedia, 2009. 2(2): p. 161-170.

19. Simoes, R., et al., Low percolation transitions in carbon nanotube networks dispersed in a polymer matrix: Dielectric properties, simulations and experiments. Nanotechnology, 2009. 20(3): p. 035703.

20. Martins, P., et al., Dielectric and magnetic properties of ferrite/poly(vinylidene fluoride) nanocomposites. Materials Chemistry and Physics, 2012. 131(3): p. 698-705.

21. Gören, A., et al., High performance screen-printed electrodes prepared by a green solvent approach for lithium-ion batteries. Journal of Power Sources, 2016. 334: p. 65-77.

22. Jaleh, B., et al., UV-degradation effect on optical and surface properties of polystyrene-TiO2 nanocomposite film. Journal of the Iranian Chemical Society, 2011. 8(1): p. 161-168.

23. Capiglia, C., et al., DSC study on the thermal stability of solid polymer electrolyte cells. Journal of Power Sources, 2003. 119-121(1): p. 826-832.

24. Wang, H.W., et al., Significant Decreased Dielectric Constant and Loss of Polystyrene-Clay Nanocomposite Materials by Using Long-Chain Intercalation Agent. Journal of Applied Polymer Science, 2004. 92(4): p. 2402-2410.

25. Lu, M., W. Zhou, and K. Mai, Effect of nano-CaCO3 on polymorphic behavior in syndiotactic polystyrene for non-isothermal crystallization. Polymer, 2006. 47(5): p. 1661-1666.

26. Zhao, X., et al., Effect of the selective localization of carbon nanotubes in polystyrene/poly(vinylidene fluoride) blends on their dielectric, thermal, and mechanical properties. Materials and Design, 2014. 56: p. 807-815.

27. Khodyuk, I.V. and P. Dorenbos, Trends and Patterns of Scintillator Nonproportionality. Ieee Transactions on Nuclear Science, 2012. 59(6): p. 3320-3331.

28. Moses, W.W., et al., Scintillator non-proportionality: Present understanding and future challenges. Ieee Transactions on Nuclear Science, 2008. 55(3): p. 1049-1053.

29. Cha, B.K., et al., Synthesis and scintillation properties of nano Gd2O 3(Eu) scintillator for high resolution X-ray imaging applications. Nuclear Instruments and Methods in Physics Research, Section A: Accelerators, Spectrometers, Detectors and Associated Equipment, 2010. 619(1-3): p. 174-176.

30. Derenzo, S.E., et al., The quest for the ideal inorganic scintillator. Nuclear Instruments and Methods in Physics Research, Section A: Accelerators, Spectrometers, Detectors and Associated Equipment, 2003. 505(1-2): p. 111-117.

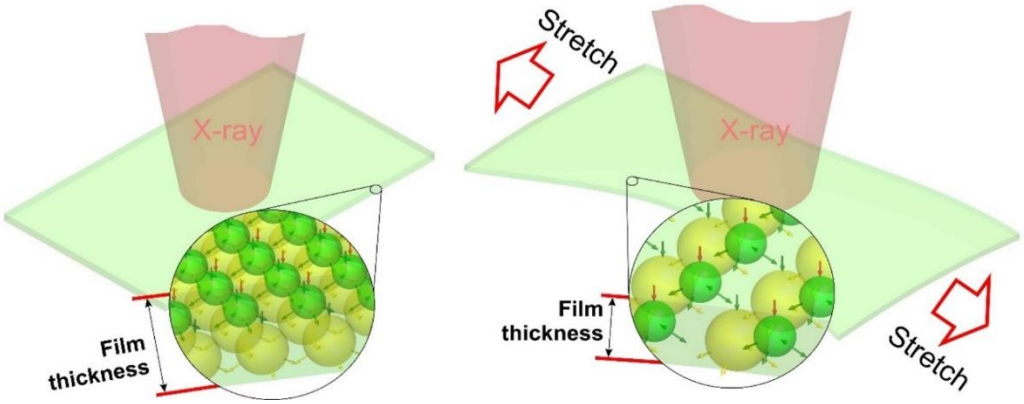

Chapter 4. Stretchable scintillator composites for indirect X-ray detectors

This chapter reports on polymer-based scintillator composites based on the thermoplastic elastomer Styrene-Ethylene/Butadiene-Styrene (SEBS) and $Gd_2O_3:Eu^{3+}$ scintillator nanoparticles, to form a polymer-based flexible and stretchable material for X-ray indirect detectors. Together with high levels of stretchability, with deformations up to 100%, the films exhibit suitable performance with low mechanical hysteresis (less than 1.5 MJ/m^3 for cycles up to 100% of strain) and reproducibly such as a scintillator material for the conversion of X-ray radiation into visible radiation. The developed material is suitable for large area and stretchable X-ray radiation detectors.

This chapter is based on the following publication: J. Oliveira, V. Correia, P. Costa, A. Francesko, G. Rocha and S. Lanceros-Mendez, *Stretchable scintillator composites for indirect X-ray detectors*, Composites Part B: Engineering, 133, pp. 226-231, (2018).

4.1. Introduction

Flexible electronics is an increasingly growing technology as it allows the development of innovative products, opening new application possibilities [1]. One step further in this concept and a new paradigm for electronics is to achieve stretchable materials that are essential to create stretchable organic electronics, sensors and novel devices [2, 3].

In this context, characteristics such as moldable, flexible, printable and stretchable [4] emerge as one of the most relevant technological research fields nowadays, aiming to improve the applicability and integration of electronic systems [4]. Thus, stretchable electronics will allow applications in close contact to the human body and improve installation on curved interfaces [5, 6], among others. In the particular case of radiation detectors, stretchability will reduce the inconvenience caused by the rigid panels of conventional detectors and will allow the integration of sensors for medical monitoring and control on three dimensional architectures/configurations [7]. Stretchable radiation detectors will allow applications in the areas of security equipment and in large strain deformation sensors for medical imaging [8, 9].

Indirect X-ray detectors based on scintillators are a key engineering tool on industrial environment as they are widely used in many business and consumer products with ever increasing frequency in areas such as medicine and security, among others [10-12]. Traditional indirect X-ray detectors are limited by the scintillators critical properties such as efficiency, response time, light yield, surface roughness and for large area applications, low flexibility and cost [13, 14]. Flexible nanocomposites have been prepared for the development of indirect radiation detectors by dispersing scintillating nanoparticles within a polymer matrix [15, 16]. The polymer matrix allows short scintillation time and low manufacturing costs when compared to current available scintillators [11]. These limitations have led to the search for novel materials [17]. Among them, X-ray detectors from polymer-based scintillator composites have sparked large attention due to their scintillation decay time, thermal stability, flexibility, low cost and an easy fabrication in large areas [11, 18].

Thus, in order to develop flexible and stretchable materials able to convert X-ray radiation into visible radiation, with appropriate mechanical properties, showing thermally stability, chemical and radiation resistance and high energy resolution [18], this work reports on a novel composite based on GDO nanoparticles and fluorescence

molecules 2,5-diphenyloxazole (PPO) and 1,4 di[2-(5phenyloxazolyl)] benzene (POPOP) able to efficiently convert X-ray radiation into visible light [19, 20], dispersed into a thermoplastic elastomer polymer. Due to their already mentioned properties, $Gd_2O_3:Eu^{3+}$ - GDO nanoparticles were selected as scintillators. Further, the overall visible light output in the X-ray to electrical conversion process was improved by incorporating the same fluorescence molecules as in the last Chapters, PPO and POPOP [22].

The polymer matrix was selected from the elastomer styrene-butadiene-styrene (SBS) family, as these materials show a chemical resistance with highly repeatable deformation [23]. However, applications of SBS in the biomedical area is not recommended due to the low biostability, associated to the double bonds of butadiene present in the elastomeric block [24, 25] . The SBS family are thermoplastic elastomers (TPE), showing properties of both rubbers and thermoplastics. They have proven suitability for the development of composite materials for strain sensors applications due to their characteristic large deformation, high flexibility and good optical resistance [26, 27]. Form this family of TPE, the co-polymer Styrene-Ethylene/Butylene-Styrene (SEBS) due to their lower butadiene ratio arises as an efficient and stable binder with high biostability, allowing the biomedical application [24]. Besides that, SEBS present an excellent radiation and temperature resistance, good mechanical properties and good optical properties [28, 29].

In this way, the main objective of this work is the development of an innovative generation of flexible and stretchable materials for large area and stretchable indirect X-ray detectors with applicability in areas such as security and healthcare.

4.2. Experimental Section

4.2.1 Materials

The thermoplastic elastomer copolymer SEBS, Calprene CH-6120, with a molecular weight of 245.33 g/mol and a ratio of Ethylene-Butylene/Styrene of 68/32, was supplied by Dynasol. Toluene was obtained from Panreac with a density of 0.86 g/cm^3 at 20 ºC. GDO nanoparticles were obtained from Nanograde® and the fluorescence molecules, PPO and POPOP were obtained from Sigma-Aldrich®. Commercial ink scintillator EJ296 was supplied by Eljen Technology. The chemicals were used as provided by the suppliers.

4.2.2. Samples Preparation

Nanocomposite films with an average thickness of ≈50 μm and nanoparticle content between 0.25 to 1.5 wt.% were prepared by solvent casting, as already described in Chapter 2, section 2.2.2. The fluorescent molecules were then added at the concentrations of 1wt.% of PPO and 0.01wt.% of POPOP, respectively [30], in some of the samples. The resulting mixture was placed under mechanical stirring, until homogeneous mixing of the components. To conclude, the solution was spread in a clean glass substrate and let dry, for 24 h at room temperature, until complete solvent evaporation.

4.2.3. Sample characterization and scintillator composite performance evaluation

The composite films with nanoparticle content of 0.50 wt.% were first sputter-coated with gold and subsequently imaged in a NanoSEM - FEI Nova 200 (FEG/SEM) scanning electron microscope (SEM). The SEM images with magnification ×5K and ×50K were recorded in several regions on the top of the film to study the morphology of the nanoparticles and their distribution in the film. Cross-sections images were also obtained, confirming an average thickness of the samples of ≈50 μm and the good distribution of the nanoparticles along the sample thickness. The ImageJ software was used to determine diameter of the particles. The optical transmittance of the samples was measured by Ultraviolet–Visible (UV-VIS) spectroscopy as described on Chapter 2 in section 2.2.3. The stress-strain measurements were performed on a mechanical testing machine (Shimadzu model AG-IS) at room temperature, with a load cell of 50 N, in the tensile mode. Samples were cut with 10 mm x 8 mm and with a thickness of 50 μm (Fischer Dualscope 603-478, digital micrometer). The mechanical measurements were carried out at a velocity of 5 mm/min. Mechanical hysteresis was performed under the same conditions for 10 loading unloading cycles at different deformation up to 100%. The scintillator material converts X-ray radiation into visible light, thus, the performance of the developed stretchable scintillators was evaluated by subjecting the samples to the X-ray radiation as described on Chapter 2 in section 2.2.3. The efficiency of the X-ray to visible conversion was evaluated with an electronic measurement system that allows to quantify the emitted visible wavelength radiation, according to the diagram shown in Scheme 1, also when the samples are subjected to different deformation levels.

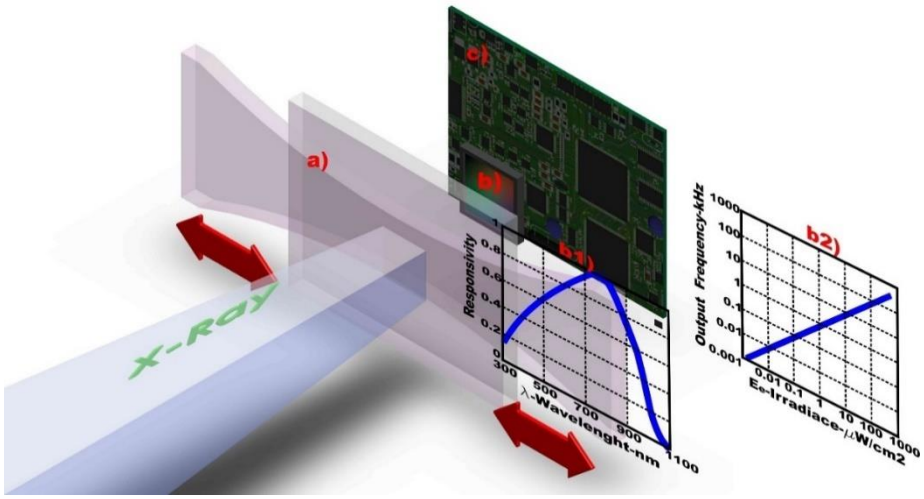

Figure 4.1 - Diagram of the experimental procedure and the radiation output read-out system for stretchable scintillators samples: a) stretchable scintillators samples, b) light to frequency conversion sensor, b1) converted visible light from the scintillator samples at the corresponding wavelength, b2) sensor (TSL235 from Texas Instruments [31]) output frequency according to irradiated power and c) electronic control system circuit.

The measurements were performed by placing the samples on a home-made support with a mechanical system allowing to apply controlled deformation to the sample (Figure 4.1a)). This support also contains the light to frequency sensor (Figure 4.1b), that convert the radiation in a visible wavelength (Figure 4.1b2), resulting in a frequency response according to the radiation intensity (Figure 4.1b2). The frequency signal response is conditioned and stored over time by an electronic control system circuit (Figure 4.1c) till the end of the experiment, as the measuring system is placed inside a protection chamber during the irradiation process for securing reasons. The electronic system was already described on Chapter 2 and 3.

4.3. Results and Discussion

Nanocomposite films with an average thickness of ≈50 µm and nanoparticle content between 0.25 to 0.75 wt.% were prepared by solvent casting method and their properties optical, mechanical and performance for X-ray detectors were studied to evaluate the performance as indirect X-ray detectors. The nomenclature SEBS/0.50S-FL is adopted in

the manuscript, identifying a SEBS sample with 0.50 wt.% of scintillator nanoparticles and with incorporated fluorescent (FL) molecules.

The morphology and distribution of the nanoparticles within in film were studied by SEM (Figure 4.2a and b). The nanoparticles for small clusters homogeneously distributed in the films (Figure 4.2b), both on the top of the film within the film (cross-section images, not shown). The surface microstructure of the film Figure 4.2a is due to styrene and butadiene rich regions of the SEBS, respectively. SEM images also allow determining that the nanoparticles are of spherical shape with ~22 nm average diameter (Figure 4.2b). The particles mostly grouped small clusters [32], evenly distributed in the film.

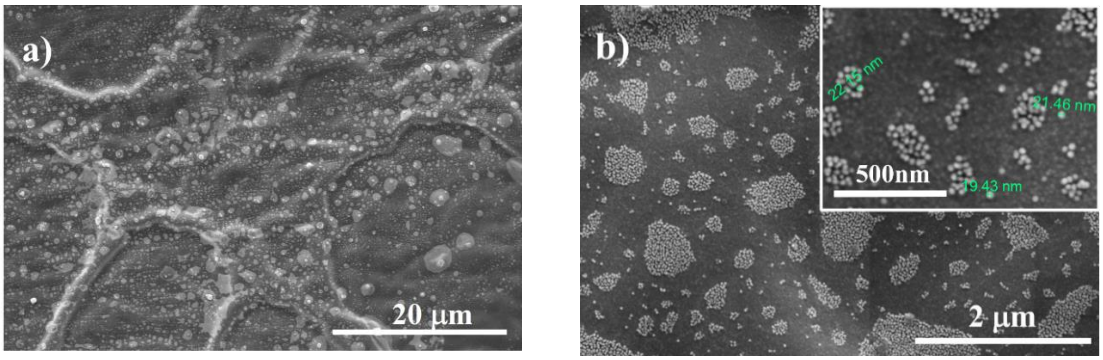

Figure 4.2 - Representative SEM images of the nanocomposite films taken with magnifications of x5K (a) and x50K (b).

The optical properties of the scintillators composites were evaluated, and the results are presented in Figure 4.3a. Figure 4.3a shows that the optical transmittance of the samples as a function of wavelength decrease with increasing scintillator filler content, as increasing filler concentration leads to light dispersion and decreased optical transparency of the films.

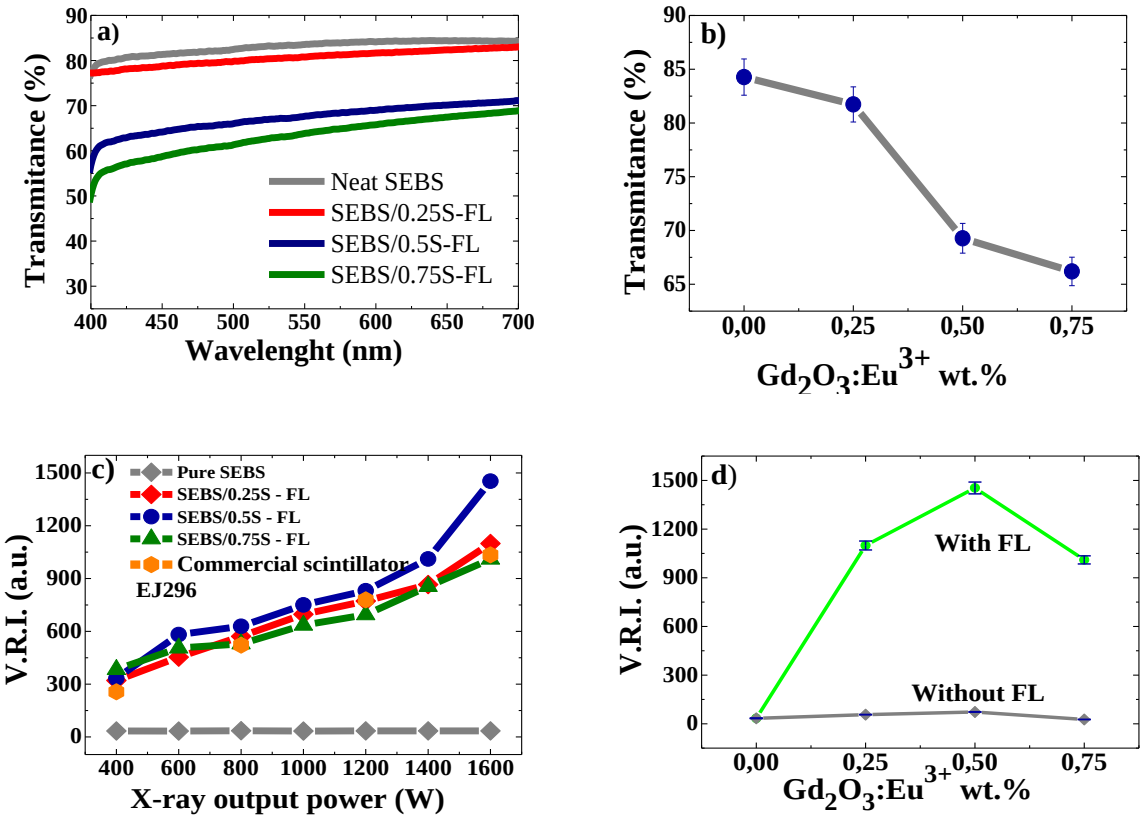

Figure 4.3 - a) Composites optical transmittance as a function of wavelength; b) Composites optical transmittance as a function of GDO content, at 611 nm; c) Visible radiation intensity (V.R.I) variation as a function of the X-ray output power (W); d) Variation of the visible radiation intensity as a function of GDO content (wt %), with and without fluorescence molecules, for a X-ray radiation power of 1600 W;

The main emission peak of the GDO is observed at ≈ 611 nm and is related to the red emission transition of Eu^{3+} under X-ray radiation [15, 22]. Figure 4.3b shows the optical transmittance as a function of GDO content, at a wavelength of 611 nm. The transmittance at ≈ 611 nm suffers a decrease with increasing of scintillator nanoparticle content due to increased light dispersion [22] which leads to the decrease of the composites transmittance from 85% for the pristine polymer to around 65% for the higher filler concentrations.

X-ray radiation was projected into the GDO/PPO/POPOP/SEBS composite and the conversion into visible light was measured, in order to test and prove the good performance of the composites for the development of X-ray indirect radiation detectors. Figure 4.3c shows the variation of the visible radiation intensity (V.R.I.) as a function of the X-ray intensity. The intensity of the converted visible radiation increases with

increasing X-ray output power. It is shown that higher X-ray power and higher scintillators nanoparticle content leads to a higher number of produced visible photons [18]. The V.R.I. of the composite was compared with the VRI of a commercial ink scintillator, EJ296. This scintillator was chosen as it is based on polyvinyltoluene, has a density of 1.02 $g.cm^{-3}$ and a scintillation efficiency of 9000 photons/MeV^{-1}. As it can be seen, the composite with 0.5 wt.% of GDO presents a better performance compared with the commercial scintillator, showing also the advantage for applications where stretchability can be taken to advantage, as it will be shown later. Figure 4.3d shows that the fluorescence molecules inclusion on the scintillation process also improves composite scintillation performance: the introduction of small amounts of fluorescence molecules and scintillator nanoparticles confirms to be the better approach for improving the performance of polymer-based composites for X-ray indirect detector applications, through the mechanism schematically represented in Figure 4.4a.

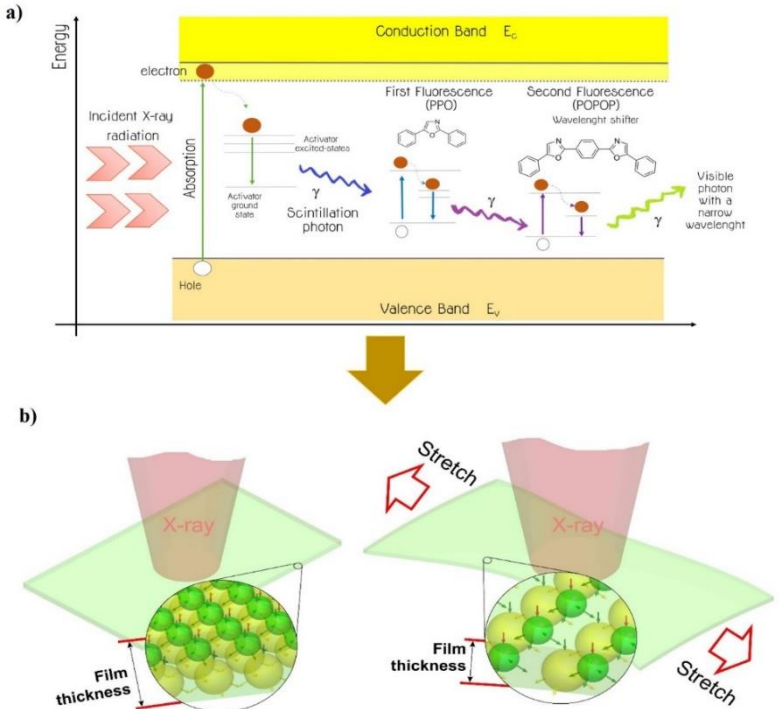

Figure 4.4 - a) Schematic representation of the main physical processed within the scintillator composite. b) Schematic representation of the distribution of the scintillators nanoparticles and fluorescence molecules upon stretching.

Figure 4.4a shows the scintillator process that occurs on the activated crystals. The interaction between the X-ray radiation and the scintillators nanoparticles generates a

deep hole and a hot electron. A sequence of relaxation process including multiplication and thermalization migration lead to a huge number of relaxed electron-hole which must be transferred to the light emitting species (In order to simplify the scintillation process understanding, the recombination of holes and the interactions that will occurs on polymer are not represented in Figure 4.4a). Then, the electrons migrate to the activator excited state and the holes in the valence band migrate to the activator ground state [33]. The transition of electrons from an activated center excited-state orbital to an activation center ground-state leads to a production of a scintillation photon [33]. The fluorescence molecules (FL) absorbs this scintillation energy that re-emits at larger wavelength, in the visible wavelength range [24]. PPO absorbs and re-emits the radiation transfer and that will increase the light yield and the POPOP additionally works as a wavelength shifter [34, 35] which will re-emit the photon that will be detected by the photodetector [36]. This process allows the conversion of the shorter emission wavelength scintillators nanoparticles at 611 nm to a longer wavelength light correspondent to the maximum photodetector spectral responsivity (The sensor responds over the light range of 300 nm to 1100 nm showing a maximum spectral response at around 800nm) [31].

It can be seen that the visible radiation yield strongly increases with GDO nanoparticle content as well as with the introduction of scintillators nanoparticles and fluorescence molecules up to 0.50 wt.%, decreasing for higher concentrations. The detected increase is a consequence of a significant contribution of the scintillator nanoparticles to the increase of the composite density which enhances the X-ray absorption. The decrease for higher particle concentration is a consequence of the decreased optical transparency of the composite, as it can be observed in Figure 4.3a.

Finally, the suitability of the developed composites for flexible and stretchable indirect X-ray detector applications was estimated. The composite with 0.50 wt.% content of GDO was chosen as it shows the best performance for the X-ray radiation conversion into visible radiation.

Figure 4.5a shows the intensity of the converted visible radiation light at an X-ray power of 1600 W as a function of the applied strain up to 100 %.

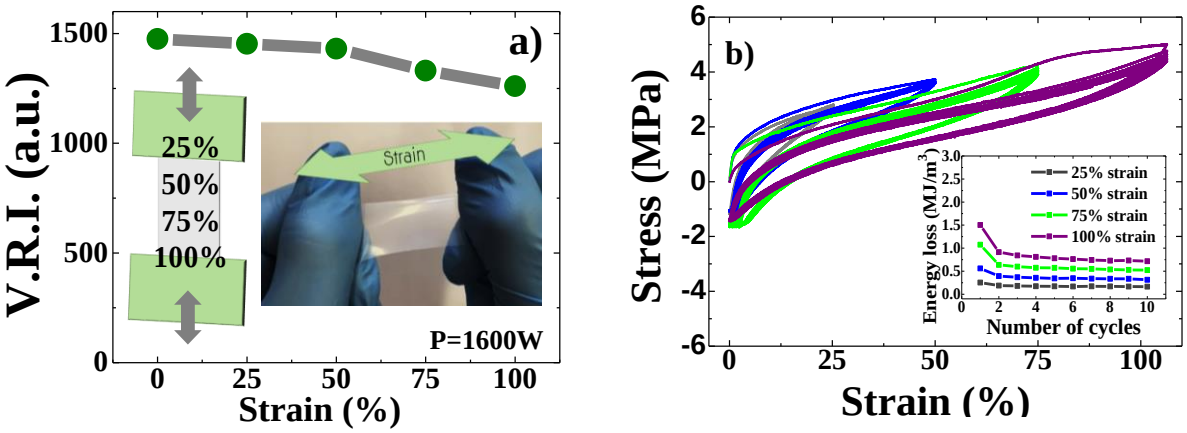

Figure 4.5 - a) Visible radiation intensity variation as a function of applied strain on the SEBS/0.5S-FL composite at an X-ray power output of 1600 W; b) strain recovery curves with the respective strain of 25, 50, 75 and 100 % for the SEBS/0.5S-FL composite and (inset) energy losses for the composites as a function of mechanical strain (between 25 % to 100 % of strain), for 10 load–unload cycles.

It is observed that increasing applied strain up to 100% leads just to a small decrease of ~13 % in the visible radiation intensity output, the scintillator material remaining fully functional. This effect is related to the reduction of the effective distribution of filler concentration, as the thickness decreases, leading to higher optimal transmittance: film stretching leads to a decrease of the film thickness, reducing thus the amount of material in the X-ray beam. Figure 4.4b shows the schematic representation of the microscopic variation of the nanoparticle distribution upon stretching: polymer stretching leads to redistribution of the fillers, having as a result a decrease in the visible radiation conversion efficiency due to a decrease of the filler content by unit area.

The reproducibility of mechanical behavior was measured by the stress-strain curves up to 100% strain, as represented in Figure 4.5b for the SEBS/0.5S-FL composite. The composite shows excellent elasticity and reproducibility over cycling tests, with a mechanical hysteresis that increases with increasing applied strain. The inset of Figure 4.5b shows the mechanical energy dissipate during 10 load-unload cycles for 25, 50, 75 and 100 % of applied strain, showing that the mechanical hysteresis leads to a stabilization after the firsts 2 or 3 cycle for the different applied strains.

Thus, this work shows the suitability of the SEBS/0.5S-FL composites for the development of large deformation indirect X-ray detectors.

4.4. Conclusions

Polymer-based scintillators materials have been developed based on thermoplastic elastomer SEBS composites with a combination of $Gd_2O_3:Eu^{3+}$ scintillator nanoparticles and fluorescence molecules, 2,5dipheniloxazol (PPO) and (1,4-bis (2,5-phenioxazolil))-benzol (POPOP), in order to enhance the visible light output.

This work demonstrated a new type of flexible and stretchable composite material for indirect X-ray detectors with simple, fast and low-cost fabrication.

The SEBS/0.5-FL composites presents suitable optical properties in the visible spectral range with an optical transmittance of ~70 % at 611 nm. Further, the composite maintains excellent elasticity after applied strains of 100% and the stretchability of the scintillator composites does not significantly affects the performance of the X-ray radiation into visible light conversion, proving to be an efficient material for the development of large area stretchable and flexible polymer-based X-ray detectors.

Further, these composites also arise as suitable and novel materials for emerging applications in the area of stretchable electronics.

4.5. References

1. Segev-Bar, M. and H. Haick, Flexible sensors based on nanoparticles. ACS Nano, 2013. 7(10): p. 8366-8378.

2. Park, J., et al., Material approaches to stretchable strain sensors. ChemPhysChem, 2015. 16(6): p. 1155-1163.

3. Knoll, G.F., Radiation Detection and Measurement. 2000: Wiley.

4. Wu, Z., K. Hjort, and S.H. Jeong, Microfluidic stretchable radio-frequency devices. Proceedings of the IEEE, 2015. 103(7): p. 1211-1225.

5. Yoon, S., K. H., and S. Chang, Highly Stretchable and Transparent Microfluidic Strain Sensors for Monitoring Human Body Motions. ACS Applied Materials & Interfaces, 2015. 7(49): p. 27562-27570.

6. Reuss, R.H., Macroelectronics: Perspectives on Technology and Applications. Proceedings of the IEEE, 2005. 93(7): p. 1239-1256.

7. Löher, T., M. Seckel, and A. Ostmann, in Electronics System Integration Technology Conference, ESTC 2010 - Proceedings2010.

8. Kim, S.J., et al., Materials for Flexible, Stretchable Electronics: Graphene and 2D Materials. Annual Review of Materials Research, 2015. 45: p. 63-84.

9. Yao, S. and Y. Zhu, Nanomaterial-Enabled Stretchable Conductors: Strategies, Materials and Devices. Advanced Materials, 2015. 27(9): p. 1480-1511.

10. Milbrath, B.D., et al., Radiation detector materials: An overview, in Journal of Materials Research2008. p. 2561-2581.

11. Cai, W., et al., Synthesis of bulk-size transparent gadolinium oxide-polymer nanocomposites for gamma ray spectroscopy. Journal of Materials Chemistry C, 2013. 1(10): p. 1970-1976.

12. Rocha, J.G., L.M. Goncalves, and S. Lanceros-Mendez, Bi 2Te 3-Sb 2Te 3 on polymeric substrate for X-ray detectors based on the seebeck effect. Microsystem Technologies, 2012. 18(1): p. 1-8.

13. Nikl, M., Scintillation detectors for X-rays. Measurement Science and Technology, 2006. 17(4): p. R37-R54.

14. Quaranta, A., et al., Optical and scintillation properties of polydimethyl-diphenylsiloxane based organic scintillators. IEEE Transactions on Nuclear Science, 2010. 57(2): p. 891-900.

15. Cha, B.K., et al., Synthesis and scintillation properties of nano Gd2O 3(Eu) scintillator for high resolution X-ray imaging applications. Nuclear Instruments and Methods in Physics Research, Section A: Accelerators, Spectrometers, Detectors and Associated Equipment, 2010. 619(1-3): p. 174-176.

16. Lujan, R.A. and R.A. Street, Flexible X-Ray Detector Array Fabricated With Oxide Thin-Film Transistors. IEEE Electron Device Letters, 2012. 33(5): p. 688-690.

17. Weber, M.J., Inorganic scintillators: Today and tomorrow. Journal of Luminescence, 2002. 100(1-4): p. 35-45.

18. Martins, P.M., et al., Gd2O3:Eu Nanoparticle-Based Poly(vinylidene fluoride) Composites for Indirect X-ray Detection. Journal of Electronic Materials, 2014. 44(1): p. 129-135.

19. Milinchuk, V.K., et al., Radiation-induced chemical processes in polystyrene scintillators. Nuclear Instruments and Methods in Physics Research, Section B: Beam Interactions with Materials and Atoms, 1999. 151(1-4): p. 457-461.

20. Oliveira, J., et al., Increasing X-ray to visible transduction performance of $Gd_2O_3:Eu^{3+}$/ P(VDF) composites by PPO/POPOP addition. Composites Part B: Engineering, 2016. 91: p. 610-614.

21. García-Murillo, A., et al., Elaboration and scintillation properties of Eu3+-doped Gd2O3 and Lu2O3 sol-gel films. Nuclear Instruments and Methods in Physics Research, Section A: Accelerators, Spectrometers, Detectors and Associated Equipment, 2002. 486(1-2): p. 181-185.

22. Oliveira, J., et al., $Gd_2O_3:Eu^{3+}$/PPO/POPOP/PS composites for digital imaging radiation detectors. Applied Physics A: Materials Science and Processing, 2015. 121: p. 581–587.

23. Allier, C.P., et al., Thin photodiodes for a neutron scintillator silicon-well detector. IEEE Transactions on Nuclear Science, 2001. 48(4 I): p. 1154-1157.

24. Ribeiro, S., et al., Electrospun styrene-butadiene-styrene elastomer copolymers for tissue engineering applications: Effect of butadiene/styrene ratio, block structure, hydrogenation and carbon nanotube loading on physical properties and cytotoxicity. Composites Part B: Engineering, 2014. 67: p. 30-38.

25. Agarwal, S., J.H. Wendorff, and A. Greiner, Use of electrospinning technique for biomedical applications. Polymer, 2008. 49(26): p. 5603-5621.

26. Wang, Z.F., et al., IEEE Conference on Nanotechnology, 2009: p. 756-757.

27. Hu, M., et al., Soluble salt-driven matrix swelling of a block copolymer for rapid fabrication of a conductive elastomer toward highly stretchable electronics. Materials and Design, 2016. 100: p. 263-270.

28. Ranade, S.V., R.E. Richard, and M.N. Helmus, Styrenic block copolymers for biomaterial and drug delivery applications. Acta Biomaterialia, 2005. 1(1): p. 137-144.

29. Gonçalves, B.F., et al., Green solvent approach for printable large deformation thermoplastic elastomer based piezoresistive sensors and their suitability for biomedical applications. Journal of Polymer Science, Part B: Polymer Physics, 2016. 54(20): p. 2092-2103.

30. Ovechkina, L., et al., Gadolinium loaded plastic scintillators for high efficiency neutron detection. Physics Procedia, 2009. 2(2): p. 161-170.

31. Instruments, T. May, 2016 [cited 2016 1 May]; Available from: http://www.ti.com.

32. Pires, A.M., et al., The effect of Eu3+ ion doping concentration in Gd2O3 fine spherical particles. Journal of Alloys and Compounds, 2002. 344(1–2): p. 276-279.

33. Derenzo, S.E., et al., The quest for the ideal inorganic scintillator. Nuclear Instruments and Methods in Physics Research, Section A: Accelerators, Spectrometers, Detectors and Associated Equipment, 2003. 505(1-2): p. 111-117.

34. Liu, C., et al., Facile Single-Precursor Synthesis and Surface Modification of Hafnium Oxide Nanoparticles for Nanocomposite γ-Ray Scintillators. Advanced Functional Materials, 2015. 25(29): p. 4607-4616.

35. Fernow, R.C., Introduction to Experimental Particle Physics. 1989: Cambridge University Press.

36. Quaranta, A., et al., Doped polysiloxane scintillators for thermal neutrons detection. Journal of Non-Crystalline Solids, 2011. 357(8-9): p. 1921-1925.

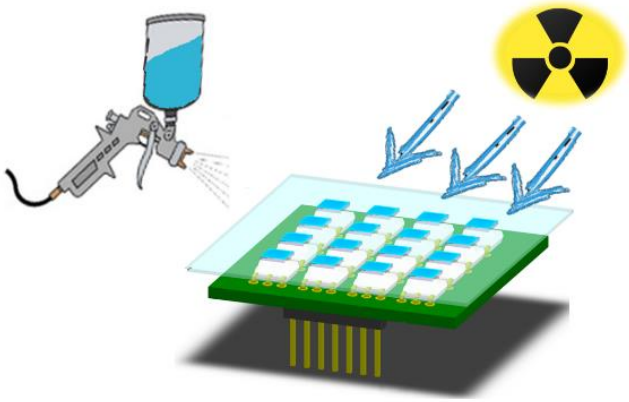

Chapter 5. Novel environmentally-friendly scintillator ink for printed radiation detectors

For application in spray-printed radiation detectors, water-based scintillator inks have been produced by combining a thermoplastic elastomer poly(vinyl) alcohol (PVA) and $Gd_2O_3:Eu^{3+}$ (GDO) scintillator nanoparticles. Formulations of these green inks with different concentrations of scintillator nanoparticles have been assessed in terms of their rheological properties: the optimal concentration of scintillator nanoparticles in the water-based ink for spray-printing was 0.75 wt.%. This optimized ink formulation exhibits a Newtonian behavior with a viscosity around 0.1 Pa.s and performance characteristics suitable for spray-printing scintillators for indirect X-ray detectors.

This chapter is based on the following publication: J. Oliveira, P. M. Martins, V. Correia, L. Hilliou, D. Petrovykh and S. Lanceros-Mendez; *Water based scintillator ink for printed X-ray radiation detectors*; Polymer testing Polymer Testing 69, pp. 26-31 (2018)

5.1. Introduction

Printing and other additive manufacturing processes are increasingly being used in technological applications [1]. The success of these processes is predicated on providing an environmentally-friendly, low-cost, and practical method for the fabrication of tailored flexible and disposable structures and devices, including electronic and biomedical devices [2-4].

X-ray detectors are among the biomedical sensors that can benefit from recent developments in materials and fabrication techniques. Applications of traditional X-ray detectors in medical imaging are limited by the low mechanical flexibility and high cost of bulk scintillators [5, 6]. In contrast, polymer-based scintillator composites [7] now offer such beneficial properties as short scintillation decay time, extended thermal stability, mechanical and chemical stability [6, 8], low cost, and facile fabrication into large areas or complex (compliant) shapes [9].

High efficiency and fast time response have been demonstrated for advanced polymer-based X-ray detectors [10]. Polymer composites with scintillator particles provide additional benefits for radiation detection in many applications [11-14] , due to the combination of the low cost of the polymer matrix and the contribution of the particles to the increase of composite density and atomic number [15].

These types of composite functional materials can be implemented using printing technologies with inks appropriately designed [16] to take advantage of the wide range of physicochemical properties and extensive possibilities for tailoring functional properties of the polymer component of the ink [17, 18]. Radiation detectors can be printed using printing techniques such as spray- or screen-printing to produce low-cost flexible sensors and devices [19, 20]. Spray-printing, in particular, is a low-cost process for producing polymer coatings [21] with a distribution of ink sufficiently uniform to be compatible with large-area printed electronics [22]. Most of the polymers used for printing technologies are processed from solutions in toxic solvents, creating environmental hazards and critical problems for biomedical applications [23]. Water-based polymer inks, therefore, would be desirable for printed-sensor applications of polymer-matrix composites.

Poly(vinyl alcohol) (PVA) is a suitable polymer in this context, being water-soluble, biocompatible, biodegradable and thus commonly used in biomedical devices, drug delivery and food packaging industry [24, 25]. The use of PVA in sensor applications also takes advantage of its chemical resistance [24] and mechanical properties [26, 27].

The beneficial properties of PVA as a polymer matrix can be complemented in a composite material by scintillator nanoparticles of europium-doped gadolinium oxide, $Gd_2O_3:Eu^{3+}$ (hereafter GDO). Furthermore, fluorescence molecules 2,5 diphenyloxazol (PPO) and (1,4-bis (2-(5-phenioxazolil))-benzol (POPOP) can be used, as already referred in previous chapters, to increase the visible light yield efficiency [29, 30], particularly in combination with GDO dispersed in a polymer matrix [31, 32].

Accordingly, a new scintillator ink based on PVA together with scintillator GDO nanoparticles and PPO and POPOP fluorescence molecules is reported here as a critical enabling step for spray-printing X-ray detectors constructed from water-based polymer composite materials able to convert X-ray radiation into visible light.

5.2. Experimental Section

5.2.1. Materials

Poly(vinyl alcohol), PVA, 98% hydrolyzed was supplied by Sigma Aldrich with a molecular weight between 13000–23000 and a density of 1.269 g/cm^3. GDO, nanoparticles were obtained from Nanograde and the fluorescence molecules from Sigma-Aldrich. Ultra-pure water with 18.2 MΩ·cm resistivity at 25 ºC was obtained from a Millipore Milli-Q system. The commercial scintillator ink EJ296, which was used for benchmarking the performance of the scintillator developed in this work, was supplied by Eljen Technology. All chemicals were used as provided by the suppliers.

5.2.2. Preparation of scintillator inks

The scintillator inks were prepared by solvent casting with nanoparticle content of 0, 0.75 and 1,5 wt.%. First, the desired amount of GDO nanoparticles and fluorescence molecules, PPO at concentration of 1wt.% and POPOP at concentration of 0.01 wt.%, were dispersed in ultra-pure water. The solutions were kept in an ultrasound bath (ATU, Model ATM40-3LCD) for 4h in order to properly disperse all the fillers. After the dispersion of the nanoparticles, PVA was added and the solution in different polymer/solvent ratios (Table 1) was magnetically stirred and heated at 90 ºC, until complete dissolution of the polymer, as reported in [31].

Table 5.1 - Scintillator inks prepared by varying $Gd_2O_3:Eu^{3+}$ filler content and polymer/solvent relative content.

Ink	GDO content (wt.%)	PVA (g) : water (ml) ratio
SC003	0	1:6
SC004	1.5	1:6
SC005	0.75	1:5
SC006	0.75	1:6
SC007	0.75	1:7
SC008	0.75	1:8

5.2.3. Preparation of the scintillator films

Scintillator films were prepared both by spray printing and by doctor-blade coating. The PVA films were printed on a polyethylene terephthalate (PET) substrate, in order to obtain flexible scintillators. The nanocomposite doctor-blade-coated films were prepared on a glass substrate with scintillator nanoparticle content between 0.25 to 1.5 wt.% and dried at 25 ºC until complete solvent evaporation. These nanocomposites films showed an average thickness of ≈ 30 μm, measured with gauge Fischer DualScope MPOR. Then, the films were removed from the substrate for characterization.

After the evaluation of the functional performance, films with concentrations of scintillator nanoparticles of 0.75 and 1.5 wt.% and produced by spray printing technique were determined to produce the highest visible light output. The nomenclature adopted in the manuscript is as follows: PVA/0.75S-FL means a PVA composite with 0.75 wt.% of scintillator nanoparticles and with incorporated fluorescent molecules (FL).

5.2.4. Characterization of scintillator ink and films

The morphology of the PVA scintillator films was analyzed by scanning electron microscopy (SEM) (FEI Quanta 650 FEG microscope) with an accelerating voltage of 5 kV. The energy dispersive X-ray (EDX) spectra were measured by an INCA 350 spectrometer (Oxford Instruments) with a primary beam voltage of 20 kV. The rheological behavior of the inks was characterized at 25º C using a stress controlled rotational rheometer MCR-300 (Anton Paar, Austria) equipped with a Couette geometry.

After loading the inks into the shearing geometry, steady shear rates were ramped from 2000 s^{-1} down to 1 s^{-1} within 15 min. This test was immediately followed by another ramp with steady shear rates from 1 s^{-1} up to 2000 s^{-1} also within 15 min. The viscosity data obtained from the two ramps overlapped, indicating that flow curves were obtained under steady state conditions and that the polymer solutions showed no thixotropy.

The optical transmittance of the samples was evaluated by Ultraviolet–Visible spectroscopy (UV-VIS) from 200 to 800 nm using the same equipment described on section 2.2.3 of Chapter 2.

For the functional performance of the films, X-ray radiation was projected into the composites and the conversion into visible light was measured as already described in previous chapters. The efficiency of this conversion was evaluated with a custom-built system that allows to quantify the emitted visible wavelength radiation [31].

5.3. Results and Discussion

5.3.1. Characterization of the PVA scintillator composites

The morphology of the PVA composite films prepared by doctor-blade technique was studied to test if the addition of the scintillator nanoparticles and fluorescence molecules influences the typical microstructure of PVA as well as to verify if the fillers are well dispersed. Figure 5.1 shows SEM images of the pristine PVA sample together with the PVA/0.75S-FL sample, the appearance of which is representative of the other composite samples.

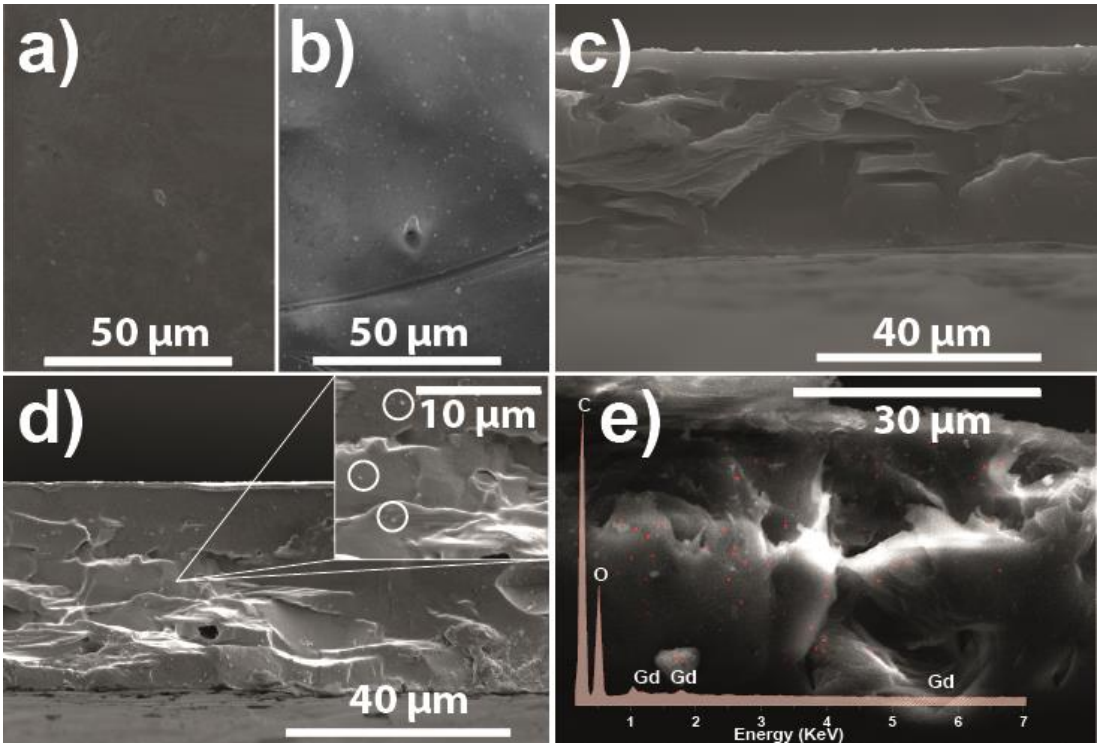

Figure 5.1 - Surface (a and b) and cross-section (c and d) SEM images of the PVA and PVA/0.75S-FL films, respectively. SEM-EDX mapping and spectrum of the PVA/0.75S-FL film (e).

Figure 5.1 shows a smooth surface for the pristine PVA films (Figure 5.1a) and for the composite (Figure 5.1b). A good filler dispersion is observed for the nanocomposite and just a few Gadolinium nanoparticle aggregates are observed at the surface and in the cross-section micrographs (white circles in the inset of Figure 5.1d). The EDX measurement revealed the bulk composition of 56 wt.% of carbon (C), 43 wt.% of oxygen (O) and 0.8 wt.% of gadolinium (Gd) for the PVA/0.75S-FL (Figure 5.1e). C and most of the O are ascribed to PVA and Gd to the GDO nanoparticles. The amount of Gd estimated by EDX (0.8 wt.%) is in good agreement with the amount of GDO nanoparticles added to the nanocomposite (0.75 wt.%), taking into account that the Gd dominates the content of the nanoparticles by weight. Conversely, Eu doped into GDO nanoparticles at 3 wt.% Eu^{3+} was not detected by EDX. EDX mapping revealed a uniform distribution of the GDO nanoparticles (red dots in Figure 5.1e) across the nanocomposite film.

The optical transmittance (Figure 5.2a) of the scintillator composites was measured as a function of wavelength and filler content (0, 0.25, 0.5, 0.75 and 1.5 wt.%). As expected, the transmittance decreases with increasing filler content in the polymer matrix,

while a relatively flat transmittance in the visible range is consistent with the uniform dispersion of the fillers observed by SEM. The inset of Figure 5.2a shows the optical transmittance as a function of GDO filler content, at a wavelength of 611 nm, which is the emission peak of the scintillator nanoparticles. For this specific wavelength, the optical transmittance decreases with increasing scintillator filler content from ~90% for the pure polymer down to ~40% for the sample with 1.5 wt.% filler content.

The scintillator process occurs due to the interaction of the X-ray radiation with the scintillator material, which generates a free electron and a deep hole pair excited to the ionization band (Scheme 5.1) [33]. Several relaxation processes follow as explain in section 4.3 on Chapter 4.

It is to notice that large contents of scintillator nanoparticles and fluorescence molecules in the composite lead to higher visible light dispersion and lower scintillator composite performance [27]: increasing filler content leads to increased composite density and higher number of scintillating nanoparticles, leading to an enhancement of X-ray absorption and conversion. On the other hand, it also leads to a decrease in the optical transparency of the polymer-based scintillator composite, due to higher light dispersion (Scheme 5.1).

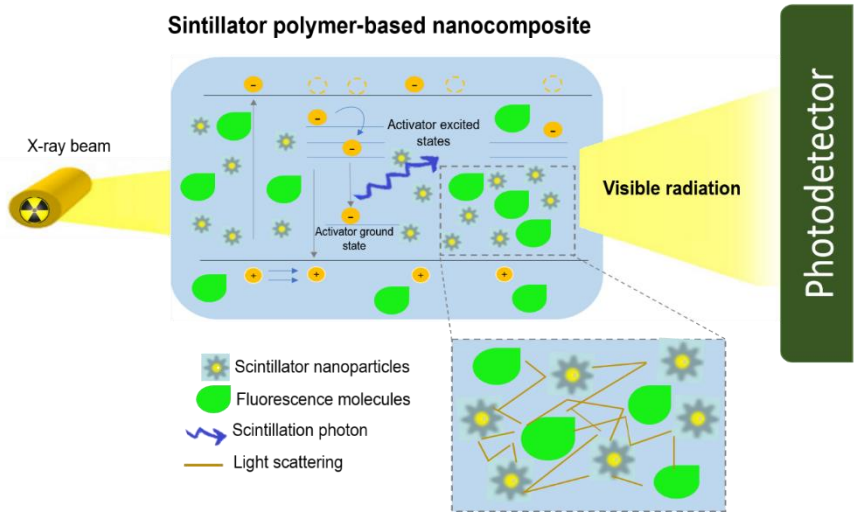

Scheme 5.1 - Schematic representation of the scintillation process induced by X-ray radiation.

Figure 5.2b shows the variation of the efficiency of the X-ray radiation conversion into visible light (visible radiation intensity, named V.R.I.) as a function of X-ray intensity

obtained for the PVA composites prepared with different nanoparticle filler contents by doctor-blade coating. The intensity of the converted visible radiation increases with increasing X-ray output power and small amounts of scintillator GDO nanoparticles, as reported in [31]. The increase of the X-ray power increases the interaction volume and hence the number of photons produced [9]. The V.R.I. increases with increasing filler content up to 0.75 wt.%, presumably because at higher concentrations the increased conversion of X-ray radiation into visible one is counteracted by the decreasing transmittance in the visible [32].

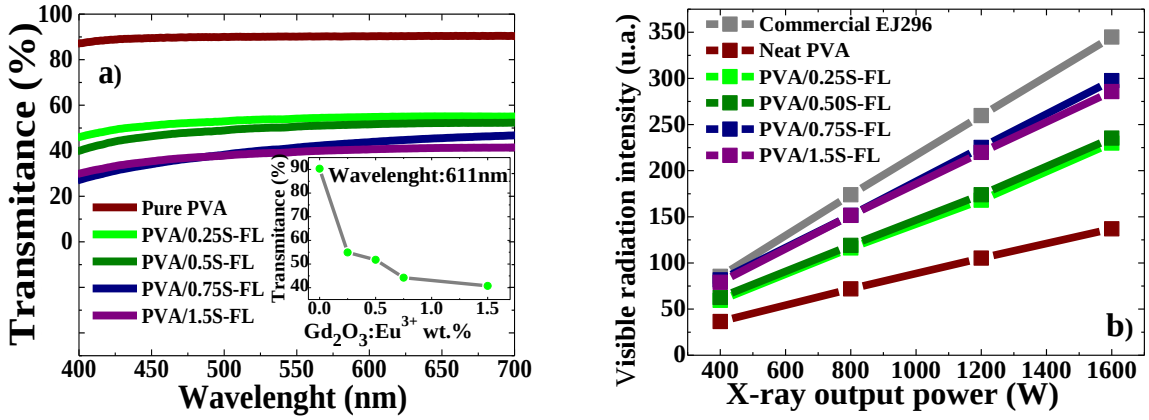

Figure 5.2 - a) Optical transmitance of the PVA composites as a function of wavelenght and GDO content (inset: optical transmittance as a function of GDO filler content, at a wavelenght of 611 nm) b) Intensity of the converted visible radiation of the composites as a function of X-ray output power.

Figure 5.2b also shows a commercial scintillator ink, EJ296, for comparison: the PVA nanocomposite scintillator with 0.75 wt.% filler content exhibits a response lower only by 14% at the highest X-ray power tested, which would not significantly influence the device performance in most applications. As noted above, composites with 0.75 and 1.5 wt.% GDO content exhibit similar scintillator performance, accordingly, inks were prepared from these formulations to evaluate their rheology for printing processes.

5.3.2. Ink characterization

For application and upscaling production of inks, the rheological behavior of the solution is critical because it affects how the ink is transferred to the substrate to form a homogeneous film. The viscosity is affected by various parameters such as temperature, molecular weight of the polymer, solvent, concentration, and additives [34]. Thus, viscosity is often used as a quality control parameter of the fluids.

To optimize ink development, the rheological behavior of the suspensions was evaluated. The shear viscosity of PVA suspensions does not exhibit any shear rate dependence (Figure 5.3a), indicating a classical Newtonian behavior [35]. In fact, the data suggest that this PVA solution is in the dilute regime, because the zero shear viscosity exhibits a linear increase with the PVA volume fraction [36]. The error bars of the extracted zero shear viscosities displayed in the inset of Figure 5.3a are large and show that variations in the viscosity of the suspensions are at the limit of torque sensivity of the rheometer (Couette geometry).

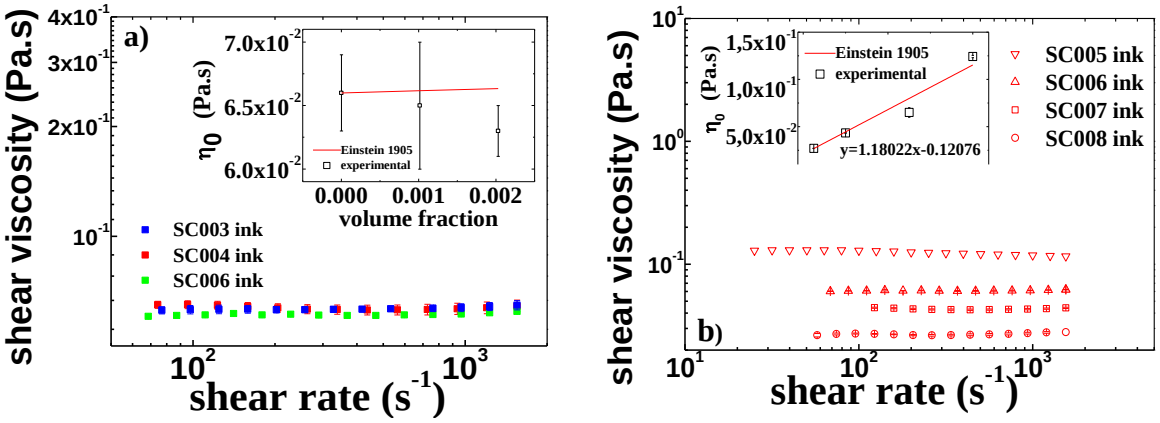

Figure 5.3 - a) Shear rate dependence of suspensions of GDO nanoparticles in PVA solution in water. Inset: zero shear viscosity of suspensions as a function of the particle volume fraction. The red line represents the Einstein equation for dilute suspensions of hard spheres; b) Shear rate dependence of 0.75 wt.% nanoparticle suspensions in PVA solutions with different PVA concentrations. Inset: zero shear viscosity of suspensions as a function of the PVA concentration.

However, a trend for decreasing zero shear viscosity η_0 with increasing particle volume fraction is observed. This trend is at odds with the Einstein behavior expected for

diluted suspensions of non-interacting hard spheres in a Newtonian solvent with viscosity η_0. Indeed, the Einstein relation is [37]:

$$\eta_0 = \eta_S(1 + 2.5\phi) \quad (5.1)$$

where ϕ is the volume fraction of spherical particles.

Flocculation between particles could lead to a mismatch between the data and the expected functional dependence but cannot explain a suspension viscosity smaller than the viscosity of the suspending medium. Indeed, flocculation of silica nanoparticles suspended in PVA suspensions has been recently associated with an increase in η_0, as large particle aggregates are formed through the H-bonding of PVA to the nanoparticles, promoting particle bridging [38]. Thus, to explain the non-Einstein behavior, other types of particle-particle and PVA-particle interactions have to be considered. Indeed, PVA is not fully hydrolyzed (98% of OH groups as reported by the PVA supplier). Accordingly, PVA chains and particles could form complexes: electrostatic repulsion between the few ester groups of the polymer chain is modulated by the presence of cations available in the solvent. The addition of particles could thus bring a polyelectrolyte effect: the dissociation of protons from the nanoparticles would cause a change in the overall conformation of PVA chain from extended to more coil-like and result in a decrease in the viscosity of the PVA solution [39].

Adding less PVA in suspensions with a constant volume fraction in particles results in a simple dilution effect of the suspending fluid. This is illustrated in Figure 5.3b, where the flow curves of suspensions with different PVA concentrations are reported. All flow curves show a Newtonian behavior, indicative of dilute systems. Indeed, the zero-shear viscosity of the suspensions increases linearly with the concentration in PVA which suggests that no interactions between PVA chains occur as expected for the dilute regime of a polyelectrolyte solution [38].

Coming back to the non-Einstein behavior suggested by the data reported in Figure 5.3a, we note that the adsorption of PVA chains on the surface of particles will effectively reduce the volume fraction of free PVA chains in the suspending medium. As suspensions are diluted and PVA concentration in the solvent remains in the dilute regime, the addition of particles will simply lead to a loss of drag forces between PVA chains and the solvent, thereby reducing the shear viscosity of the suspensions. Rheological data show that all tested formulations exhibit viscosities suited for doctor-blade application, which is a

versatile technique, tolerant to a wide range of viscosities [35]. As far as spraying is concerned, viscosity levels reported in Figure 5.3 are within the range of reported values for successful spraying. The rheology of spraying process, however, is far from being fully understood. Spraying involves shear rates far above those tested in Figure 5.3 and contributions from surface tension, gravity, and extensional viscosity. Furthermore, because of the huge shear rates occurring during spraying, issues such as inertial and jetting instabilities cannot be ignored (and cannot be assessed with the rotational rheometer employed in the present study). As a proof-of-concept, a prototype scintillator film was produced by spray printing.

5.3.3. Development of printed scintillator films by spray printing technique

The ink selected for producing the printed active scintillator layer was the SC005 (viscosity of about 0.1 Pa.s). The active layer with an average thickness of ≈30 μm was deposited on a PET substrate by spray-printing process (Figure 5.4a). The adhesion of printed films to substrate was tested to successfully resist removal by the standard tape test and showed a good stick between the sprayed films and the PET substrate. The spray-printed film exhibits the same functional performance in the conversion of the X-ray radiation into visible light as the composites obtained by doctor-blade coating. The V.R.I. follows the same trends (results not shown) as the results presented in Figure 5.2b.

To evaluate the performance as a scintillator, the film was printed on a photodetector matrix and selectively illuminated by focusing the incident X-ray beam on different photodetectors. An electronic system with RF communication was used to measure all the photodetectors simultaneously, effectively producing a radiation detector with a large area and evaluating the potential of the scintillator film for imaging applications. Figure 5.4a shows the schematic representation of the photodetector matrix connected to the RF system [31].

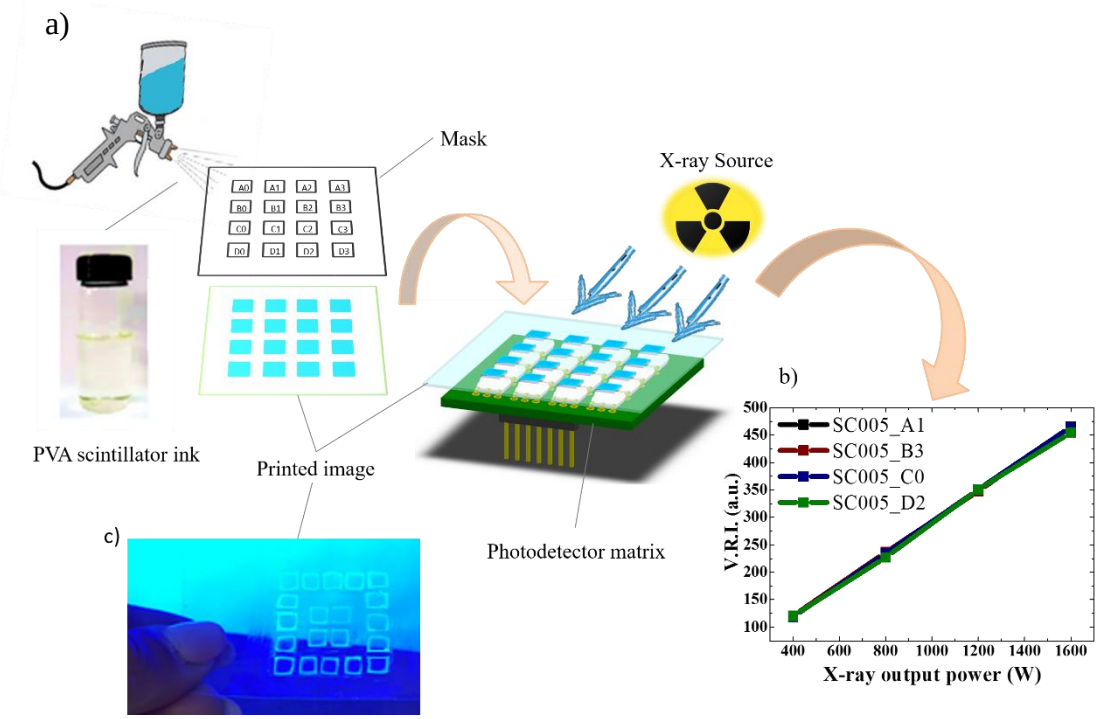

Figure 5.4 - a) Schematic representation of the construction of the prototype of the spray-printed scintillator film; b) variation of the visible radiation intensity (V.R.I.) as a function X-ray output power in different photodetectors of the matrix, c) Visualization of images printed with water-based scintillator ink.

Figure 5.4b shows the variation of the visible radiation intensity (V.R.I.) as a function X-ray output power in different photodetectors of the matrix. The V.R.I. shows an increase with increasing X-ray power, analogous to the samples prepared by doctor-blade coating (Figure 5.2b). Notably, the printed devices exhibit a constant and linear behavior, independently of the selectively illuminated photodetector, indicating a good reproducibility of the printing process and a uniform dispersion of the fillers.

Thus, it is demonstrated that an environmentally-friendly scintillator ink based on PVA allows the developed spray printable scintillator composites to be applied for the fabrication of indirect X-ray detectors.

5.4. Conclusions

A water-based scintillator ink was developed and optimized. The ink formulations include ultrapure water as a solvent and PVA as a binder. The test films were produced

by doctor-blade coating and by spray-printing. The printed films were used for the optimization of the scintillator filler concentration and showed a homogeneous distribution of scintillator nanoparticles. The rheological characterization of the inks suggests that they behave as Newtonian fluids in the dilute regime. The optimized ink with 0.75 wt.% content of scintillator nanoparticles was printed on top of a photodetector matrix as a prototype device, which confirmed a reproducible and linear conversion of the X-ray radiation into visible light by the spray-printed nanocomposite films. This successful prototype device indicates that the ink developed in this work is suitable for the preparation of spray-printed indirect X-ray detectors by a green-solvent approach.

5.5. References

1. Lee, S., et al., Three-dimensional Printing of Silver Microarchitectures Using Newtonian Nanoparticle Inks. ACS Applied Materials and Interfaces, 2017. 9(22): p. 18918-18924.

2. Wisitsoraat, A., et al., Printed organo-functionalized graphene for biosensing applications. Biosensors and Bioelectronics, 2017. 87: p. 7-17.

3. Tematio, C., et al., Design and characterization of conductive biopolymer nanocomposite electrodes for medical applications, in Materials Science Forum2017. p. 1921-1926.

4. Levi, D.S., N. Kusnezov, and G.P. Carman, Smart materials applications for pediatric cardiovascular devices. Pediatric Research, 2008. 63(5): p. 552-558.

5. Nikl, M., Scintillation detectors for X-rays. Measurement Science and Technology, 2006. 17(4): p. R37-R54.

6. Quaranta, A., et al., Optical and scintillation properties of polydimethyl-diphenylsiloxane based organic scintillators. IEEE Transactions on Nuclear Science, 2010. 57(2 PART 2): p. 891-900.

7. Bliznyuk, V.N., et al., New Efficient Organic Scintillators Derived from Pyrazoline. ACS Applied Materials and Interfaces, 2016. 8(20): p. 12843-12851.

8. Righetti, M.C., et al., Thermal and mechanical properties of PES/PTFE composites and nanocomposites. Journal of Applied Polymer Science, 2013. 130(5): p. 3624-3633.

9. Martins, P.M., et al., Gd2O3:Eu Nanoparticle-Based Poly(vinylidene fluoride) Composites for Indirect X-ray Detection. Journal of Electronic Materials, 2014. 44(1): p. 129-135.

10. Basiricò, L., et al., Direct X-ray photoconversion in flexible organic thin film devices operated below 1 v. Nature Communications, 2016. 7.

11. Cai, W., et al., Synthesis of bulk-size transparent gadolinium oxide-polymer nanocomposites for gamma ray spectroscopy. Journal of Materials Chemistry C, 2013. 1(10): p. 1970-1976.

12. Fraboni, B., et al., Organic semiconducting single crystals as solid-state sensors for ionizing radiation. Faraday Discussions, 2014. 174: p. 219-234.

13. Zhao, Y.S., H. Zhong, and Q. Pei, Fluorescence resonance energy transfer in conjugated polymer composites for radiation detection. Physical Chemistry Chemical Physics, 2008. 10(14): p. 1848-1851.

14. Lawrence, W.G., et al., Quantum dot-organic polymer composite materials for radiation detection and imaging. IEEE Transactions on Nuclear Science, 2012. 59(1 PART 2): p. 215-221.

15. Martins, P., et al., Tailored Magnetic and Magnetoelectric Responses of Polymer-Based Composites. ACS Applied Materials and Interfaces, 2015. 7(27): p. 15017-15022.

16. Wei, Y., et al., Highly Stable and Sensitive Paper-Based Bending Sensor Using Silver Nanowires/Layered Double Hydroxides Hybrids. ACS Applied Materials and Interfaces, 2015. 7(26): p. 14182-14191.

17. Deng, H., et al., Progress on the morphological control of conductive network in conductive polymer composites and the use as electroactive multifunctional materials. Progress in Polymer Science, 2014. 39(4): p. 627-655.

18. Obitayo, W. and T. Liu, A review: Carbon nanotube-based piezoresistive strain sensors. Journal of Sensors, 2012. 2012.

19. Khan, S., L. Lorenzelli, and R.S. Dahiya, Technologies for printing sensors and electronics over large flexible substrates: A review. IEEE Sensors Journal, 2015. 15(6): p. 3164-3185.

20. Sousa, R.E., et al., High performance screen printable lithium-ion battery cathode ink based on C-LiFePO4. Electrochimica Acta, 2016. 196: p. 92-100.

21. Hunter, B.S., et al., Low-voltage polymer/small-molecule blend organic thin-film transistors and circuits fabricated via spray deposition. Applied Physics Letters, 2015. 106(22).

22. Khim, D., et al., Spray-printed organic field-effect transistors and complementary inverters. Journal of Materials Chemistry C, 2013. 1(7): p. 1500-1506.

23. Mouret, A., et al., Eco-friendly solvents and amphiphilic catalytic polyoxometalate nanoparticles: A winning combination for olefin epoxidation. Green Chemistry, 2014. 16(1): p. 269-278.

24. Baker, M.I., et al., A review of polyvinyl alcohol and its uses in cartilage and orthopedic applications. Journal of Biomedical Materials Research - Part B Applied Biomaterials, 2012. 100 B(5): p. 1451-1457.

25. Kadajji, V.G. and G.V. Betageri, Water soluble polymers for pharmaceutical applications. Polymers, 2011. 3(4): p. 1972-2009.

26. Bao, C., et al., Poly(vinyl alcohol) nanocomposites based on graphene and graphite oxide: a comparative investigation of property and mechanism. Journal of Materials Chemistry, 2011. 21(36): p. 13942-13950.

27. Kanoun, O., et al., Flexible carbon nanotube films for high performance strain sensors. Sensors (Switzerland), 2014. 14(6): p. 10042-10071.

28. Liu, X., et al., Fabrication of highly a-axis-oriented Gd_2O_3:Eu^{3+} thick film and its luminescence properties. Optical Materials, 2008. 31(2): p. 126-130.

29. Shmurak, S.Z., et al., Spectroscopy of composite scintillators. Physics of the Solid State, 2012. 54(11): p. 2266-2276.

30. Nurmukhametov, R.N., et al., Fluorescence and absorption of a polystyrene-based scintillator exposed to UV laser radiation. Journal of Applied Spectroscopy, 2007. 74(6): p. 824-830.

31. Oliveira, J., et al., Gd_2O_3:Eu^{3+}/PPO/POPOP/PS composites for digital imaging radiation detectors. Applied Physics A: Materials Science and Processing, 2015.

32. Oliveira, J., et al., Increasing X-ray to visible transduction performance of Gd_2O_3:Eu^{3+}/ P(VDF) composites by PPO/POPOP addition. Composites Part B: Engineering, 2016. 91: p. 610-614.

33. Derenzo, S.E., et al., The quest for the ideal inorganic scintillator. Nuclear Instruments and Methods in Physics Research, Section A: Accelerators, Spectrometers, Detectors and Associated Equipment, 2003. 505(1-2): p. 111-117.

34. Voigt, M.M., et al., Gravure printing inverted organic solar cells: The influence of ink properties on film quality and device performance. Solar Energy Materials and Solar Cells, 2012. 105: p. 77-85.

35. Barnes, H.A., J.F. Hutton, and K. Walters, An Introduction to Rheology. 1989: Elsevier.

36. de Gennes, P.G., Scaling Concepts in Polymer Physics. 1979: Cornell University Press.

37. Einstein, A., Eine neue Bestimmung der Moleküldimensionen. 1905: Buchdruckerei K.J. Wyss.

38. Kim, S., et al., Structural Development of Nanoparticle Dispersion during Drying in Polymer Nanocomposite Films. Macromolecules, 2016. 49(23): p. 9068-9079.

39. Dobrynin, A.V., R.H. Colby, and M. Rubinstein, Scaling theory of polyelectrolyte solutions. Macromolecules, 1995. 28(6): p. 1859-1871.

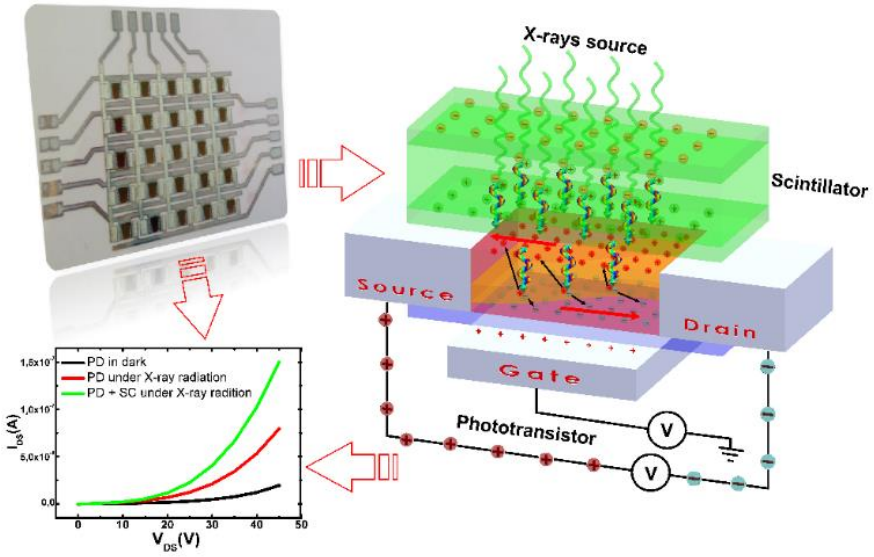

Chapter 6. All-printed indirect X-ray detector based on OTFT photodetectors

In this work, inkjet-printed photodetector array, based on organic thin-film transistor (OTFT) architecture, have been developed and applied for the indirect detection of X-ray radiation using a scintillator ink as X-ray absorber. The about 93% increase of the photocurrent of the photodetectors from about 53 nA under illumination to about 102 nA under X-ray radiation with the scintillator located on top of the photodetector proves the suitability of the developed printed device for X-ray detection applications.

This chapter is based on the following publication: J. Oliveira, V. Correia, E. Sowade, I. Etxebarria, R. D. Rodriguez, K. Y. Mitra, R. R. Baumann, S. Lanceros-Mendez; "*Indirect X-ray detectors based on inkjet-printed photodetectors with a screen-printed scintillator layer"*; ACS Applied Materials & Interfaces, Vol. 10, Issue 15, pp.12904 -12912 (2018)

6.1. Introduction

Photodetectors allow the conversion of light into measurable current signals, being a common component of optoelectronic systems. Photodetectors are thus found in many applications such as automated gates and doors, digital versatile discs (DVD), blue-ray devices, night vision systems, and remote controls [1, 2]. Further, they are also implemented in radiation medical imaging [3], including systems for radiography [4], mammography [5], computed tomography (CT) [6] , spectroscopy devices and integrated sensors for lab-on-a-chip applications [7]. Miniaturization, large-area applicability, selectivity, and high responsivity are key factors that need to be take into account for new developments in this field [8, 9].

The materials typically used for X-ray radiation detection, i.e., conversion of the ionizing radiation into an electrical signal, are mainly based on charge-coupled device (CCD) and complementary metal-oxide-semiconductor (CMOS) technology [2]. However, these methods show limitations regarding the processing into pixelated photodetector matrices applied to large and non-flat areas [10]. The most common material used for this type of radiation photodetector is silicon. Silicon shows limitations related to the low radiation absorption coefficient [11], which results in the need of high thickness silicon layers in order to obtain high performing devices [12, 13]. Nano-structuring of silicon layers can be used to improve the photon absorption, but this approach results in a remarkable cost increase which limits the commercial implementation [14].

Thus, there has been an increasing interest on the development of alternative materials for detecting radiation. In particular, efforts are being directed to the development of a new generation of photodetectors for radiation detection, combining easy manufacturing, flexible and seamless integration capabilities and mechanical flexibility [15]. Besides that, several applications, ranging from security control to industrial and medical diagnostics [16], require thin, conformable sensor panels, with a lower exposure to radiation dose of X-ray imaging systems and for large-area [17]. Printed photodetectors based on organic materials are well-qualified candidates to fulfil the above-mentioned requirements.

All recent investigations related with printed photodetectors have been directly connected with the improvement of light sensitivity yield, the compatibility with silicon and flexible electronics for integration, and should be adapted to low-temperature solution processing [18]. Printed photodetectors show significant advantages in comparison to

solid-state devices. They can have large active areas, can be processed at low temperatures, offer an well-adjustable spectral sensitivity, and they are inexpensive and easily fabricated [12]. Printing technologies are additive processes that allow a patterned material deposition, the economizing of material usage and the manufacturing at competitive costs [19].

Among the different printing techniques, inkjet printing [20-22] is a fully digital technology where the print image is formed by the ejection of single droplets on pre-defined positions of a substrate. The droplets are directly transferred to the substrate without the need for masks which facilitates varying pattern design and customization.

Printed photodetectors are being produced by e.g., inkjet [23], spraying [24, 25] and screen printing [26] based on materials such as polymers, silver nanoparticles, carbon nanotubes [24], metal oxide and even colloidal quantum dots. The combination of low-cost fabrication methods such as printing technologies, represent key advantages of organic semiconductor photodetectors over their silicon-based counterparts [23].

The deposition of multilayer stacks of different functional materials provides a simple form of depositing thick films (some nanometers) layer-by-layer onto a surface of any kind or any shape. Multilayers stacks allow to fabricate a sequence of layers, each layer with specific structure and properties, being a rather general approach for the fabrication of devices. This approach has been successfully applied for the development of multilayer ink-jet printed passive components [27].

In layer-by-layer deposition, the precise structure of each layer depends on a precise set of deposition parameter, which will determine the structure and properties of each layer, but that will allow high level of reproducibility, if the processing parameters are maintained strictly constant [27, 28].

Several concepts have been proposed to promote the advantages of organic semiconductors in medical flat-panel X-ray photodetectors, such as easy processing, flexibility and the possibility of large area fabrication with a low effective cost [29]. Organic photodetectors (OPDs) are very attractive for this application as they are inexpensive and can be flexible showing a promising alternative to silicon-based photodetectors [25, 30]. Organic photodetectors show a strong absorption coefficient, enabling the operation with thin layers. Furthermore, these materials can be tuned to improve the absorption spectra selectivity, as well as the optical bandgap and the electronic transport properties [31, 32]. Most importantly, organic materials are

advantageous in terms of processing since they can be formulated as inks and fabricated by printing technologies, which reduces photodetectors cost [12, 32].

There are two different approaches for medical X-ray detection systems classified as direct and indirect methods [33]. The direct method uses photoconductive materials with high X-ray sensitivity and typically requires high operation bias voltage. The indirect method uses scintillator materials that absorb the X-ray radiation and convert it into visible light [34]. The photodetectors sensitive to visible light convert the light from the scintillator located on top of them into electric signals, thus allowing the indirect detection of X-ray radiation.

Both direct and indirect methods still face limitations and high costs when large areas or flexible applications are required. Polymer composites based on scintillator nanoparticles allow the design and overcome such limitations as well as innovative, novel applications thanks to their high efficiency, flexibility and low-cost production [35].

Several works have explored the use of photodetectors for indirect X-ray detection based either on polymer thin-films filled with scintillator and fluorescence molecules [35, 36], inorganic high-Z nanocomposites [37] or carbon nanotubes [38] to enhance the sensitivity to X-rays and consequently reduce the radiation dose. However, consistent approaches are still required to reach unfailing and reproducible deposition of multilayer stacks of different functional materials.

In this work, a novel device for X-ray indirect detection was developed based on a thin-film transistor organic photodetector architecture fabricated by inkjet and screen printing scintillator inks. A further interesting feature for applications is that the devices were manufactured in a standard laboratory environment (no cleanroom) and at low temperatures compatible with polymer substrates.

6.2. Experimental details

6.2.1. Materials for the fabrication of the photodetectors

Polyethylene naphthalate (PEN) films (Dupont Teijin Q65FA) with a thickness of 125 μm were employed as flexible polymeric substrates. UTDAgIJ1 conductive silver nanoparticle ink from UT DOTS (UT Dots Inc., USA) was applied for the manufacturing of the electrodes. The applied dielectric material was cross-linked poly-4-vinylphenol (c-PVP, PVP purchased from Sigma Aldrich with a Mw. of about 25000). PVP was dissolved at room temperature in 10 mL propylene glycol monomethyl ether acetate

(PGMEA), and magnetically stirred for 3 hours. Poly(melamine-coformaldehyde) methylated (PMFM, from Sigma Aldrich, Mw. of about 432, 84 wt.% in 1-butanol) was added as a crosslinking agent under stirring for 2h. The ratio of PVP to PMFM was 2:1. Before printing, the conductive silver nanoparticle and the dielectric inks were filtered through 0.2 µm syringe filters to ensure the removal of residual agglomerations. FS0096, a p-type polymer from Flexink (Flexink Ltd., UK) dissolved in mesitylene and tetralin mixture was used as amorphous organic semiconductor (OSC).

6.2.2. Fabrication of the printed photodetectors

Inkjet printing was performed with a Dimatix Materials Printer (DMP) 2831 (Fujifilm Dimatix Inc., USA), equipped with 16 nozzles piezoelectric printhead with a nominal drop volume of about 10 pL and a nozzle-to-nozzle spacing of 254 µm. For all the inks, the printing process was carried out with a maximum jetting frequency of 5 kHz and a well-adjusted, optimized control signal (waveform) for each individual ink formulation, as represented in figure 6.1.

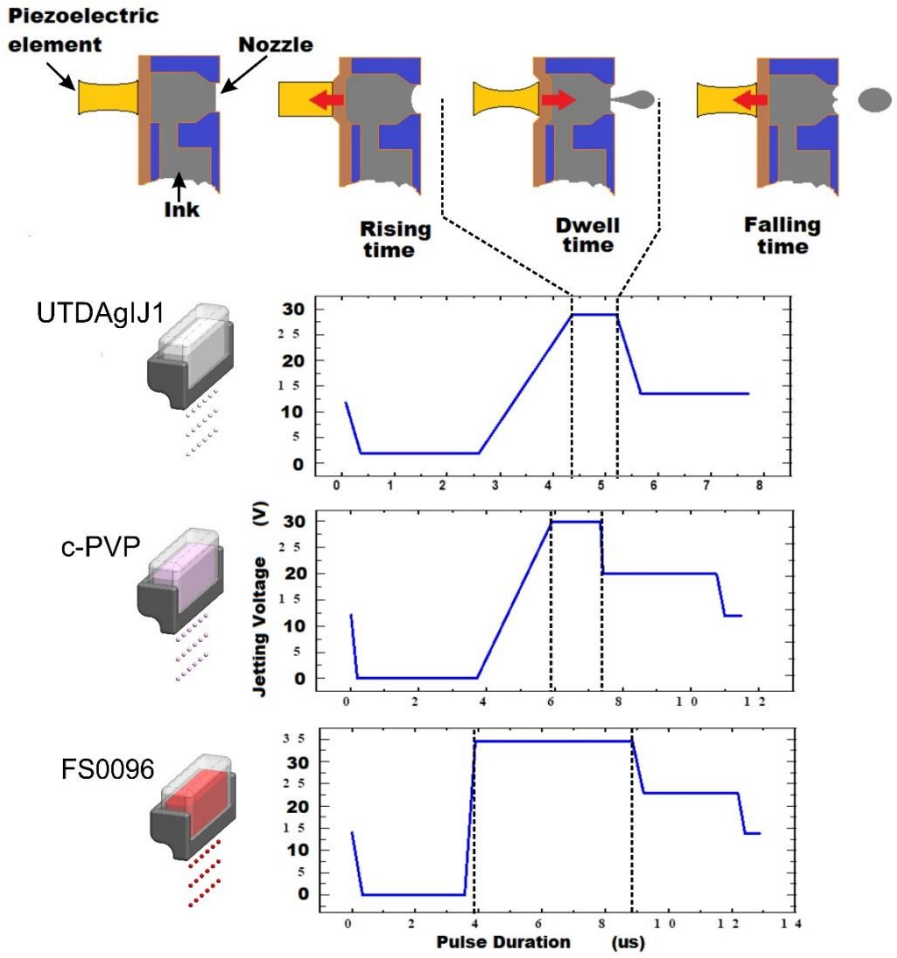

Figure 6.1 - Silver nanoparticles, dielectric and OSC ink jetting waveform.

Figure 6.1 shows the optimized jetting waveforms used for the different ink formulations. The adjustment of the print waveform can be divided into three parts, represented in Figure 6.1: rising time, dwelling time and falling time. The rising time setting allows to define the amount of ink that will be ejected through the nozzle, defining the drop size. The setting of the dwelling time parameters allows to define how the drop leaves the nozzle. Finally, it is necessary to define the shape of the falling time, corresponding to the process of separating the drop from the nozzle, this step being critical to ensure that there is no formation of satellite drops. The maximum drop ejection voltage was 35 V and the drop ejection frequency was limited to 5 kHz for higher repeatability.

Figure 6.2a shows the organic thin-film transistor (OTFT) architecture of the printed photodetectors consisting of four different layers: (i) a bottom gate layer using the silver nanoparticle ink, (ii) an insulating dielectric layer based on c-PVP, (iii) 12 interdigitated

source-drain (S-D) electrodes using the silver nanoparticle ink, and (iv) a semiconducting layer on top of the stack. Further, the 5 x 5 sensors matrix layout is presented in Figure 6.2b. The spacing between S-D electrode fingers in the digital design was 120 µm and represents the channel length of the TFT. The width of the individual finger electrodes in the design was 26000 µm and the channel length was 40 µm.

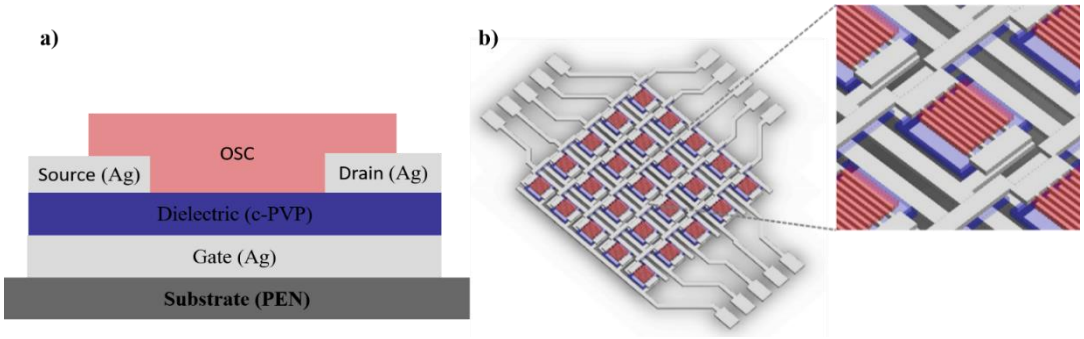

Figure 6.2 - a) Schematic image of the TFT-based photodetector device structure; b) layout of the inkjet printed 5 x 5 photodetector matrix.

Before printing, the PEN substrate was cleaned with ethanol and then dried by a nitrogen flow to remove any remaining particles. For the deposition of the bottom gate, the silver ink was jetted using a print resolution of 635 dpi that corresponds to a drop space of 40 µm. During the process of printing, the cartridge and substrate temperature was set to 35 ºC and 40 ºC respectively. The post-printing procedure for the printed silver layer consisted of drying and sintering in an oven (JP Selecta 2005164) at 150 °C for 30 minutes. Subsequently, two layers of c-PVP were printed using a print resolution of 1270 dpi (drop space of 20 µm), with both the substrate and printhead temperature set to room temperature (~ 28 ºC). Finally, curing of the dielectric layer took place at 150 °C for 30 minutes in an oven. For the S-D electrodes, the silver nanoparticle ink was jetted with print resolution of 635 dpi and just 1 nozzle, in order to achieve higher print accuracy.

The post-printing treatment of the silver layer was the same as indicated earlier. The final layer for the OTFT stack (photodetector) was the OSC, that was printed with a substrate temperature of 35 ºC and printhead temperature set to room temperature (~ 28 ºC). Then, the layer was cured in an oven at 100 ºC for 10 minutes. During the printing, the used drop space was 20 µm and the quality check of the printed patterns was performed using the microscope Leica DM4000 M.

6.2.3. Development and application of the scintillator ink

A polymer-based scintillator ink formulation based on gadolinium oxide doped with europium ($Gd_2O_3:Eu^{3+}$ - GDO) as scintillator material and the fluorescence molecules 2,5-dipheniloxazol (PPO) and 1,4-bis-(2-(5-phenioxazolil))-benzol (POPOP) was formulated following the procedure described in [36]. GDO was selected as scintillator nanoparticles due to the characteristics already mentioned in previous chapters [39-41].

The thermoplastic elastomer copolymer Styrene-Ethylene/Butylene-Styrene (SEBS) Calprene CH-6120, with a molecular weight of 245.33 g/mol and a ratio of Ethylene-Butylene/Styrene of 68/32, supplied by Dynasol was used as the polymer matrix to develop a flexible ink with suitable adhesive properties. It has been proven that this combination of materials is able to efficiently convert X-ray radiation into visible light [34]. Thus, the formulation of the scintillator ink was as follows: 0.5 wt.% of GDO scintillator nanoparticles (Nanograde) and 1 wt% of PPO (Sigma-Aldrich D210404) and 0.01wt.% of POPOP (Sigma-Aldrich P3754) were added to toluene (Panreac with a density of 0.86 g/cm^3 at 20 ^{o}C) and placed for dispersion in an ultrasound bath for 3 hours.

After the complete dispersion of the scintillator nanoparticles and fluorescence molecules, SEBS was added with a ratio of 1:4 (1 g of polymer was added to 4 ml of solvent) to the solution and placed in a Teflon™ mechanical stirrer at 150 rpm until complete dissolution and homogeneous mixing of all components. Finally, a scintillator ink formulation was obtained with a viscosity between 2 and 5 Pa.s suitable for screen printing.

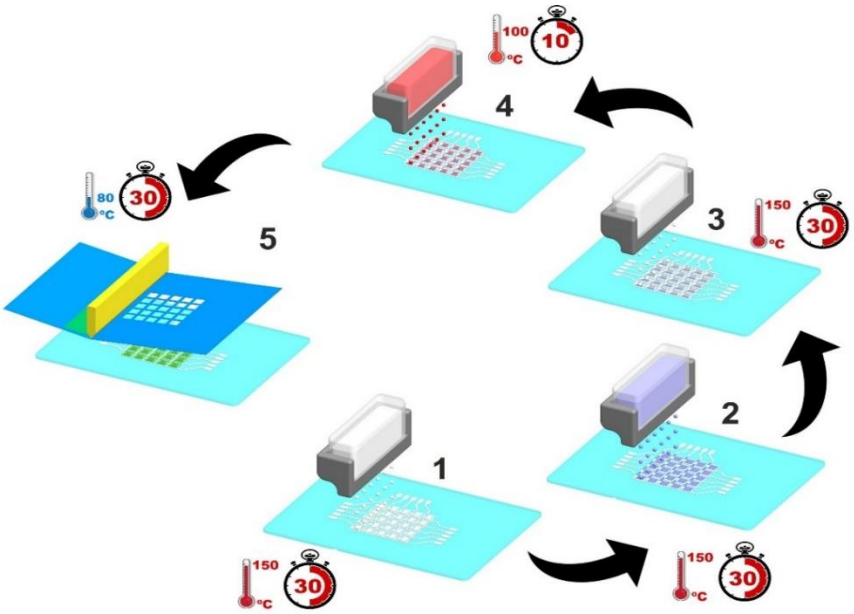

Figure 6.3 - Schematic representation of the printing processes used for the fabrication of the photodetector array and respective cure conditions: inkjet printing of 1) silver bottom layer; 2) dielectric layer of c-PVP ink; 3) silver layer corresponding to the drain and source electrodes; 4) OSC layer and screen-printing of 5) the scintillator ink.

The scintillator ink was deposited on top of the photodetectors by the screen printing technique as represented in Figure 6.3 - process 5, using a home-made manual screen-printing machine. The screen-printer was fabricated in stainless steel and presents a support for the substrate that can be adjusted on the x and y axis. Further, it shows a frame to add and fix the screen mesh that can be adjusted in the z axis to ensure the required distance to the substrate support. A polyester mesh screen was used in the printer. The dimensions of the aluminum frame attached to the mesh was 450 x 350 mm^2 with a profile of 20 × 20 mm^2. The mesh count for the printing screen was 65 threads/cm, the thread diameter was 52 µm, and the square-edged mesh opening was 102 µm. The squeegee orientation angle was set to 45º relative to the print substrate and the tension on the mesh was 20 N. After printing, the samples were oven-cured at 80 °C for 30 minutes. Figure 6.3 summarizes the different steps for the fabrication of the X-ray detection devices.

6.2.4. Characterization of the printed photodetectors

Scanning electron microscopy (SEM) images were obtained with a Zeiss Auriga microscope. The system is equipped with a focused gallium ion beam (FIB) tool Zeiss 1560XB Cross Beam. FIB cuts were performed to obtain cross-sectional images of the layer stack in order to determine the thickness and the structure of the individual layers. Micro Raman spectroscopy experiments were performed under green and infrared laser excitations, 514.7 nm and 532 nm, and 785 nm, respectively. Absorption spectra of the active layers were obtained by using the UV/Vis microreflectance spectrometer TIDAS S MSP 800 (J&M Analytik AG, Esslingen, Germany) connected to a Zeiss Axio Imager M2m microsope. The light source of the microscope was used to illuminate the samples through the microscope objective lenses. The reflected light was collected by the same lenses and guided to the spectrometer by optical fibres. The electrical characterization of the photodetectors is equal to the electrical characterization of an organic thin-film transistor (OTFT). In order to ensure the uniformity and reproducibility of the results, the functionality of the printed photodetectors array was analysed for all 25 OTFT within the array. The percentage of functional OTFTs was over 80% relative to the total number of printed OTFT. This is also the same for different printed OTFT arrays. Furthermore, the photodetector and especially the active, semiconducting layer was exposed to a light source as shown in Figure 6.4.

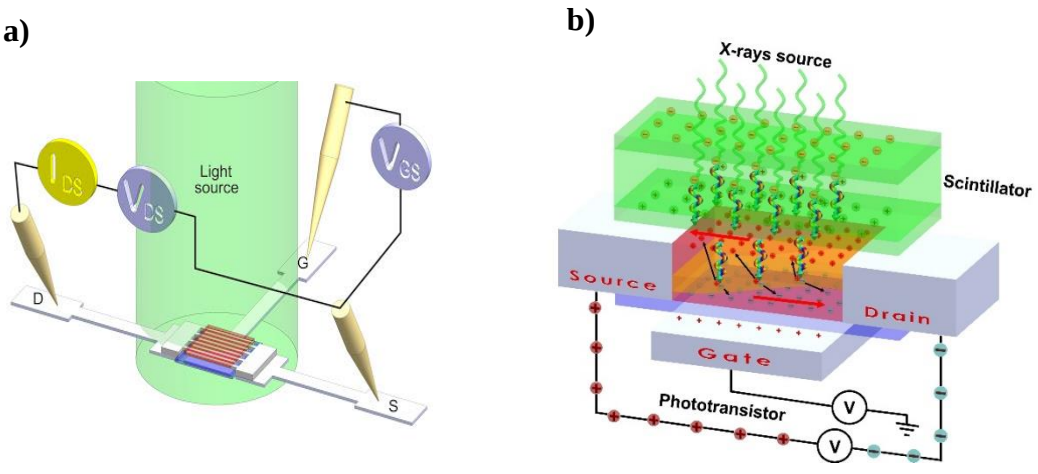

Figure 6.4 - a) Schematic representation of the electrical and functional characterization setup of the transistor-based photodetectors for X-ray detection. The OTFT characterization parameters, voltage drain-source (V_{DS}), current drain-source

(I_{DS}) and voltage gate-source (V_{GS}) were measured, using the terminals drain (D), source (S) and gate (G); b) schematic representation of the experimental procedure with the final device, with the scintillator placed on top of the photodetectors, and representation of the main physical process taking place in the all-printed device.

The electrical measurements were performed with the QuadTech 1920 Precision LCR Meter. The electrical operation properties of the printed photodetectors were characterized with a 2400 source/meter and a 6457 picoammeter with integrated voltage source from Keithley (Keithley Instruments, Cleveland, OH, USA) controlled by LABView program developed for current vs. voltage (I-V) characteristic measurements. The probe station was directly connected to the photodetector using gold-coated round tips. The IEEE1620 standard test method was used for the characterization of the organic transistors. All measurements were performed at room temperature, in dark and multi-wavelength light conditions, achieved with a broadband Xenon arc lamp (Xenon XBO 75W/2 OFR, Osram, Munich, Germany) coupled via a 44-position bandpass filter wheel and appropriate focusing optics to a 100 μm core diameter multimode fibre, that allows to obtain a wavelength variation between 362 nm and 1000 nm. The I_{DS}-V_{DS} curve was obtained applying a fixed V_{GS} when a light source was focused on the active area of the photodetector. The process was made for each wavelength (between 400 nm to 700 nm) and for each different applied V_{GS} (from 5 to 45 V).

The performance of the printed photodetector under X-ray radiation with and without the printed scintillator layer was measured by subjecting the samples to the X-ray radiation produced by a Bruker D8 Discover diffractometer using Cu Kα incident radiation (wavelength of 1.54056 angstroms) and in same conditions referred in Chapter 2 in section 2.2.3. The efficiency of the X-ray to visible conversion was evaluated with an electronic measurement system that allows to quantify the emitted visible wavelength radiation, as described in previous chapters.

6.3. Results and discussion

The microstructure and the thickness of the printed layers for the printed photodetectors were obtained by the scanning electron microscopy (SEM) as shown in

Figure 6.5 a). The cross-sectional images were obtained by partial material removal using a FIB.

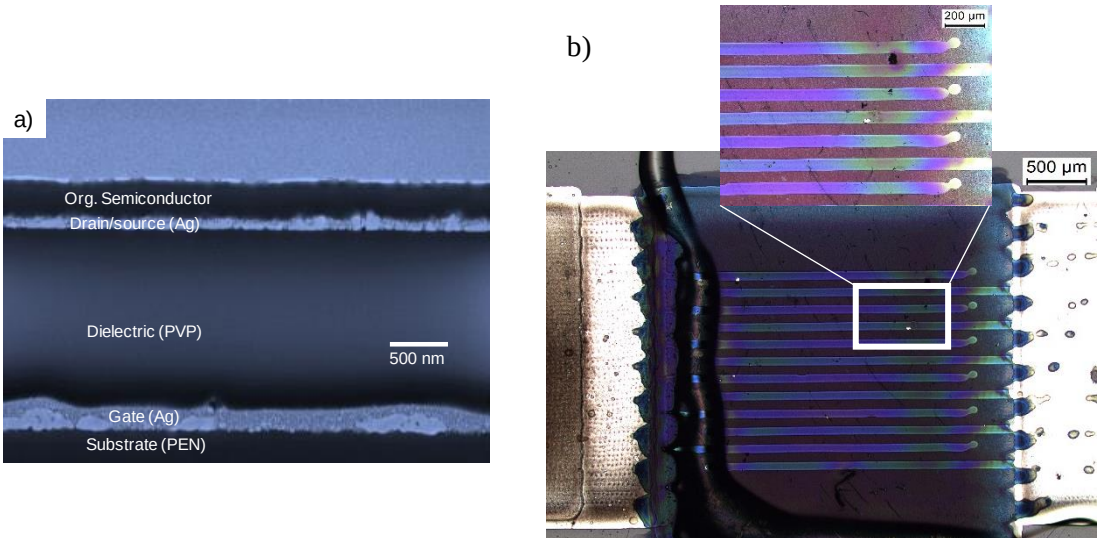

Figure 6.5 - a) Cross-section analysis by scanning electron microscopy of the organic printed photodetector showing the different layers of the heterostructure. b) photograph of the TFT channel with a width of about 26000 µm and a channel length of about 57 µm.

In Figure 6.5 a), it is observed that the silver electrodes are comparably rough and depending on the lateral position with different microstructural morphology, *e.g.* silver nanoparticle agglomerations are observed along the layer. The average layer thickness of the gate electrode is about 200 ± 40 nm. The average layer thickness of the S-D electrodes is just half of the gate electrode with about 100 ± 30 nm. The dielectric has a thickness of about 1500 ± 30 nm and the organic semiconductor a thickness of about 300 ± 30 nm. The different layer thicknesses are caused by the substrate ink interaction of the different ink formulations and by the different print parameters indicated in the experimental section.

The UV/Vis micro-reflectance spectroscopy was performed for the OSC layer and is show in figure 6.6a. The OSC layer absorbs radiation with a wide and large band in the range of approximately 550 nm to 700 nm and narrower less intense bands below 430 nm and in the range of about 830 to 950 nm.

The interface between the metal contact electrode, the dielectric and the organic semiconductor at the device channel plays a crucial role with regard to the performance

of any organic semiconductor device [42]. In organic photodetectors, a field in which electrons and holes play various roles in determining the functionality and performance of organic devices, e.g., charge injection/extraction, charge separation, and charge transport are highly dependent on the quality and reliability of the interface of the printed devices. Carrier injection from metal electrodes to semiconductors and its electrical transport are important key factors in electronic devices [43-45]. Thus, the choice of the electrodes is as important as the selection of organic semiconductor (OSC). In order to evaluate the metal electrode/polymer interface, Raman spectroscopy was performed (Figure 6.6b). It was observed that the interaction with the metal electrode affects some of the Raman modes marked by asterisks (*) in Figure 6.6b. It is also observed from the photoluminescence (PL) spectra averaged over the channel and electrode regions (excitation wavelength of PL spectra is 532 nm), Figure 6.6c and 6.6d, respectively, that the photon emission from the organic semiconductor gets quenched for the polymer located at the electrode region. This slight quenching is spectrally selective affecting the emission band located around 733 nm. This is contrary to the case of the band at 775 nm that experiences a slight increase over the electrode region with respect to the channel. Figure 6.6e shows the PL intensity map averaged over the emission range from 660 nm to 830 nm, where the PL quenching over the electrode at the bottom side of the image is clearly visible. In figure 6.6f it is shown the intensity ratio map between the bands at 733 nm and 778 nm. These results are particularly interesting because they show a way to increase the light emission and so the performance of the device as an X-ray detector, for example, by decreasing the lateral dimensions of the interdigitated electrodes. Indeed, the Ag electrodes act as a pool of charge carriers that result in a de-doping effect on the polymer quenching the emission band [46]. According to the position of Raman modes that are affected, we can tentatively attribute these vibrations to the carbon vibrations shown in figure 6.6b.

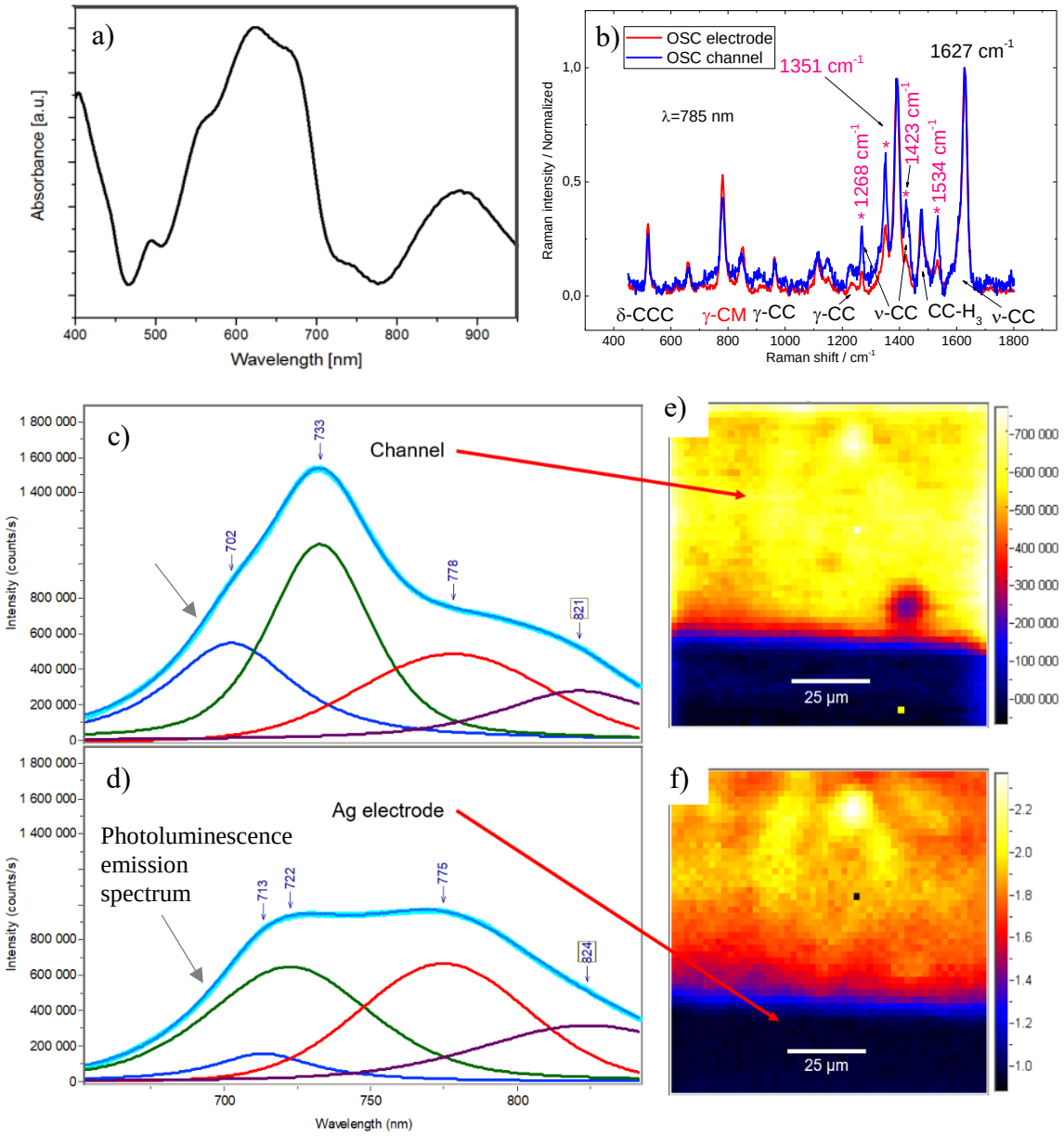

Figure 6.6 - a) UV/Vis micro-reflectance spectra of OSC layer; b) Raman spectra averaged over the Ag electrode and channel regions. The different modes affected by the interaction of the polymer with the electrode are marked by asterisks (*); The photoluminescence emission spectra (light blue curve) averaged over the channel region c) and the electrode region d) with different modes deconvolved by fitting with 4 different emission bands (blue, red, green and purple curves); e) The emission map shown for the intensity within the spectral region around 733 nm. f) Map obtained from the intensity ratio between the emission around 733 nm and 775 nm.

The absorbance spectrum of the OSC layer is very important for the operation principle of photodetector, since the indirect detection method is used with a scintillator,

positioned or printed over the photodetector array, converting X-ray radiation in visible light [47]. The emitted visible light from scintillator interacts with the active material of the photodetector and should be converted into electron-hole pairs, which represents the imaging charge [48]. Therefore, the OSC layer of the printed photodetector needs to generate photo-activated charge carriers because of the radiation of the scintillator. Most of the available OSC with Highest Occupied Molecular Orbital - Lowest Unoccupied Molecular Orbital (HOMO-LUMO) band gap energy ranging from 1.5 - 3.0 eV show photo-induced charge carrier effects in the visible light spectrum of about 400 nm to 700 nm. Based on the maximum absorbance of the OSC layer, the band gap energy is about 1.70 eV.

The photodetector needs to be functional in the range of the visible radiation wavelength. Thus, a correct selection of the OSC is necessary which should be suitable for the required application and the detected light should also have a matching within a wavelength range that matches the absorption spectrum of the active layer and scintillator material [49, 50]. In this case, the OSC should be suitable to wavelengths on the visible light range. This fact is due to the absorption/emission spectra and quantum efficiency of the scintillator material, which converts the X-ray radiation into visible radiation. During the scintillation process, several relaxation processes occurs and leads to a large number of relaxed electron-hole pairs which are transferred to states of lower energy and the corresponding emission of light (Figure 6.4b), as explained on previous Chapter 4 in section 4.3. The fluorescence molecules (POPOP and PPO) absorb this scintillation energy and re-emits at higher wavelength, in the visible wavelength range that should be detected for the active material of the photodetector, inducing the photogenerated charge carriers in the OSC [51]. Under a potential difference (external bias on the device) those carriers will result in a current increase, as represented on Figure 6.4b.

To evaluate the electrical response and performance of the printed photodetectors, the I-V characteristics were measured in dark and under illumination. The wavelength for the illuminated measurement method (about 630 nm) was selected in order to match the maximum absorbance of the active layer present in the photodetector, in order to absorb in the spectral region were the emission of the scintillating material. The spectral peak of the photodetector absorbance should be matching with the visible light radiation as an assumed requirement to maximize application sensitivity to the application [1, 52].

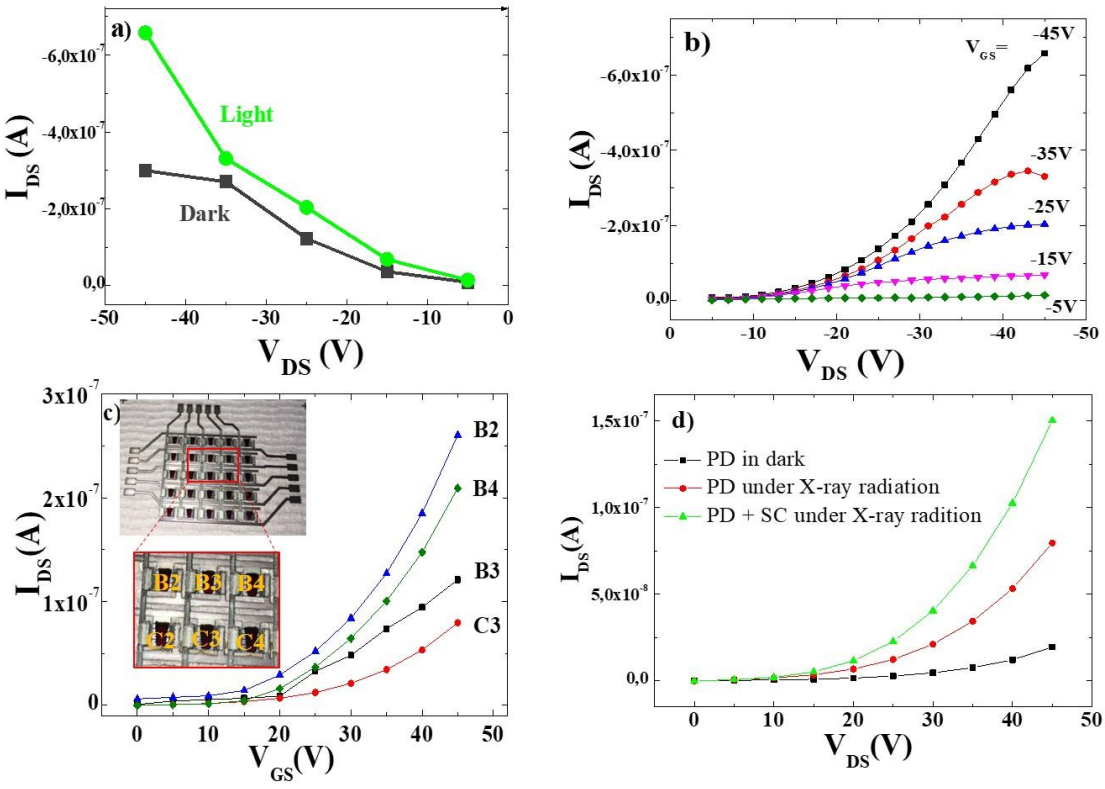

Figure 6.7 - a) I–V characteristics of the printed photodetectors (PD) measured in dark and under light radiation (630 nm) as a function of the applied drain-source voltage; b) I-V output curved for the PD under illumination; c) Electrical response of randomly-selected PD from the 5 x 5 TFT matrix (channel: length of 57 µm, width of 26000 µm (image in the inset)), under X-ray radiation ($P_{X\text{-ray beam}}$ = 1600 W and a voltage applied on system of 45 V), as a function of the gate-source voltage; d) I-V curves of one of the single PD present in the PD array in dark (black curve), and under X-ray radiation with (green curve) and without (red curve) scintillator (SC) film (B2, B3, B4 and C3 are the nomenclature used to identify each PD: the different PD on the array are identified by a letter, which corresponds to the line, and with a number, which indicates the column of the 5 x 5 PD array), as a function of the drain-source voltage ($P_{X\text{-ray beam}}$ = 1600 W and a voltage applied bias of 45 V).

Figure 6.7a shows the electrical characteristics of the photodetector array obtained from I–V measurements in dark and under light radiation with a wavelength of about 630 nm. At -45 V bias, the dark current was about 300 nA, while under illumination the photocurrent was more than doubled with about 660 nA. It is concluded that the photodetector under illumination shows an increase in the drain-source current of

approximately 120% with respect to the device under dark. This indicates a good performance of the printed device to be used as a photodetector, relative with the photodetectors present in literature, which present photocurrents in the range of 20 to 200 nA [23, 53, 54]. The wavelength of illumination is in the spectral range response of the active layer (OSC layer) present on the photodetector array. The performance of the photodetector array was measured considering different applied negative voltages, 5, 15, 25, 35 and 45 V, respectively. Figure 6.7b shows that the printed photodetector array has its maximum response at 45 V.

After that, the electrical response of the photodetector array (PD in Figure 6.7. Image in the inset of Figure 6.7c) was evaluated under X-ray radiation. The Figure 6.7c shows that the photodetector matrix has a consistent response, with the same electrical behavior when the radiation was applied independently of the single pixel, i.e. when the radiation is applied to every single photodetector, the electrical response is the same, independently of the photodetector within the array. The consistent response demonstrates the uniformity of the photodetectors response within the array, which is also extended to different photodetector arrays, as expected due to the reproducibility of printing technologies for device fabrication. For the indirect detection, the scintillator material used (SC in the graph, Figure 6.7d) was printed on top of the photodetector matrix by screen printing technology as described in experimental section. The printed film has a thickness of around 30 µm and a transmittance of about 70 %, measured by Ultraviolet–Visible (UV-VIS) spectroscopy in a range between 200 to 800 nm with a 1 nm step in a UV-2501PC spectrometer, in order to allow the light passing through it to the OSC layer.

The intensity of the converted visible radiation of this scintillator printed film increases with increasing X-ray output power. The scintillator nanoparticles content was optimized for this specific scintillator based on the work already reported [36] in order to have a higher number of produced visible photons [55]. It is to notice that other scintillator nanoparticles could be used, such as Gd_2O_2S:Tb [56], Lu_2O_3:Eu [57] and Gd_2O_2S:Eu [58] but, in this case, the specific scintillator output spectra should be taken into consideration to design and fabricate the specific photodetector in order to maximize visible to electrical signal conversion. Figure 6.7d shows the response of the photodetector under X-ray radiation. The conditions of the X-ray power, voltage of 40 kV and a power from 0 to 1600 W were optimized based on previous chapters [34, 35]. In the following, the results with a $P_{X\text{-ray beam}}$ of 1600 W are shown. At lower X-ray power, the trend is the same as at 1600 W. After analysing the stability of the of the device upon ten X-ray radiation on/off

cycles, the printed photodetector shows a stability of the signal of 98% for V_{DS} from 20 to 45 V, being therefore the variations within experimental error and therefore, no radiation aging is detected. The current intensity shows an increase with increasing applied voltage. At higher voltages (45 V) a higher electrical response of the photodetector under X-ray radiation (53 nA) is observed in comparison with the photodetector in dark (19 nA). This increase is more pronounced when the scintillator material is on top of the photodetector (102 nA). This represents an increase of the current intensity of about 93% and proves the good performance of the printed scintillator material. The printed X-ray detector responsivity is approximately 1.457 µA/W, under X-ray irradiation. Thus, in this work the development of a novel generation of flexible, all printed, and large-area devices applied on fields like security or medical imaging, for the detection of X-ray radiation was successfully demonstrated.

6.4. Conclusions

The development of a novel generation of all printed and flexible indirect X-ray detectors based on polymer-based scintillator inks and inkjet printed photodetector TFT-based array has been successfully demonstrated.

The electrical response of the photodetector shows a dark current about 300 nA, while under illumination the photocurrent was about 660 nA, which corresponds to an increase of around 120 %, demonstrating the good performance of the printed device as a photodetector. Regarding to the performance as X-ray detection, after printing the scintillator ink, it was observed a higher electrical response of the photodetector under X-ray radiation (53.1 nA) in comparison with the photodetector in dark (19.5 nA). This increase is strongly improved when the scintillator material is on top of the photodetector (102.4 nA). This increase of 93 % in the current intensity of the device under X-ray radiation shows the suitability of the printed scintillator and all the devices for applications in the X-ray radiation detection area, concerning the results already reported [29, 59] of different photodetectors for indirect X-ray detection. Thus, a novel all-printed X-ray detection device for indirect radiation detector was manufactured with a combination of two different printing methods, inkjet and screen printing. These devices show a very promising performance for emerging large-area and low-cost flexible optoelectronics, which can be applied to, *e.g.*, medical imaging or security industry.

6.5. References

1. Yotter, R.A. and D.M. Wilson, *A review of photodetectors for sensing light-emitting reporters in biological systems.* IEEE Sensors Journal, 2003. **3**(3): p. 288-303.

2. Spahn, M., *X-ray detectors in medical imaging.* Nuclear Instruments and Methods in Physics Research, Section A: Accelerators, Spectrometers, Detectors and Associated Equipment, 2013. **731**: p. 57-63.

3. Pacella, D., *Energy-resolved X-ray detectors: The future of diagnostic imaging.* Reports in Medical Imaging, 2015. **8**: p. 1-13.

4. Spahn, M., *Flat detectors and their clinical applications.* European Radiology, 2005. **15**(9): p. 1934-1947.

5. Pani, S., et al., *High energy resolution hyperspectral X-ray imaging for low-dose contrast-enhanced digital mammography.* IEEE Transactions on Medical Imaging, 2017. **36**(9): p. 1784-1795.

6. Cole, L.E., et al., *Gold nanoparticles as contrast agents in X-ray imaging and computed tomography.* Nanomedicine, 2015. **10**(2): p. 321-341.

7. Pais, A., et al., *High-sensitivity, disposable lab-on-a-chip with thin-film organic electronics for fluorescence detection.* Lab on a Chip, 2008. **8**(5): p. 794-800.

8. De Fazio, D., et al., *High Responsivity, Large-Area Graphene/MoS2 Flexible Photodetectors.* ACS Nano, 2016. **10**(9): p. 8252-8262.

9. Xie, C. and F. Yan, *Flexible Photodetectors Based on Novel Functional Materials.* Small, 2017. **13**(43).

10. Liu, N., et al., *Large-area, transparent, and flexible infrared photodetector fabricated using P-N junctions formed by N-doping chemical vapor deposition grown graphene.* Nano Letters, 2014. **14**(7): p. 3702-3708.

11. Casalino, M., et al., *State-of-the-art all-silicon sub-bandgap photodetectors at telecom and datacom wavelengths.* Laser and Photonics Reviews, 2016. **10**(6): p. 895-921.

12. Pace, G., et al., *Printed photodetectors.* Semiconductor Science and Technology, 2015. **30**(10).

13. Wegrzecka, I. and M. Wegrzecki, *Silicon photodetectors - The state of the art.* Opto-electronics Review, 1997(2): p. 137-146.

14. Baeg, K.J., et al., *Organic light detectors: Photodiodes and phototransistors.* Advanced Materials, 2013. **25**(31): p. 4267-4295.

15. Koppens, F.H.L., et al., *Photodetectors based on graphene, other two-dimensional materials and hybrid systems.* Nature Nanotechnology, 2014. **9**(10): p. 780-793.

16. Wojciechowski, J.R., et al., *Organic photodiodes for biosensor miniaturization.* Analytical Chemistry, 2009. **81**(9): p. 3455-3461.

17. Basiricò, L., et al., *Direct X-ray photoconversion in flexible organic thin film devices operated below 1v.* Nature Communications, 2016. **7**.

18. Konstantatos, G. and E.H. Sargent, *Nanostructured materials for photon detection.* Nature Nanotechnology, 2010. **5**(6): p. 391-400.

19. Kang, B.J., C.K. Lee, and J.H. Oh, *All-inkjet-printed electrical components and circuit fabrication on a plastic substrate.* Microelectronic Engineering, 2012. **97**: p. 251-254.

20. Piqué, A. and D.B. Chrisey, *Direct-write Technologies for Rapid Prototyping Applications: Sensors, Electronics, and Integrated Power Sources*. 1st ed, ed. s. Edition. 2002: Elsevier.

21. Singh, M., et al., *Inkjet printing-process and its applications.* Advanced Materials, 2010. **22**(6): p. 673-685.

22. Seifert, T., et al., *Additive manufacturing technologies compared: Morphology of deposits of silver ink using inkjet and aerosol jet printing.* Industrial and Engineering Chemistry Research, 2015. **54**(2): p. 769-779.

23. Lilliu, S., et al., *Inkjet-printed organic photodiodes.* Thin Solid Films, 2011. **520**(1): p. 610-615.

24. Falco, A., et al., *Fully-sprayed and flexible organic photodiodes with transparent carbon nanotube electrodes.* ACS Applied Materials and Interfaces, 2014. **6**(13): p. 10593-10601.

25. Tedde, S.F., et al., *Fully spray coated organic photodiodes.* Nano Letters, 2009. **9**(3): p. 980-983.

26. Pierre, A. and A.C. Arias. *High-detectivity printed organic photodiodes for large area flexible imagers*. in *Technical Digest - International Electron Devices Meeting, IEDM*. 2017.

27. Correia, V., et al., *Design and fabrication of multilayer inkjet-printed passive components for printed electronics circuit development.* Journal of Manufacturing Processes, 2018. **31**: p. 364-371.

28. Batool, S., et al., *Layer-by-layer fabrication of nacre inspired epoxy/MMT multilayered composites.* Journal of Applied Polymer Science, 2018. **135**(14).

29. Büchele, P., et al., *X-ray imaging with scintillator-sensitized hybrid organic photodetectors.* Nature Photonics, 2015. **9**(12): p. 843-848.

30. Krebs, F.C., et al., *A round robin study of flexible large-area roll-to-roll processed polymer solar cell modules.* Solar Energy Materials and Solar Cells, 2009. **93**(11): p. 1968-1977.

31. Sahu, S. and A.J. Pal. *Photodetectors based on organic semiconductors: Optimization of device architectures*. in *Proceedings of the 14th International Workshop on the Physics of Semiconductor Devices, IWPSD*. 2007.

32. Pierre, A., et al., *High Detectivity All-Printed Organic Photodiodes.* Advanced Materials, 2015. **27**(41): p. 6411-6417.

33. Rocha, J.G., et al., *X-ray image detector based on light guides and scintillators.* IEEE Sensors Journal, 2009. **9**(9): p. 1154-1159.

34. Oliveira, J., et al., *Increasing X-ray to visible transduction performance of* $Gd_2O_3:Eu^{3+}$/ P(VDF) *composites by PPO/POPOP addition.* Composites Part B: Engineering, 2016. **91**: p. 610-614.

35. Oliveira, J., et al., $Gd_2O_3:Eu^{3+}$*/PPO/POPOP/PS composites for digital imaging radiation detectors.* Applied Physics A, 2015. **121**(2): p. 581-587.

36. Oliveira, J., et al., *Stretchable scintillator composites for indirect X-ray detectors.* Composites Part B: Engineering, 2018. **133**: p. 226-231.

37. Kang, Z., et al., *CdTe quantum dots and polymer nanocomposites for x-ray scintillation and imaging.* Applied Physics Letters, 2011. **98**(18).

38. Boucher, R.A., et al., *A carbon nanotube based x-ray detector.* Nanotechnology, 2016. **27**(47).

39. Paik, T., et al., *Designing tripodal and triangular gadolinium oxide nanoplates and self-assembled nanofibrils as potential multimodal bioimaging probes.* ACS Nano, 2013. **7**(3): p. 2850-2859.

40. Cai, W., et al., *Synthesis of bulk-size transparent gadolinium oxide-polymer nanocomposites for gamma ray spectroscopy.* Journal of Materials Chemistry C, 2013. **1**(10): p. 1970-1976.

41. Gu, M., et al., *Preparation and luminescence properties of transparent Gd2O3:Eu thick film.* Guang Pu Xue Yu Guang Pu Fen Xi/Spectroscopy and Spectral Analysis, 2010. **30**(3): p. 603-606.

42. Sirringhaus, H., N. Tessler, and R.H. Friend, *Integrated optoelectronic devices based on conjugated polymers.* Science, 1998. **280**(5370): p. 1741-1744.

43. Kanagasekaran, T., et al., *A new electrode design for ambipolar injection in organic semiconductors.* Nature Communications, 2017. **8**(1).

44. Yamane, H., et al., *Impact of interface geometric structure on organic-metal interface energetics and subsequent films electronic structure.* Journal of Electron Spectroscopy and Related Phenomena, 2009. **174**(1-3): p. 28-34.

45. Koch, N., et al., *Influence of molecular conformation on organic/metal interface energetics.* Chemical Physics Letters, 2005. **413**(4-6): p. 390-395.

46. Furukawa, Y., *Electronic absorption and vibrational spectroscopies of conjugated conducting polymers.* Journal of Physical Chemistry, 1996. **100**(39): p. 15644-15653.

47. Antonuk, L.E., et al., *Strategies to improve the signal and noise performance of active matrix, flat-panel imagers for diagnostic X-ray applications.* Medical Physics, 2000. **27**(2): p. 289-306.

48. Nikl, M., *Scintillation detectors for X-rays.* Measurement Science and Technology, 2006. **17**(4): p. R37-R54.

49. Coling, D. and B. Kachar, *Principles and application of fluorescence microscopy*. Vol. 14. 2001, California.

50. Ploem, J.S. and H.J. Tanke, *Introduction to fluorescence microscopy*. Vol. 10. 1987: Oxford University Press.

51. Derenzo, S.E., et al., *The quest for the ideal inorganic scintillator.* Nuclear Instruments and Methods in Physics Research, Section A: Accelerators, Spectrometers, Detectors and Associated Equipment, 2003. **505**(1-2): p. 111-117.

52. Kubitscheck, U. and P. Reiner, *Fluorescence Microscopy: From Principles to Biological Applications*. Fluorescence Microscopy: From Principles to Biological Applications. 2013, Germany: Wiley-VCH.

53. Li, Y., et al., *All Inkjet-Printed Metal-Oxide Thin-Film Transistor Array with Good Stability and Uniformity Using Surface-Energy Patterns.* ACS Applied Materials and Interfaces, 2017. **9**(9): p. 8194-8200.

54. Sowade, E., et al., *Up-scaling of the manufacturing of all-inkjet-printed organic thin-film transistors: Device performance and manufacturing yield of transistor arrays.* Organic Electronics: physics, materials, applications, 2016. **30**: p. 237-246.

55. Martins, P.M., et al., *Gd2O3:Eu Nanoparticle-Based Poly(vinylidene fluoride) Composites for Indirect X-ray Detection.* Journal of Electronic Materials, 2014. **44**(1): p. 129-135.

56. Cha, B.K., et al., *Fabrication and imaging characterization of high sensitive CsI(Tl) and Gd2O2S(Tb) scintillator screens for X-ray imaging detectors.* Radiation Measurements, 2010. **45**(3-6): p. 742-745.

57. Kalyvas, N., et al., *Studying the luminescence efficiency of Lu 2O 3:Eu nanophosphor material for digital X-ray imaging applications.* Applied Physics A: Materials Science and Processing, 2012. **106**(1): p. 131-136.

58. Seferis, I., et al., *Light emission efficiency and imaging performance of Lu2O 3:Eu nanophosphor under X-ray radiography conditions: Comparison with Gd2O2S:Eu.* Journal of Luminescence, 2014. **151**: p. 229-234.

59. Starkenburg, D.J., et al., *Thin film organic photodetectors for indirect X-ray detection demonstrating low dose rate sensitivity at low voltage operation.* Journal of Applied Physics, 2017. **122**(22).

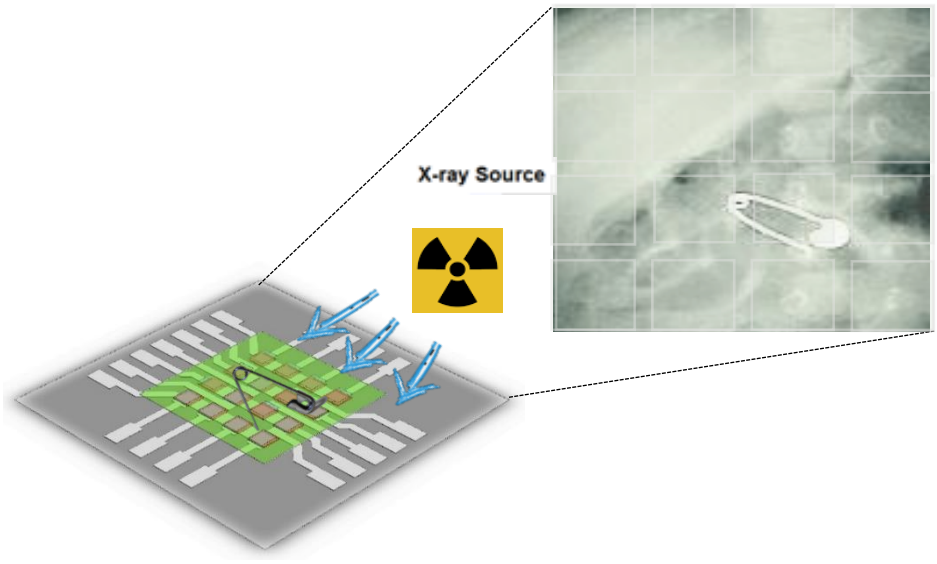

Chapter 7. Conclusions and future work

This chapter presents the main conclusions of the work, devoted to the development of polymer-based scintillator composites for indirect X-ray radiation detectors. Further, some suggestions for future works are also provided.

7.1. Conclusion

The development of polymer-based scintillator materials has been demonstrated as a suitable approach for the fabrication of a new generation of flexible and large area radiation detectors. Those materials can be produced based on different polymer matrix composites from thermoplastics and thermoplastic elastomers as well as using polymers with intrinsic scintillation behavior. Indirect X-ray radiation detectors are mainly based on scintillator materials that convert X-ray into visible radiations, latter read by photodetectors. Thus, high performance scintillating layers have to be developed, compatible with high throughput processing techniques, such as printing technologies.

In this scope, the present work has produced novel polymer matrix composite formulations for X-ray radiation detectors that can be processed by solvent casting as well as by different printing technologies such as spray and screen printing. This approach allows to overcome of the current limitation on the application of X-ray detectors in large areas and extend the applicability to the development of flexible and even stretchable solutions.

Thus, thin polymer-based scintillators have been developed by combining scintillating $Gd_2O_3:Eu^{3+}$ nanoparticles with 2,5 diphenyloxazol (PPO) and (1,4-bis (2-(5-phenioxazolil))-benzol (POPOP) fluorescence molecules and different polymer matrix. First, a biocompatible and non-biodegradable polymer, poly(vinylidene fluoride - P(VDF)) was used for applications in biomedical imaging. The inclusion of fluorescence molecules allows to achieve higher yield of visible light output, allowing the X-ray incident radiation. It has been shown that the introduction of fluorescence molecules has no influence in the main polymer characteristics, including polymer phase, slightly decreases the optical transmittance of the composites films (8%) and increases the visible light output in 40%. Also, it has been proven that the introduction of fluorescence molecules in the scintillator composites is a suitable strategy for improving the overall X-ray to visible light conversion efficiency of the materials without sacrificing the homogeneity and transparency, allowing the development large area and/or flexible polymer-based X-ray detectors.

Further, polystyrene was introduced as the polymer matrix as it shows intrinsic scintillator characteristics and it is a synthetic polymer with high temperature stability and radiation resistance, as well as high transparency over a broad spectral range ($\lambda > 290$ nm). It has been demonstrated that despite the introduction of fluorescence molecules and scintillator nanoparticles decreases the optical transmittance of the composites films

in ≈50%, the visible light yield increases 2000% at a 1600 W X-ray output power with the inclusion of fluorescence molecules and $Gd_2O_3:Eu^{3+}$ nanoparticle filler content of 7.5 wt.%.In order to achieve novel materials to apply in the area of stretchable electronics, a polymer-based scintillator material has been developed based on thermoplastic elastomer Styrene-Ethylene/Butadiene-Styrene (SEBS) composites. As in the previous cases, $Gd_2O_3:Eu^{3+}$ was used as active scintillator material and PPO and POPOP as fluorescence molecules. Thus, a new type of flexible and stretchable composite material for indirect X-ray detectors was developed simple and low-cost fabrication.

The developed composites show suitable optical properties in the visible spectral range with an optical transmittance of ~70%. Further, the composite maintains excellent mechanical properties and elasticity after the application of strains up to 100%. Further, it was concluded that the stretching process does not significantly affects the X-ray to visible light conversion characteristics, proving to be an efficient approach for the development of large area stretchable and flexible polymer-based X-ray detectors.

Finally, a more environmentally-friendly and low-cost approach has been explored for the fabrication of flexible devices to be implemented by printing technologies. Thus, water-based scintillator inks were produced by combining the thermoplastic elastomer poly(vinyl) alcohol (PVA) with scintillator nanoparticles and fluorescence molecules. Scintillator films were prepared both by spray printing and by doctor-blade in order to achieve the best concentration of the scintillator particles (0.75 wt.%) and also the best properties of the scintillator ink. This optimized ink formulation exhibits a Newtonian behavior with a viscosity around 0.1 Pa.s. The performance of the ink was evaluated by printing on a photodetector matrix and selectively illuminated by focusing the incident X-ray beam on different photodetectors, presents on the array, confirming a reproducible and linear conversion of the X-ray radiation into visible light. This successful prototype device indicates that the developed ink is suitable for the preparation of spray-printed indirect X-ray detectors by a green-solvent approach.

Once novel scintillator composites were developed, a functional all-printed prototype was fabricated in order to fully demonstrate the potential of the technological approach. First, an inkjet-printed 5 x 5 photodetector array was fabricated based on an organic thin-film transistor (OTFT) architecture and applied for the indirect X-ray radiation detection using a scintillator ink as X-ray absorber. The architecture of each printed photodetectors consisting on four different layers: a bottom gate layer using the silver nanoparticle ink, an insulating dielectric layer based on c-PVP, 12 interdigitated source-drain (S-D)

electrodes using the silver nanoparticle ink, and a semiconducting layer on top of the stack. The spacing between S-D electrode fingers in the digital design was 120 µm and the selected width of the individual finger electrodes in the design was 26000 µm and the channel length was 40 µm.

The electrical response of the printed photodetector shows an increased output of around 120%, once the dark current is about 300 nA while under illumination increases to approximately 660 nA, indicating the good performance of the printed device as a photodetector.

A polymer-based scintillator ink was optimized based on the thermoplastic elastomer copolymer SEBS. After the placement of the scintillator material on top of the photodetector by screen printing, the performance of the device as an X-ray detection was evaluated. The increase of the photocurrent of the photodetector in about 93%, from about 53 nA without the application of X-ray radiation up to 102 nA under X-ray radiation, with the scintillator located on top of the photodetector proves the suitability of the developed printed device for X-ray detection.

Thus, this work successfully demonstrates that polymer-based scintillator composites and inks for printing technologies can be developed, allowing the implementation of novel strategies for the fabrication of indirect X-ray detectors. Further, it is demonstrated the development of all-printed X-ray radiation detectors, which represents very promising approach for a new generation of large-area and low-cost flexible devices.

7.2. Future work

In the present work, it has been proven that it is possible to produce scintillator composites for radiation detectors and to apply them by printing technologies. In this sense, some interesting studies can be carried out to further explore the developed materials and technological approaches:

- Some important characteristics of the device must be quantified, such as the noise from scattered radiation, sensitivity, resolution, response time and stability over time.

- The developed printed photodetectors must be evaluated for medical imaging, comparing the obtained results with the current devices.

- To develop novel scintillating nanoparticles focusing to the present application. Thus, visible light output and frequency, response time and stability can be tailored or improved. Further, higher performance fluorescent molecules with tailored characteristics for specific applications can be developed.

- Adjust the optical detection to another radiation types by expanding the present approach of composite and ink development by using other active nanoparticles, this will allow the application of these detectors in areas of biological and environmental interest.

- Develop a process chain for a manufacturing both flat and curved X-ray indirect photodetectors, with high reproducibility and reliability.